

MODEL
MOBILITY
TIRES
SOILS

2096

U-
462

4024162

RE-516

TECHNICAL REPORT NO. 12109 (LL152)

DEVELOPMENT OF MATHEMATICAL MODEL
FOR PNEUMATIC TIRE-SOIL
INTERACTION IN LAYERED SOILS

November 1975



U.S. ARMY
TANK-AUTOMOTIVE
COMMAND
CONTRACT
DAAEO7-75-C-0066

4024162

by

LESLIE L. KARAFIATH

RESEARCH DEPARTMENT
GRUMMAN AEROSPACE CORPORATION
BETHPAGE, NEW YORK 11714

TACOM

MOBILITY SYSTEMS LABORATORY

U.S. ARMY TANK AUTOMOTIVE COMMAND Warren, Michigan

Approved for public release; distribution unlimited.

20020725112

DEVELOPMENT OF MATHEMATICAL MODEL FOR
PNEUMATIC TIRE-SOIL INTERACTION IN LAYERED SOILS

Final Report No. 12109 (LL152)

by

Leslie L. Karafiath

Prepared Under Contract DAAE07-75-C-0066

for

United States Army Tank-Automotive Command
Mobility Systems Laboratory
Warren, Michigan

by

Research Department
Grumman Aerospace Corporation
Bethpage, New York 11714

November 1975

Approved by: *Charles E. Mack, Jr.*
Charles E. Mack, Jr.
Director of Research

FOREWORD

Improvement of land mobility technology — a major goal of the U.S. Army Tank-Automotive Command (TACOM) — requires simulation of the interaction of the terrain, the vehicle, and man. Under TACOM contracts, Grumman has developed mathematical models of rigid wheel-soil and pneumatic tire-soil interaction conceived as alternate submodels in the AMC (Army Material Command) Mobility Model. In these first generation mathematical models, the terrain was assumed homogeneous throughout its depth and characterized by one set of Coulomb strength parameters. A great number of tire tests have been performed in homogeneous soil beds at the U.S. Army Engineers Waterways Experiment Station and elsewhere. These have made validating these models possible for a great variety of homogeneous soil conditions.

In the field, however, soil conditions are rarely homogeneous. Precipitation and evaporation give rise to a moisture gradient throughout the depth profile of the terrain and to corresponding changes in the strength properties of soil. Characterization of such soil conditions requires the consideration of Coulomb strength parameters that vary with depth, either discretely or continuously. Theoretical research performed under the present contract has shown that the plasticity theory can be applied for the determination of stress states in nonhomogeneous soil conditions. In this report, the results of this research are presented together with their application in the tire-soil model for the consideration of nonuniform and layered soil conditions.

ABSTRACT

Mathematical models of tire-soil interaction have been developed for nonhomogeneous soil conditions where the soil strength varies either continuously or discretely with depth. New methods of solving the differential equations of plasticity for soils have been developed for the bearing capacity problem in two-layer soils. Composite slip line fields obtained by these methods and the associated bearing stresses are shown for two cases: upper layer stronger than the lower layer and upper layer weaker than the lower layer. An approximate procedure, based on these composite slip line fields, is given for the estimation of bearing stresses in two-layer soils. This approximate procedure is applied in a tire-soil model expanded for the consideration of two-layer soils. The simulation of tire performance by this expanded model is compared with results of small-scale mobility tests performed at the U.S. Army Engineer's Waterways Experiment Station (WES) in layered soils.

Field methods of determining soil properties in layered soils are examined, and a modification of ring shear tests is recommended for the determination of the strength of individual layers in layered soils.

ACKNOWLEDGMENT

The work reported herein was performed for the Mobility Systems Laboratory of the U.S. Army Tank-Automotive Command (TACOM), Warren, Michigan, under the general supervision of Dr. Jack G. Parks, Chief of the Engineering Science Division and Mr. Zoltan J. Janosi, Supervisor, Research and Methodology Function. Mr. Zoltan J. Janosi was also technical monitor. Their help and valuable suggestions in carrying out this work are gratefully acknowledged.

Experiments performed at the U.S. Army Engineer Waterways Experiment Station in two-layer soils were used for the validation of the tire-layered soil model. The author thanks Mr. C. J. Nuttall for his helpful cooperation in obtaining this experimental information.

Dr. Edward A. Nowatzki, Associate Professor of Civil Engineering at the University of Arizona, was consultant on the project. Mr. G. Homfeld assisted in the performance of cone penetration experiments.

TABLE OF CONTENTS

<u>Section</u>	<u>Page</u>
I Scope of Work	1
II Theoretical Background	2
III Consideration of Continuous Variation of Soil Strength with Depth in the Tire-Soil Model	5
IV The Effect of Discrete Layering on the Magnitude and Distribution of Failure Stresses ..	18
Problems Encountered	18
Relative Strength of Layers	20
Solution Method for Case 1	23
Solution Method for Case 2	34
Evaluation of the Effects of Discrete Layering on the Failure Normal Stresses	40
V Tire-Soil Model for Two-Layer Soils	43
VI The Tire-Layered Soil Model and the Problem of Slipperiness	53
VII Field Determination of Properties of Layered Soils	56
Plate Sinkage Test	56
Cone Penetration Tests	57
Ring Shear Tests	61
VIII Conclusions and Recommendations	64
IX References	66
Appendix: Flowcharts	68

LIST OF ILLUSTRATIONS

<u>Figure</u>		<u>Page</u>
1	Strength Variation with Depth z for Constant ψ Intercept	6
2	Strength Variation with Depth z Without Restrictions	6
3	Scheme for Computing the Variables σ and θ at Nodal Point i,j for Strength Varying with Depth z	7
4	Comparison of Pull Performances for Soil Strength Varying with Depth	10
5	Distribution of Normal and Shear Stresses and Tire Deformation, Case 1, 20% Slip	12
6	Distribution of Normal and Shear Stresses and Tire Deformation, Case 2, 20% Slip	13
7	Rear Slip Line Fields	15
8	Development of Interface Shear Stresses in Cohesive Soil	16
9	Computation of Nodal Points at Layer Interfaces .	19
10	Mohr-Coulomb Relationships for Cases 1 and 2	22
11	Mohr-Coulomb Relationships for Cases 3 and 4	22
12	Variation of δ Angle at the Layer Interface	27
13	Normal Stresses in the Active ($k = -1$) and in the Passive ($k = +1$) Case in Relation to the Normal Stress on the Failure Plane	27
14	Scheme for Composition of Slip Line Fields for Case 1	27
15	Composite Slip Line Fields in Two-Layer Soils for Case 1	28

<u>Figure</u>		<u>Page</u>
16	Kinematic Slip Line Field for $\phi = 0$, Strong Bottom Layer	30
17	Bearing Stresses Computed on the Basis of Composite Slip Line Fields for Two-Layer Systems	31
18	Composite Slip Line Field with Base Friction	35
19	Scheme for Composition of Slip Line Fields for Case 2	35
20	Composite Slip Line Fields for Two-Layer Soils in Case 2	38
21	Bearing Stresses Computed on the Basis of Composite Slip Line Fields, Case 2	39
22	Approximate Determination of Bearing Stresses for Two-Layer Soils	41
23	Scheme of Computations for the Tire-Soil Model for Two-Layer Soils	45
24	Interface Normal Stress Distribution in the Case of Two-Layer Soils	46
25	Results of Cone Penetration Tests in Two-Layer Clay Soil	58
26	Results of Cone Penetration Tests in Multilayered Clay Soils	59
27	Results of Cone Penetration Tests in Two-Layer Sand	60
28	Schematic Arrangement of Ring Shear Test with Surcharge	63

LIST OF SYMBOLS

A	singular point
a through j	characteristic points along slip line field boundaries
B,b	width of tire
c	cohesion
CGR	cone index gradient
CI	cone index
D,d	diameter
D_{φ}	constant for the variation of φ with depth
D_{coh}	constant for the variation of cohesion with depth
e	base of natural logarithm
h	thickness of upper layer
i,j	slip line and nodal point designations
j_o, K	constants in slip-developed friction equation
p_i	inflation pressure
p_l	limit pressure
q	normal stress
R	radius of undeflected tire
r	radius of deflected tire
s	strength
x,z	coordinates
α	central angle (measured from vertical)

α_e	entry angle
α_m	angle of separation
α_r	rear angle
α'	angle defining start and end of tire deflection
α_{if}	angle of interference in forward field
α_{ir}	angle of interference in rear field
γ	unit weight of soil
δ	angle of inclination of resultant stress to normal, angle of shear mobilization, deflection in Waterways Experiment Station terminology
ϵ	deflection coefficient
θ	angle between x-axis and major principal stress
κ	$1 - 2\delta/d$
μ	$\pi/4 - \phi/2$
σ	$(\sigma_1 + \sigma_3)/2 + \psi$
σ_n	normal stress
$\sigma_{1,3}$	principal stresses
τ	shear stress
τ_i	interface shear stress
τ_{max}	maximum available shear strength
τ_{mob}	mobilized shear strength
ϕ	angle of internal friction
ψ	$c \cot \phi$

I. SCOPE OF WORK

The scope of work, as originally described in the RFP work statement, was to establish a mathematical simulation of tire-soil interaction for soil conditions that vary with depth. Within this general scope emphasis was placed on the following items:

- Development of solution methods for the differential equations of plasticity for soil strength varying continuously with depth
- Development of solution methods for the differential equations of plasticity for discrete variation of soil strength with depth (layered systems)
- Application of the above solution methods in tire-soil interaction simulation
- Evaluation of present field techniques of soil property determination to assess their suitability to characterize soil with a variable strength profile

II. THEORETICAL BACKGROUND

A characteristic feature of soil deposits is that their strength and other properties inherently vary with depth. In soil mechanics, many theories and analytical methods have been put forward to allow proper consideration of this feature in the solution of the various soil engineering problems. As early as in 1934 Froehlich (Ref. 1) proposed the use of an elastic modulus linearly increasing with depth for the computation of settlements and developed appropriate formulas using the theory of elasticity. Burmister applied the theory of elasticity for the computation of stresses and displacements in layered systems (Ref. 2). In elasticity, he considered two kinds of boundary conditions at the layer interfaces: 1) full continuity of stresses and displacements across the interface (no limitations on shear stresses on account of shear strength of soils) and 2) continuity of normal stress and normal displacement with a frictionless interface that allows relative displacement of the adjoining layers along the interface. In his theory each layer is considered homogeneous and is characterized by its elastic modulus and Poisson's ratio. The numerical evaluation of the general equations for layered systems set forth by Burmister indicated that the boundary conditions at the layer interface, the ratio of the elastic moduli of the adjoining layers, and the ratio of the upper layer thickness to the dimensions of the loaded area strongly influence the distribution of stresses due to surface loading.

In tire-soil interaction problems of interest the stress levels in soil far exceed those for which the theory of elasticity applies. In the theory of plasticity there is no general treatment of layered systems. Sokolovskii (Ref. 3) treated a very

special case of layered systems — that of a "lamellar medium" — where the layering is such that on horizontal planes the shear stresses may not exceed a value defined by a Coulomb type failure condition along the horizontal plane. In the theory of plasticity for soils, as it was pointed out in Ref. 4, the deformations in the soil that occur prior to the plastic state are disregarded, and the stress states are calculated solely on the basis of Mohr-Coulomb yield criterion. As a consequence, in a logical expansion of the plasticity theory to layered systems the boundary conditions at layer interfaces have to be defined in terms of stresses alone, as follows: Normal and shear stresses across the interface boundary must be continuous. The shear stress at the interface may not exceed the shear strength of either adjoining layer. In mathematical terms:

$$\begin{aligned}\tau_i &\leq c_\ell + \sigma_n \tan \varphi_\ell \\ \tau_i &\leq c_u + \sigma_n \tan \varphi_u\end{aligned}\tag{1}$$

In plasticity theory, elastic deformations are not considered. However, the displacements due to plastic flow are subject to certain restraints. (A detailed discussion of the theory of velocity fields that applies to these restraints is given in Ref. 5.) The application of the theory of velocity fields to the boundary conditions at the interface yields the following boundary conditions: Velocity vectors normal to the interface must either be equal in both layers or greater in the upper layer than in the lower layer so that separation along the boundary cannot occur. Velocity vectors tangential to the interface, however, can and usually will be different so that one layer can slide past the other.

Solutions of the plasticity theory for soils constitute zones of plastic equilibrium, also known as slip line fields. Certain

problems such as the bearing capacity or tire-soil interaction problems require a composition of various types of zones (active, passive, and radial zones). Solutions in layered systems will also be composed of various zones that meet the boundary conditions at the layer interface. The adjoining zones in the two layers are not required to be of the same type, and various configurations are possible as long as the boundary conditions at the interface are satisfied. These are discussed in more detail in Section IV.

The consideration of a continuous variation of strength properties in the solution of the differential equations of plasticity is discussed in Ref. 6 for the case of a nonlinear Mohr-Coulomb strength envelope. The case where the strength properties vary with depth poses essentially the same type of problem as a nonlinear failure envelope and requires only a modification of the numerical solution procedures.

The problem of bearing capacity of soils exhibiting strength properties that vary with depth either discretely or continuously has been treated by various researchers, most of them using the single failure surface mechanism approach applied in soil mechanics for stability analyses. Tcheng (Ref. 8) performed bearing tests on layered systems using sand and a special grease to model cohesive soils. Brown and Meyerhof (Ref. 9) investigated the bearing capacity of two-layer purely cohesive soils. Salencon (Ref. 10) treated the problem of bearing capacity of a purely cohesive soil with linearly varying strength analytically. Yamaguchi and Terashi (Ref. 11) presented analytical solutions to special bearing capacity problems on multilayered ground.

III. CONSIDERATION OF CONTINUOUS VARIATION OF SOIL STRENGTH WITH DEPTH IN THE TIRE-SOIL MODEL

The methods of numerical computations for the determination of the geometry of slip line fields and associated stresses have been discussed in detail in Refs. 4 through 6. For brevity, only the differences in the computation methods necessitated by the consideration of strength variation with depth are discussed herein.

The variation of the strength properties with depth considered in the tire-soil model are shown in Figs. 1 and 2. Figure 1 shows the case where the ψ intercept at the σ -axis is constant, while Fig. 2 shows the more general situation when the ψ intercept varies with the assumed variation of soil strength. Because of this variation of the ψ intercept the numerical solution methods for the differential equations of plasticity for soils presented in Ref. 6 have to be modified. In these solutions the principal stress variable, σ , is defined as the distance of the center of the Mohr circle from the intersection of Mohr-Coulomb envelope with the σ -axis ($-\psi$). If ψ varies with depth, then the σ values have to be adjusted to this variation. Figure 3 shows the schematic diagram of the computation of variables at an i,j nodal point with respect to this variation. In practice, it was found that one iteration on the ψ values for the determination of the appropriate strength values was satisfactory.

A more detailed flow chart for the computation of a single slip line field (subroutine SLFI) for variable strength is given in the appendix. In the computer program represented by the flow chart, the following variation of the strength parameters with depth is assumed.

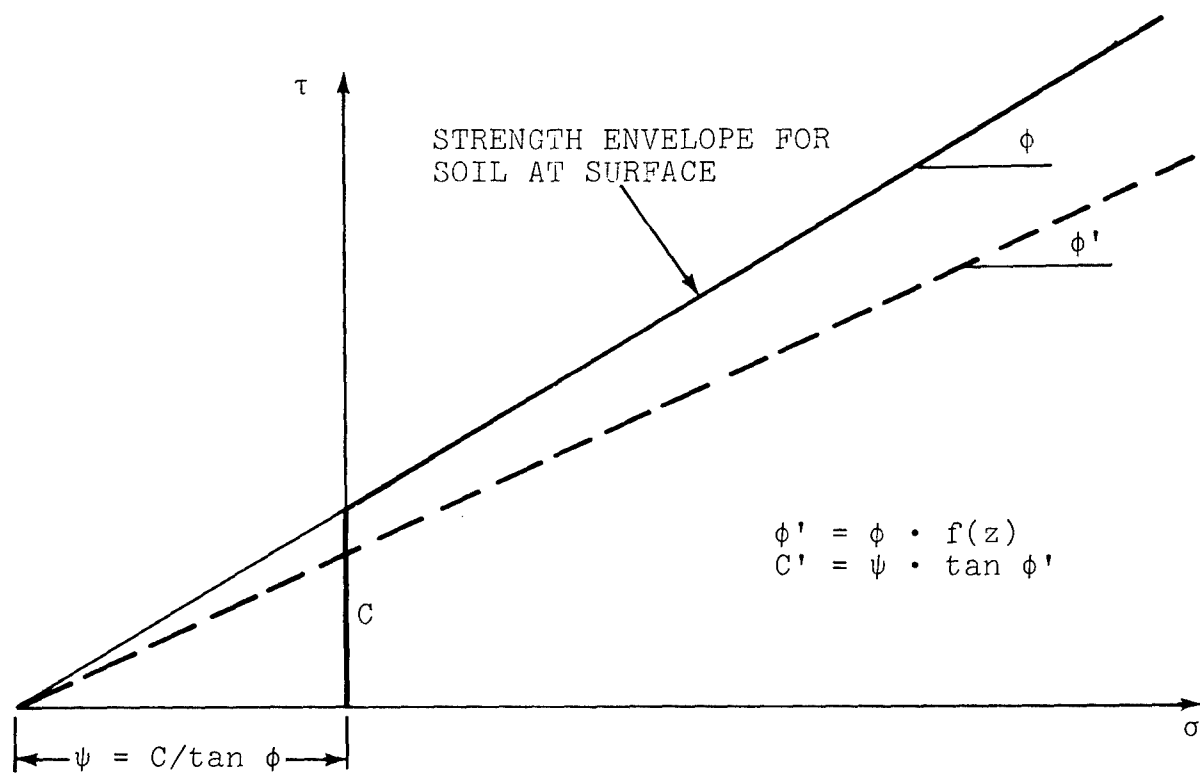


Fig. 1 Strength Variation with Depth z for Constant ψ Intercept

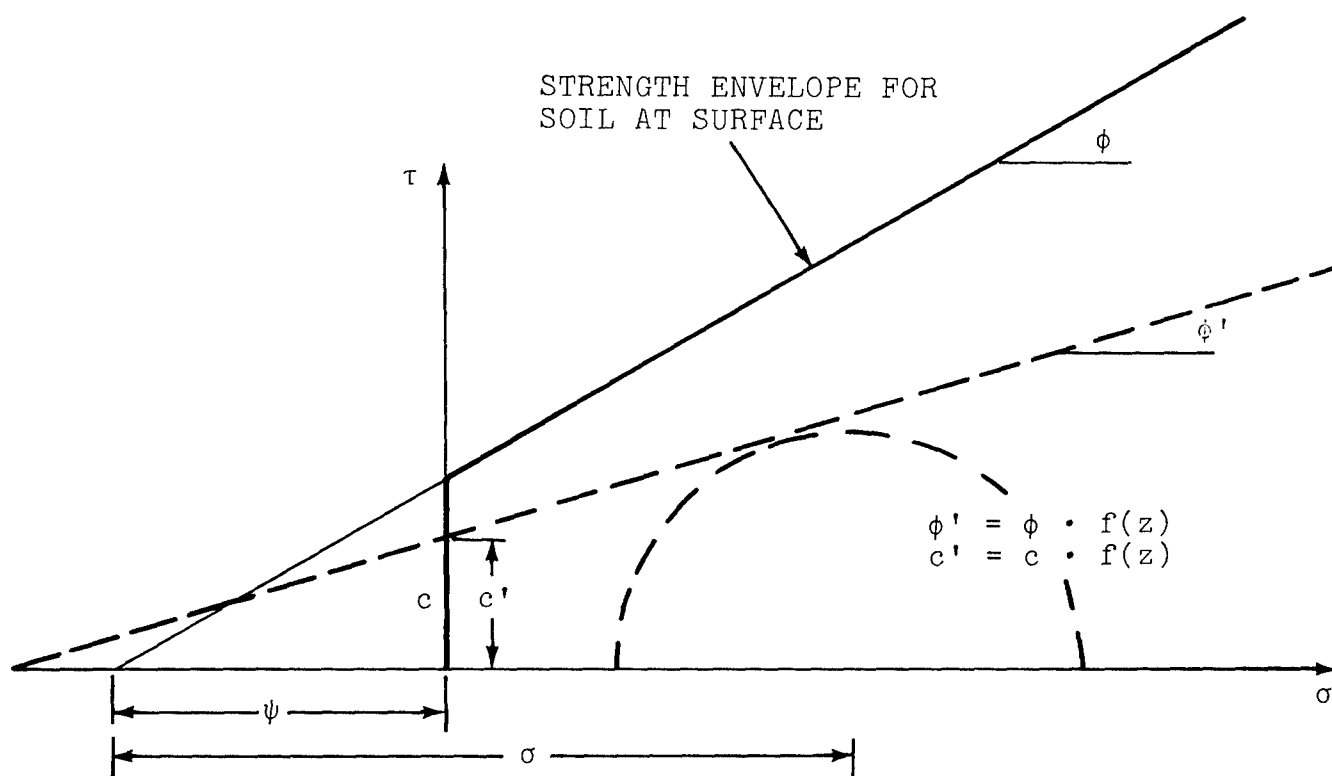


Fig. 2 Strength Variation with Depth z Without Restrictions

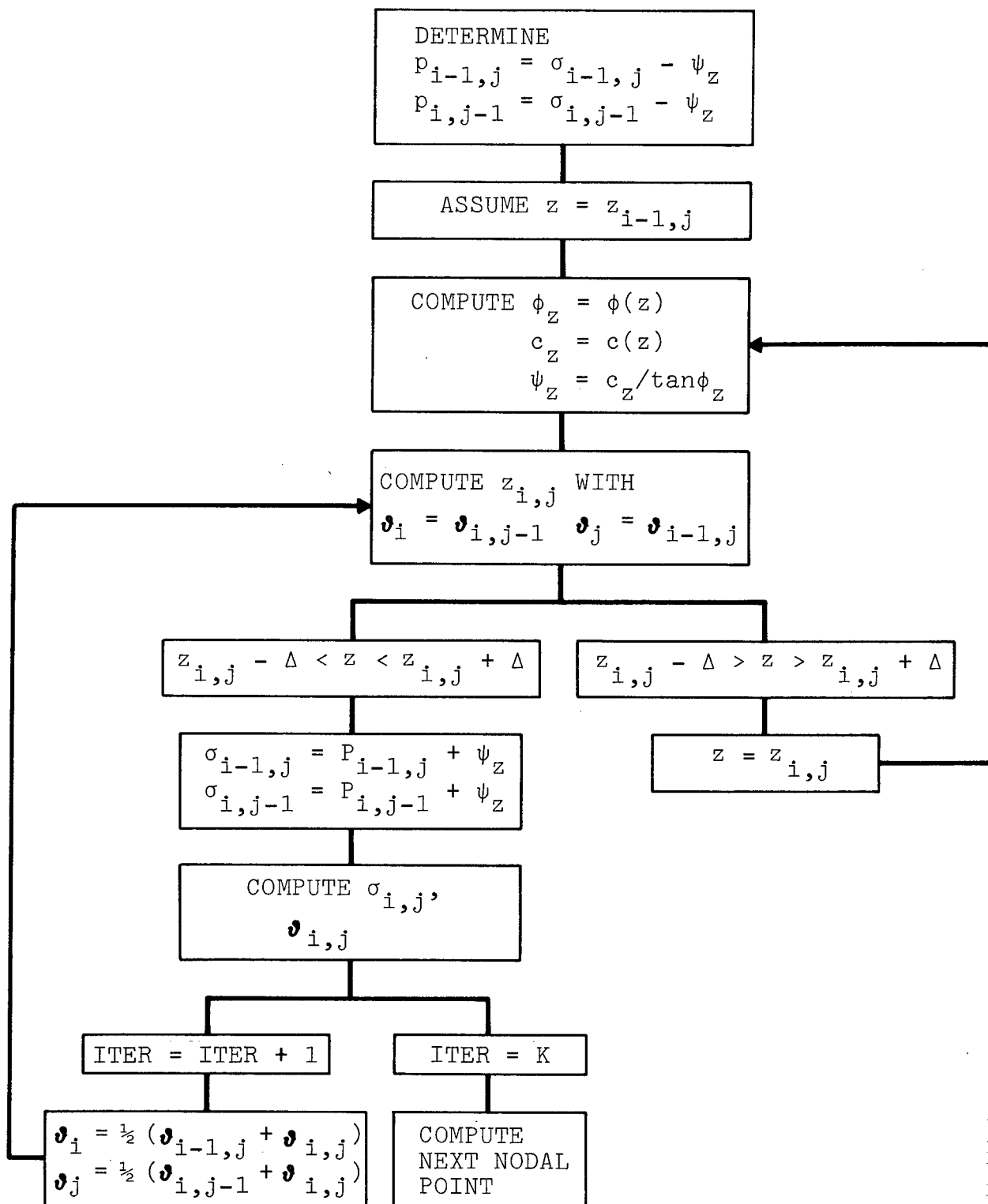


Fig. 3 Scheme for Computing the Variables σ and v at Nodal Point i, j for Strength Varying with Depth z .

$$\varphi_z = \varphi(1 + D_\varphi z)$$

$$c_z = c(1 + D_{coh} z) \quad (2)$$

$$\psi_z = c_z \cotan \varphi_z$$

Designation of the variables in the subroutine for the computation of a single slip line field is as follows. Double subscripted variables:

$$X(I,J) = x_{i,j} \quad (\text{x coordinate of nodal point})$$

$$Z(I,J) = z_{i,j} \quad (\text{z coordinate of nodal point})$$

$$S(I,J) = \sigma_{i,j} \quad (\frac{1}{2}(\sigma_1 + \sigma_3) + \psi)$$

$$T(I,J) = \theta_{i,j} \quad (\text{direction of major principal stress})$$

$$P(I,J) = \sigma_{i,j} - \psi_z = \frac{1}{2}(\sigma_1 + \sigma_3)$$

The dimension statements for these subscripted variables correspond to a 43 x 15 grid ($I = 1$ to 43, $J = 1$ to 15) for the computation of the geometry of slip line fields.

Single subscripted variables designate the following values of the variables at the interface at the "j" line intersections.

$$D(J) = \sigma_j \quad (\text{interface friction angle})$$

$$H(J) = \alpha_j \quad (\text{central angle})$$

$$Q(J) = q_j \quad (\text{normal stress})$$

$$E(J) = \tau_j \quad (\text{shear stress})$$

$$U(J) = x_j \quad (\text{x coordinate of interface})$$

$$V(J) = z_j \quad (\text{z coordinate of interface})$$

$A(J)$, $B(J)$, $C(J)$ are auxiliary variables.

Constants and Parameters:

$R\phi$	=	radius
$G\phi$	=	γ (unit weight)
COH	=	c (cohesion at surface)
PHI	=	ϕ (friction angle at surface)
D1	=	δ (interface friction angle)
$A\phi$	=	α_e (entry angle in arc)
AM	=	α_m (central angle at end of field)
A1	=	α_s (tangent angle to log spiral)
PL	=	p_ℓ (limit pressure)
XX	=	- 1 for front field
XX	=	+ 1 for rear field
XX	=	2 for rear field only
DEPHI	=	D_ϕ (constant for ϕ variation with depth)
DECON	=	D_{coh} (constant for c variation with depth)

The main program for the computation of drawbar pull, torque, and sinkage is essentially the same as reported for the tire-soil model for uniform strength in Ref. 7.

Typical results obtained with the tire-soil model modified for variable strength are shown in Fig. 4 where pull performance relationships are shown for four cases, each depicting a different variation of soil strength with depth. Common input conditions for these cases were:

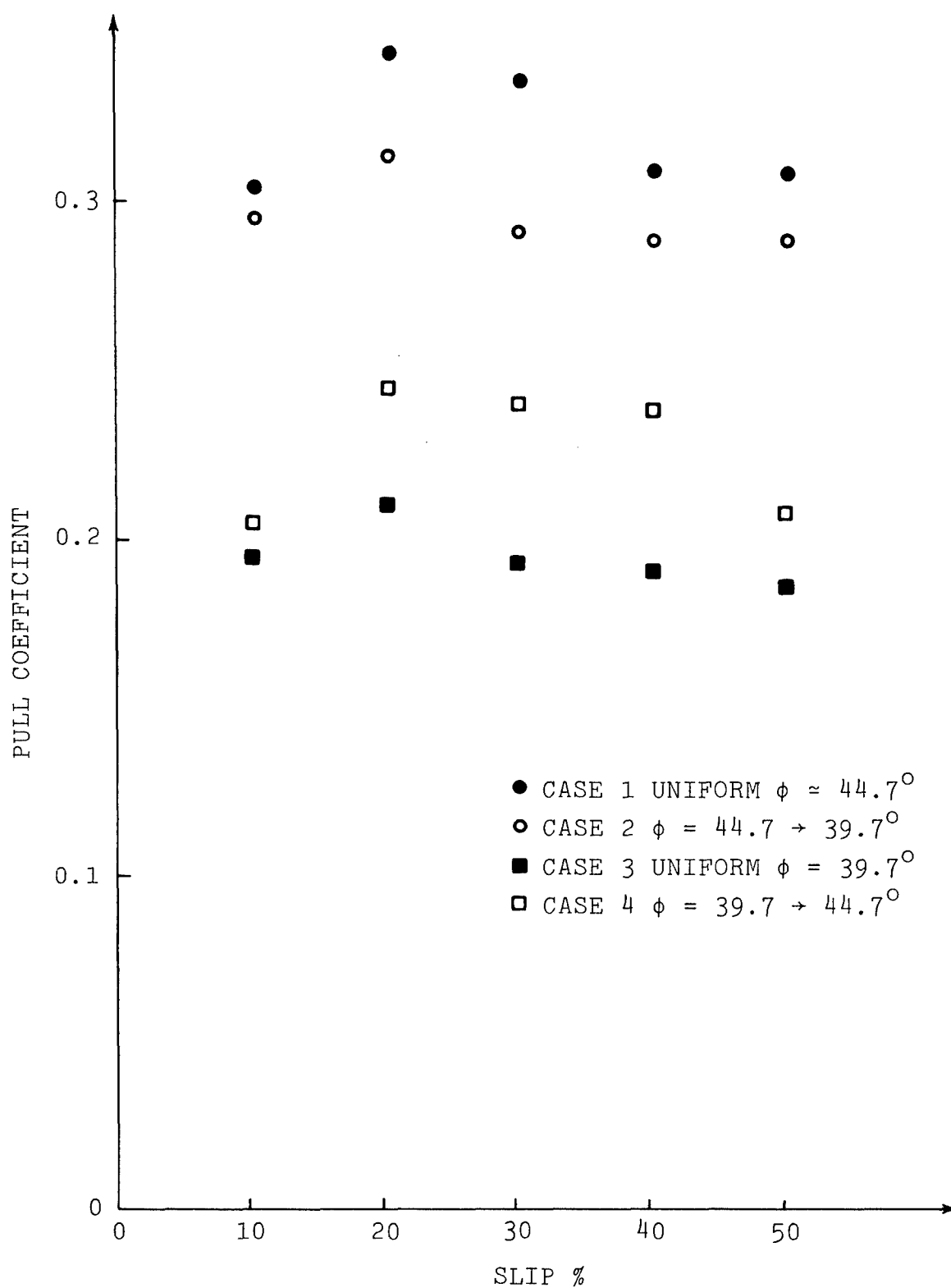


Fig. 4 Comparison of Pull Performances for Soil Strength Varying with Depth

Tire Characteristics

Tire size	9.00 - 14
Nominal radius	1.18 ft
Nominal width	0.74 ft
Inflation pressure	18.7 psi
Deflection	25%
Deflection coefficient	0.88
Load	850 lb

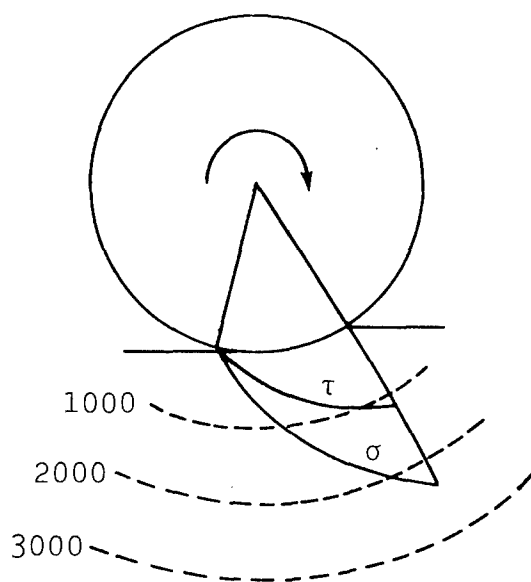
Soil

Yuma Sand

Case No. 1 represents uniform conditions corresponding to a cone index gradient (CGR) of 15, or $\phi = 44.7^\circ$. In Case No. 2, the soil strength decreases linearly from $\phi = 44.7^\circ$ at the surface to $\phi = 39.7^\circ$ at the deepest point of the slip line field. Case No. 3 again represents uniform conditions where the soil strength equals $\phi = 39.7^\circ$, the minimum soil strength in Case No. 2. This friction angle corresponds to a CGR of 5.5. Finally, in Case No. 4, the soil strength increases linearly from $\phi = 39.7^\circ$ to $\phi = 44.7^\circ$ at the deepest point of the slip line fields. As is seen from Fig. 4, the pull performance for variable shear strength is close to that in a uniform soil having the same strength as the variable strength profile at the surface.

Figure 5 shows the computed distribution of normal and shear stresses and, in the upper part, the deflection of the tire for Case No. 1 at 20 percent slip, as obtained with the computer graphics program. Figure 6 shows the same for Case No. 2. Note that in the radial plot a rigid wheel with the nominal tire diameter is shown for the convenience of plotting; the tire deformation

TIRE
DEFLECTION



σ = NORMAL STRESS IN LB/SQ FT
 τ = SHEAR STRESS IN LB/SQ FT

Fig. 5 Distribution of Normal and Shear Stresses and Tire Deflection, Case No. 1, 20% Slip

TIRE
DEFLECTION

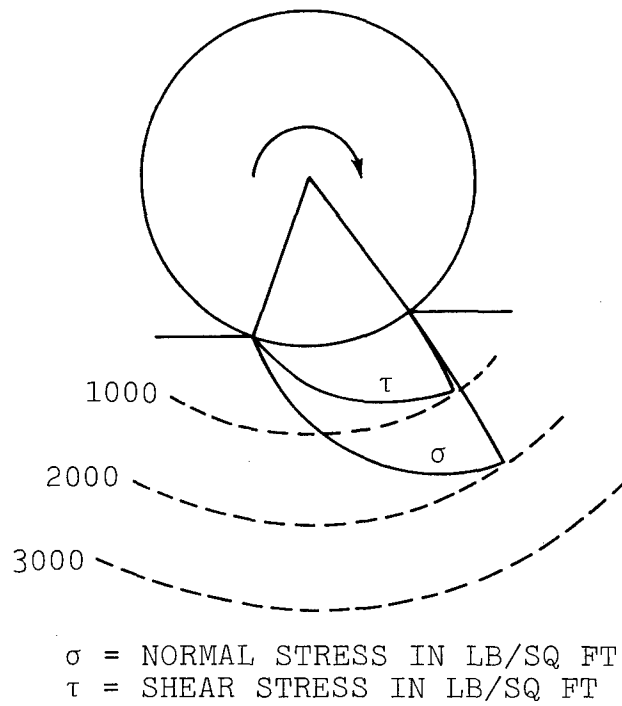
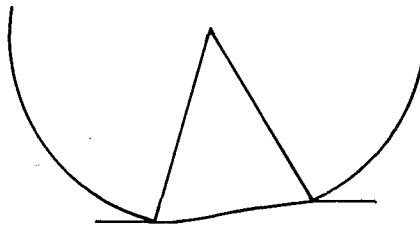


Fig. 6 Distribution of Normal and Shear Stresses and Tire Deflection, Case No. 2, 20% Slip

is shown separately at the top. The difference in the interface stresses computed for the two cases is, indeed, minor and results in little difference in pull performance.

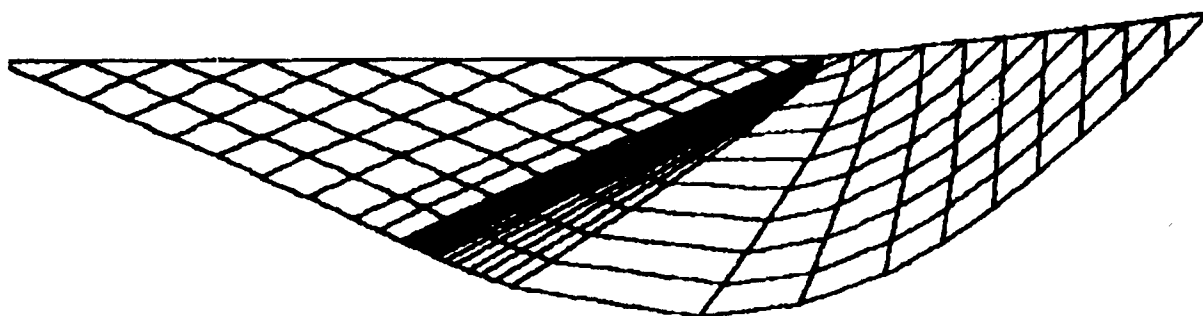
The effect of a decreasing shear strength on the slip line fields that develop underneath a tire is that the slip line fields encompass a greater depth than those for uniform strength.

Figure 7a shows a typical rear slip line field obtained for the conditions of Case 2 where the shear strength decreased from about 45° at the surface to about 33° at the point of the field. For comparison, the slip line field for Case 1 uniform strength ($\phi = 45^\circ$) is also shown (Fig. 7b).

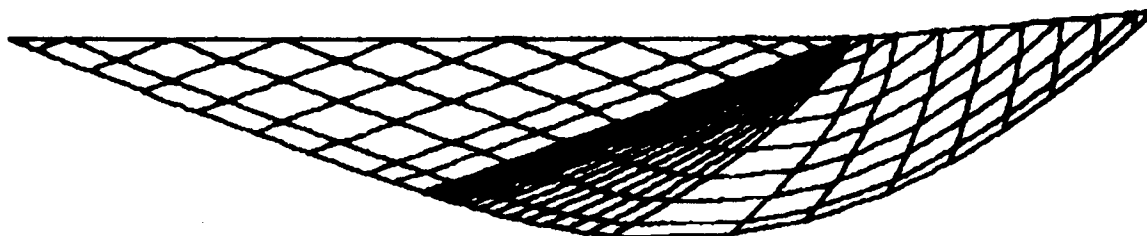
The growth of the slip line field in the z direction due to a decreasing shear strength results in encountering layers of less and less strength. At some rate of strength decrease, a progressive process takes place for which no slip line field solution may be found. This is interpreted as a condition where complete and deep reaching failure would take place in the soil under the tire load, indicating a "no go" condition.

In conclusion, in sand the surface strength is the dominating factor, but there is a limit to the rate of decrease at which a no go situation occurs. In cohesive soils the situation is very similar, as far as the limit of strength decrease is concerned at which no go condition sets in. The effect of strength decrease on pull performance is less pronounced than in sand and sometimes paradoxical in that higher pull performance is obtained with decreasing strength. The explanation of this paradox is shown in Fig. 8. The development of the interface shear stress depends on the angle δ and equals

$$\tau = (\sigma_n + \psi) \tan \delta \quad (3)$$



a) FOR CASE 2, ϕ DECREASING FROM 45° TO 33°



b) FOR CASE 1, $\phi = 45^\circ$

Fig. 7 Rear Slip Line Fields

In this equation $\psi \tan \delta$ is the contribution of the cohesion to the interface stress that may be called adhesion. The pull performance is governed by the ratio of the interface shear stress to the normal stress, or $\tan \delta'$ in Fig. 8. A decreasing shear strength reduces the normal stresses while not affecting τ that depends on the surface shear strength and δ . Thus, in cohesive soils the τ/σ_n ratio generally increases as the shear strength decreases with depth. If the effect of the increase of the τ/σ_n ratio is not set off by an increase in sinkage, then pull performance improves with a shear strength that decreases with depth.

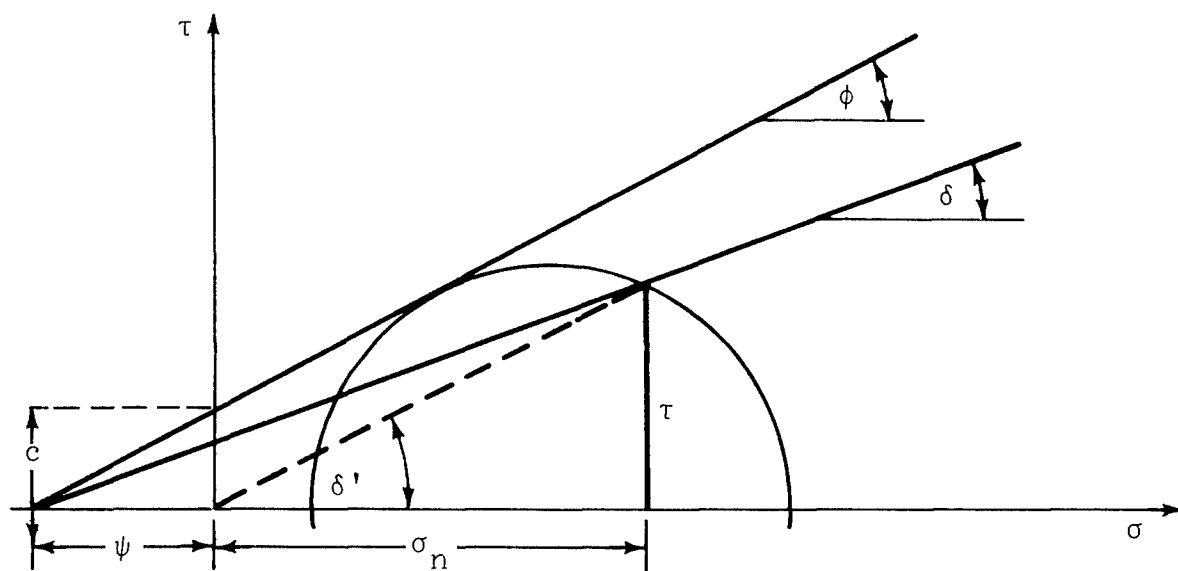


Fig. 8 Development of Interface Shear Stresses in Cohesive Soil

The conclusions that can be drawn from the tire-soil model for soil strength varying with depth is that the surface strength has more influence on the pull performance than the strength of the

underlying layers as long as the strength decrease does not result in a critical no go situation. It is recommended that criteria for the rate of strength decrease that results in such a situation be established by further research.

In these analyses a linear variation of soil strength with depth was assumed. Other relationships that describe strength variation with depth may also be assumed and appropriately introduced into the program. No difficulties are expected to occur with other forms of strength variation as long as the variation is smooth.

IV. THE EFFECT OF DISCRETE LAYERING ON THE MAGNITUDE AND DISTRIBUTION OF FAILURE STRESSES

The concept of tire-soil interaction developed for homogeneous soil conditions postulates that the soil is in the plastic state of failure whenever the failure stresses at the tire-soil interface are less than the limit pressure characteristic of the tire. Stresses in soil in the plastic state of failure are determined by the numerical integration of the differential equations of plasticity for soils; the orientation of failure surfaces and the extent of the plastic state are represented by the slip line field obtained in the course of numerical integration.

To develop a method for determining the effect of discrete layering on tire-soil interaction, the problem of constructing a single slip line field must first be solved. Since this problem has not been treated previously in two-layer soils, it is expedient to choose an approach where the problems of discrete layering may be solved without the complications inherent in the slip line field calculations in the tire-soil interaction problem. The simple two dimensional bearing capacity case is suitable for this purpose.

PROBLEMS ENCOUNTERED

Originally it was planned to develop solution methods for the bearing capacity of two-layer soils by using a common grid system in both layers and use auxiliary nodal points at the locations where the slip lines cross the interface boundary. Computer programs were written for the necessary algorithms for the computation of the coordinates and stress states at these auxiliary points, but unexpected problems arose in connection with certain situations illustrated in Fig. 9. In the numerical computation scheme, the

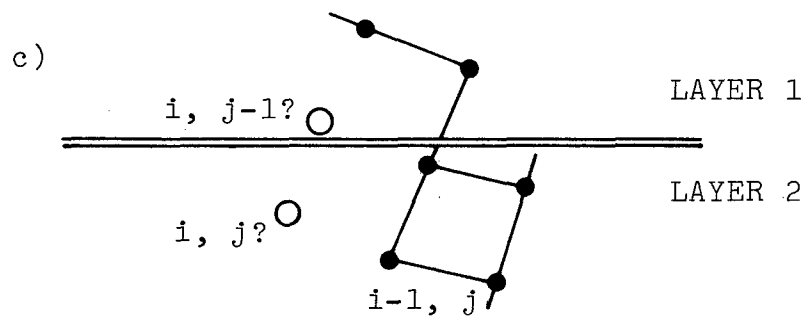
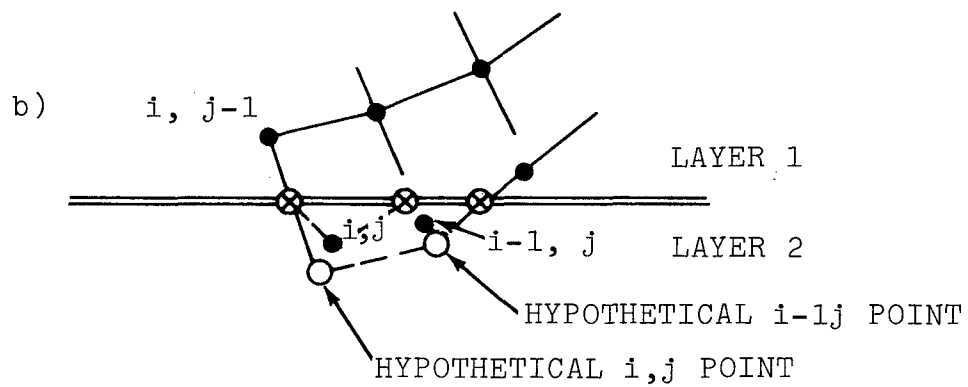
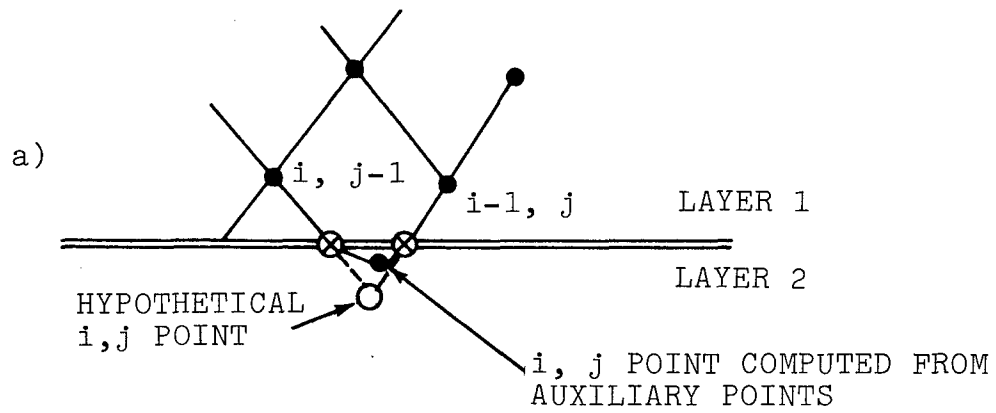


Fig. 9 Computation of Nodal Points at Layer Interfaces

variables are computed at an i,j point from the values at the $i-1,j$ and $i,j-1$ points. If both of these points are in the same layer (as shown in Fig. 9a), there is no problem. If the two points are in different layers, but hypothetical points (as they were in the adjacent layer) may be computed (as shown in Fig. 9b), the problem solution requires additional storage of data for hypothetical points. The problem for which no satisfactory solution has been found is shown in Fig. 9c, where the nodal points required to compute a hypothetical point for i,j are not in the same layer and a hypothetical $i,j-1$ point is not available from previous computations. Various methods have been tried to overcome this problem by using estimated values for these points, but none has proved to be generally satisfactory.

From the many trial computations performed for this approach it became evident that using separate grid systems in the two layers has a better chance of success. It was also concluded that different solution methods would be required, depending upon whether the upper layer is stronger than the lower one, or vice versa.

RELATIVE STRENGTH OF LAYERS

There are several cases with respect to the relative strength of the layers in a two-layer system.

Case 1

For a given normal stress, σ_n , and for $\sigma_u < \sigma_1$, i.e.,

$$c_u + \sigma_n \tan \phi_u < c_1 + \sigma_n \tan \phi_1 \quad (4)$$

The subscripts u and 1 refer to upper and lower layer, respectively. This condition is represented schematically by the Mohr-Coulomb construction shown in Fig. 10.

Case 2

For a given normal stress, σ_n , and for $\sigma_1 < \sigma_u$, i.e.,

$$c_1 + \sigma_n \tan \phi_1 < c_u + \sigma_n \tan \phi_u \quad (5)$$

This condition is represented schematically in Fig. 10a also, except that the u and 1 subscripts are everywhere interchanged.

Case 3

There is a "crossover" normal stress, σ_c , where the strength of the upper layer equals that of the lower layer. For $\sigma_n < \sigma_c$,

$$c_1 + \sigma_n \tan \phi_1 < c_u + \sigma_n \tan \phi_u \quad (6)$$

and for a given normal stress, σ_n , greater than the crossover normal stress, σ_c ,

$$c_u + \sigma_n \tan \phi_u < c_1 + \sigma_n \tan \phi_1 \quad (7)$$

This condition is shown schematically in Fig. 11.

Case 4

Case 4 is the reverse of Case 3 with the u and 1 subscripts interchanged.

If the maximum normal stress at the interface is less than σ_c in a certain problem, then Cases 3 and 4 revert to Cases 1 and 2, respectively. If σ_c is within the range of normal stresses that are transmitted through the interface in a certain situation, then there is relatively little difference in the strength of the two layers, and an acceptable approximation may be found by treating the case at homogeneous soil with strength properties averaged

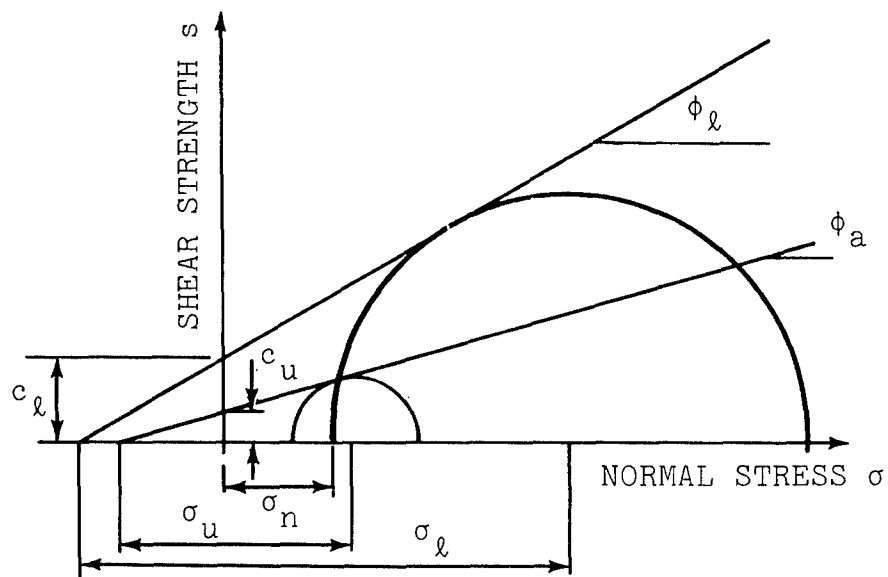


Fig. 10 Mohr-Coulomb Relationships for Case 1 and Case 2
(Exchange Subscripts)

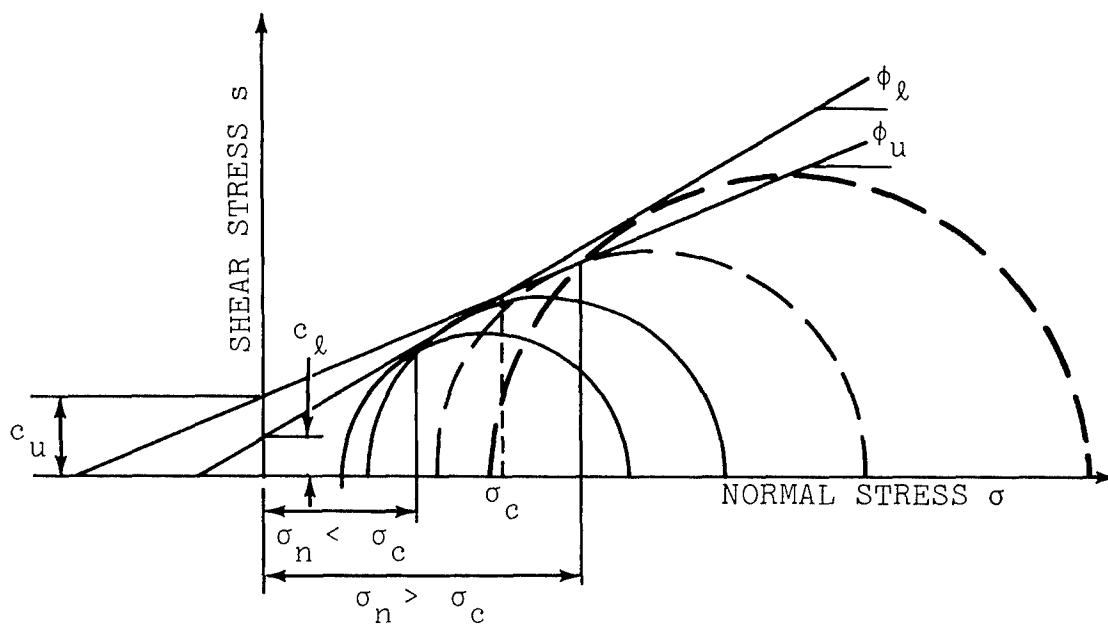


Fig. 11 Mohr-Coulomb Relationships for Case 3 and Case 4
(Exchange Subscripts)

between the two layers. For these reasons the solution method discussed in the following are restricted to Case 1 and 2.

SOLUTION METHOD FOR CASE 1

A solution of the simple two dimensional bearing capacity problem must satisfy the boundary conditions at both the surface and at the layer interface. The boundary conditions at the layer interface require the continuity of normal and shear stresses across the interface with the additional condition that the shear stress may not exceed the strength of the weaker layer. Since the strength of soils depends on the normal stress, it is convenient to express the condition on shear strength in terms of the layer interface friction angle δ (a concept similar to the tire-soil interface friction angle). The strength of the upper layer may be expressed as

$$s_u = (c_u + \sigma_n) \tan \phi$$

and the shear stress at the interface

$$\tau_u = (c_u + \sigma_n) \tan \delta_u$$

$$\tau_\ell = (c_\ell + \sigma_n) \tan \delta_\ell$$

$$(c_u + \sigma_n) \tan \delta_u = (c_\ell + \sigma_n) \tan \delta_\ell \leq (c_u + \sigma_n) \tan \phi_u$$

$$\delta_u < \phi$$

$$\tan \delta_\ell = \frac{c_u + \sigma_n}{c_\ell + \sigma_n} \tan \delta_u \leq \frac{c_u + \sigma_n}{c_\ell + \sigma_n} \tan \phi_u \quad (8)$$

The shear stresses and δ_u angles generated at the layer interface by a slip line field in the upper layer vary from 0 in the passive zone to

$$\tau_{\max} = (c_u + \sigma_n) \tan \phi_u$$

and

$$\delta_u = \phi_u$$

at the point where the interface is tangent to a "j" slip line. At this point, the interface is a slip line and $\delta_u = \phi_u$. The variation of δ_u angle in a slip line field is shown in Fig. 12. The slip line field in the area (ABCDE) may be constructed without interference from the lower layer. The dash-dot line to the right from the point where $\delta_u = \delta_{\max}$ indicates the variation of δ for hypothetical uniform soil conditions, i.e., that would occur along the line of the interface if soil conditions did not change across that line.

The θ angle, the direction of the major principal stress, is computed from the δ angle as follows (Ref. 12)

$$\theta = (1 - k) \frac{\pi}{4} + (k\Delta - \delta) \quad (9)$$

where

$$\Delta = \arcsin \frac{\sin \delta}{\sin \phi}$$

$$k = +1 \quad \text{in the passive case}$$

$$k = -1 \quad \text{in the active case}$$

The passive case $k = +1$ includes all stress states where

$$\sigma_{nf} > \sigma_n > \sigma_3$$

and the active case ($k = -1$) all stress states where

$$\sigma_{nf} < \sigma_n < \sigma_1$$

σ_{nf} = normal stress at the failure plane (Fig. 13)

Point D at the interface (Fig. 12) (where $\sigma_n = \sigma_{nf}$ and $\sigma_u = \varphi_u$) is the point that separates the $k = +1$ and $k = -1$ stress states. The variation of the θ angle along the line of the interface in the hypothetical uniform case would be continuous even though k could change at point "d" from -1 to $+1$, since Eq. (9) yields the same value for θ with either value, if $\delta_u = \varphi_u$. In this case

$$\Delta = \arcsin 1 = \frac{1}{2} \pi$$

$$k = +1 \quad , \quad \theta = \frac{1}{2}(\frac{1}{2} \pi - \varphi) = \frac{1}{4} \pi - \frac{1}{2} \varphi \quad (10)$$

$$k = -1 \quad , \quad \theta = \frac{1}{2} \pi + \frac{1}{2}(-\frac{1}{2} \pi - \varphi) = \frac{1}{4} \pi - \frac{1}{2} \varphi$$

In the case of the bearing capacity problem, the only conceivable solutions are those where the character of stress state (the "k" value) does not change across the interface. (A change in the k value would result in a permissible, but inappropriate stress discontinuity along the interface.) Thus, the boundary conditions at the interface for a slip line field solution in the lower layer are characterized by a $k = -1$ along (DC) and a $k = +1$ value along (DF). The θ values along the interface can be computed by Eq. (9). At an infinitesimal distance to the right of point D, θ in the lower layer could be computed using $k = +1$, while at an infinitesimal distance to the left, it could be computed using $k = -1$. While in the upper layer this change of the sign of k does not affect the continuity of θ , in the lower layer, where $\delta < \varphi$, there will be a discontinuity in θ at this point. This situation has been recognized as identical to that at the singular point of the bearing capacity case (point A in Fig. 12) requiring a radial zone to accommodate this discontinuity. Since the boundary conditions along (DC) are also defined by the continuity condition on the normal and shear stresses, a slip line

field can be constructed in the lower layer for any assumed variation of δ (or θ) along DF. In lieu of anything better, it was assumed that δ along DF would change the same way as in the case of uniform soil conditions.

The slip line field in the lower layer yields the normal and shear stresses at the DF portion of the interface from which the values of all four variables (x , z , σ , and θ) for the upper layer strength parameters can be computed. These constitute the boundary conditions for which an active zone type slip line field may be constituted in the upper layer. Thus, the solution in Case 1 consists of three fields, as shown in Fig. 14. Field (abcd) is a regular slip line field cut off at the interface. Field (cdefghi) is a bearing capacity field consisting of the regular three zones but for a variable δ as boundary conditions at the interface. Field (efij) consists only of an active zone. For the computation of this field, auxiliary points are needed in the zone bounded by the line (jklm).

A computer program was written for the computation of a composite slip line field comprising the three types of fields shown in Fig. 14. Typical composite slip line fields are shown in Fig. 15a through 15g for the following strength properties of the two layers:

Fig.	Upper Layer			Lower Layer		
	c (lb/sq ft)	ϕ (deg)	γ (lb/cu ft)	c (lb/sq ft)	ϕ (deg)	γ (lb/cu ft)
15a	10	30	100	14.50	40	100
15b	10	30	100	10	35	100
15c	80	20	100	100	25	100
15d	50	20	100	100	20	100
15e	50	10	100	80	10	100
15f	10	20	100	10	30	100
15g	10	10	100	20	12	100

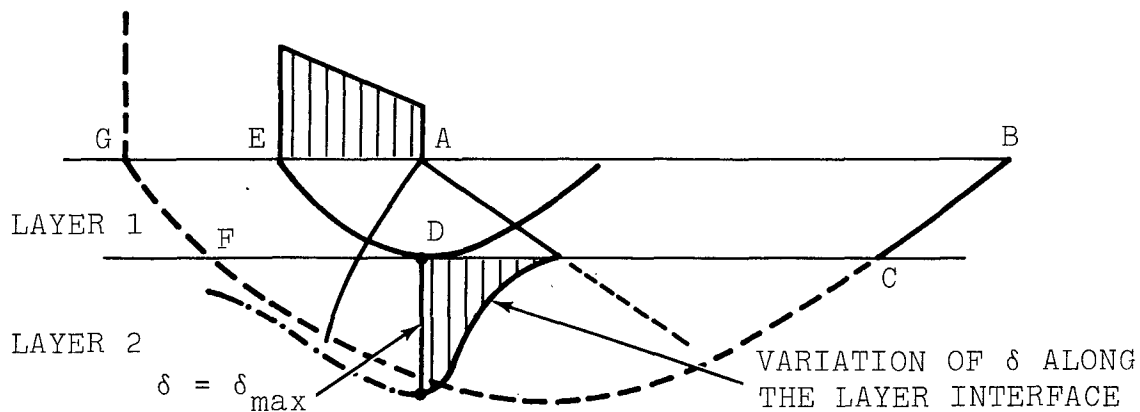


Fig. 12 Variation of δ Angle at the Layer Interface

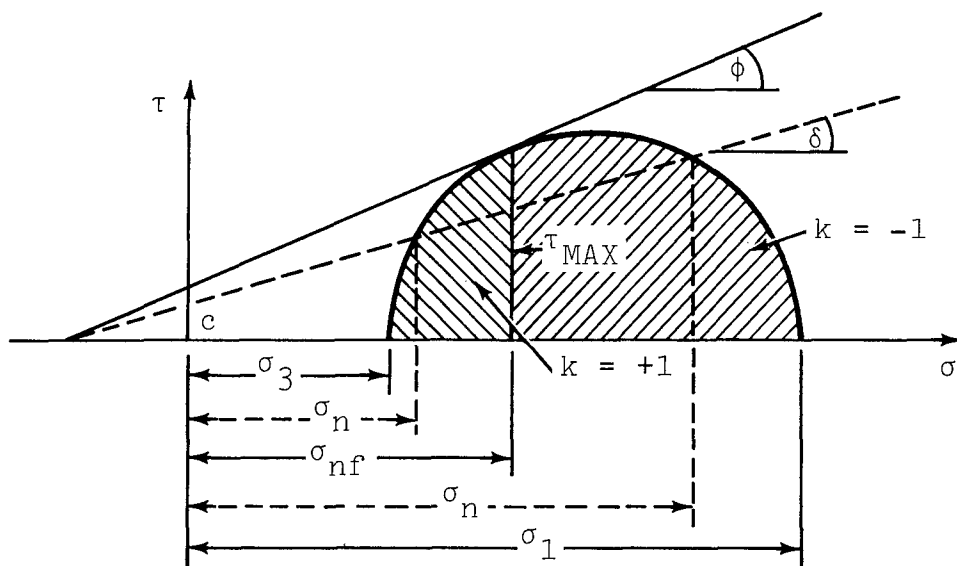
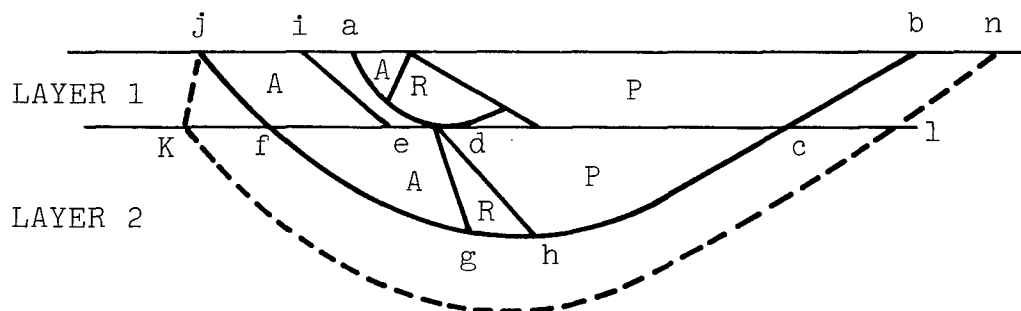


Fig. 13 Normal Stresses in the Active ($k = -1$) and in the Passive ($k = +1$) Case in Relation to the Normal Stress on the Failure Plane



ZONES: A = ACTIVE, B = PASSIVE, C = RADIAL

Fig. 14 Composite Slip Line Field for Case 1

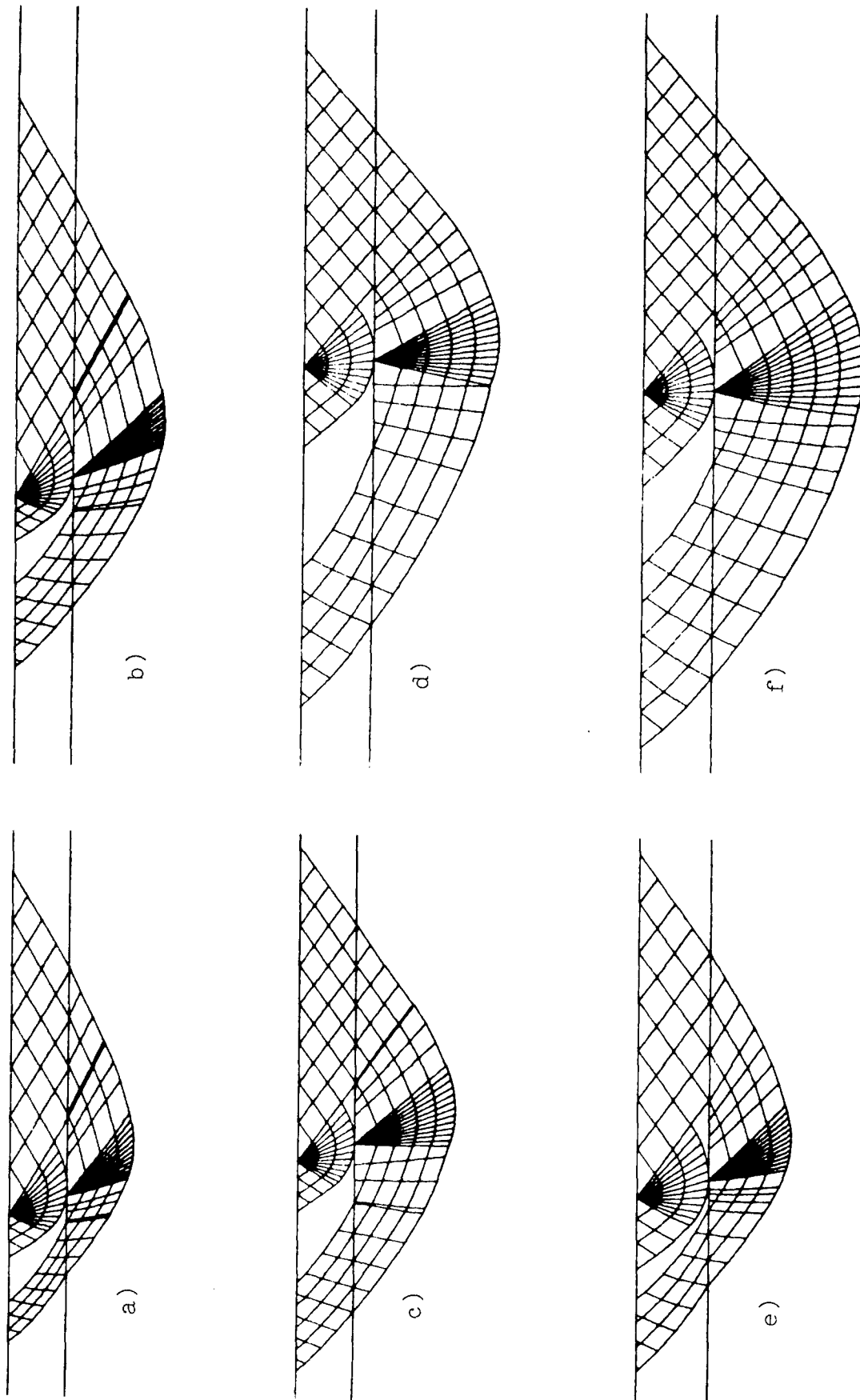


Fig. 15 Composite Slip Line Fields in Two-Layer Soils for Case 1

The construction of these composite slip line fields is not necessarily feasible for all combinations of the strength properties of the two layers. If the upper layer is very weak compared to the lower one, then the last portion of the composite field (eijk in Fig. 14) cannot be constructed. The reason for this is that the upper weak layer cannot transmit stresses high enough to result in a plastic state of failure in the lower, stronger layer. The composite field represents situations where both layers are in the plastic state of failure under the applied load.

The case when the relative strength of the two layers is such that the lower, stronger layer is not in the plastic state failure under the applied load requires another method of analysis of the stresses in the upper layer. Generally, the constraints on a stress field in the upper layer exercised by a rigid base are such that there is no complete solution for the bearing capacity problem (an incomplete solution would leave the stress states in certain areas unresolved). In such a case kinematically admissible slip line fields (upper bound solutions) may be used to estimate an upper bound for the bearing stresses. Such a field for the case of $\phi = 0$ is shown in Fig. 16. Implications of such a slip line field are discussed in connection with the problem of slipperiness in Section VI.

Typical bearing stresses calculated on the basis of composite slip line fields are shown in Figs. 17a through 17e for the following conditions:

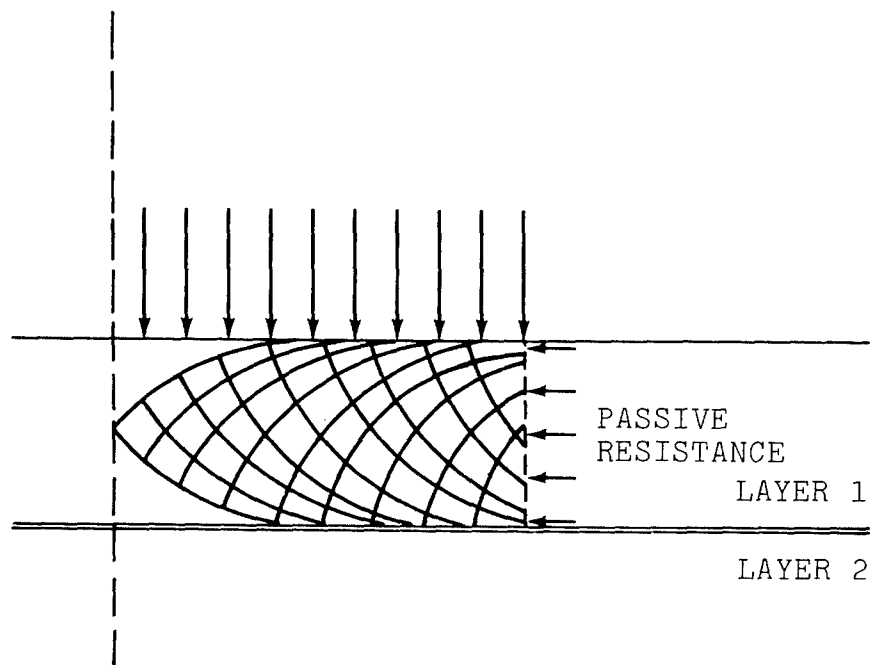


Fig. 16 Kinematic Slip Line Field for $\phi = 0$, Strong Bottom Layer

	Upper Layer			Lower Layer		
Fig.	c (lb/sq ft)	ϕ (deg)	γ (lb/cu ft)	c (lb/sq ft)	ϕ (deg)	γ (lb/cm ft)
17a	10	30	100	14.5	40	100
17b	80	20	100	100	25	100
17c	10	35	100	10	30	100
17d	0.2	30	100	0.24	35	100
17e	10	20	100	10	30	100

In these figures square or diamond symbols indicate the bearing stresses obtained from the composite slip line fields. Dashed lines show, for comparison, bearing stresses computed for

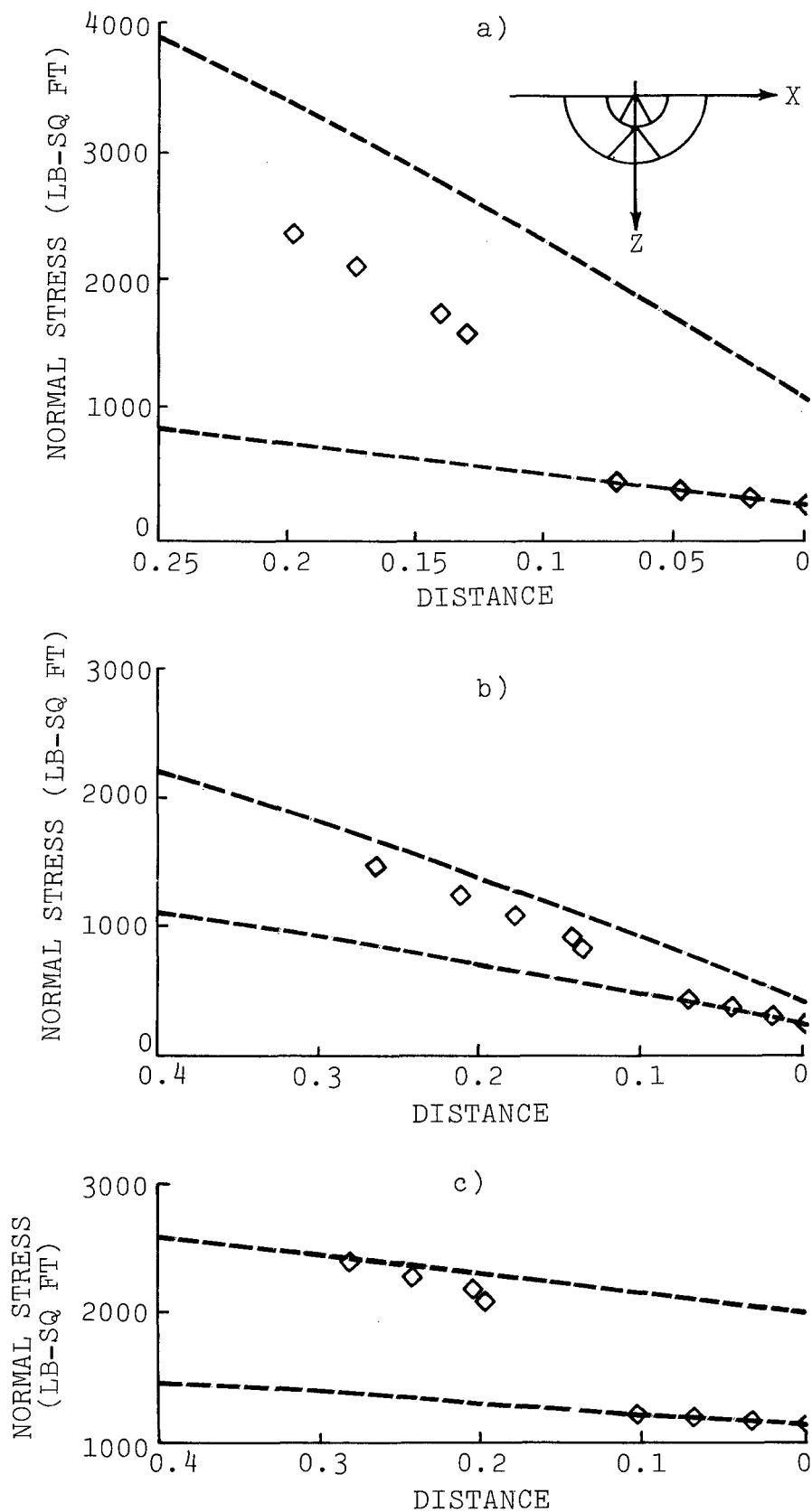


Fig. 17 Bearing Stresses Computed on the Basis of Composite Slip Line Field for Two-Layer Systems, Sheet 1 of 2

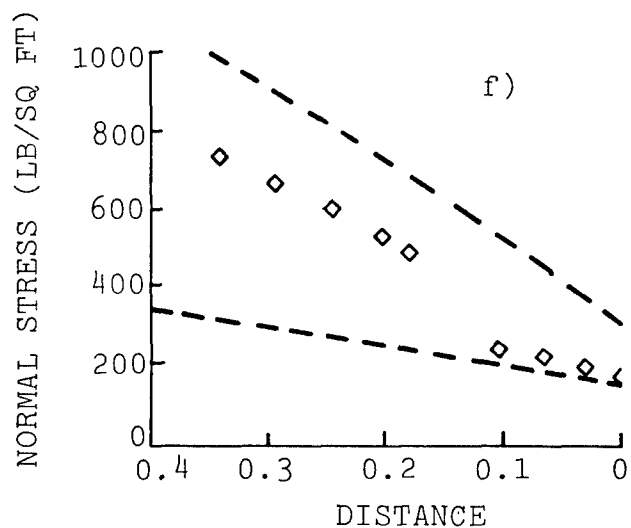
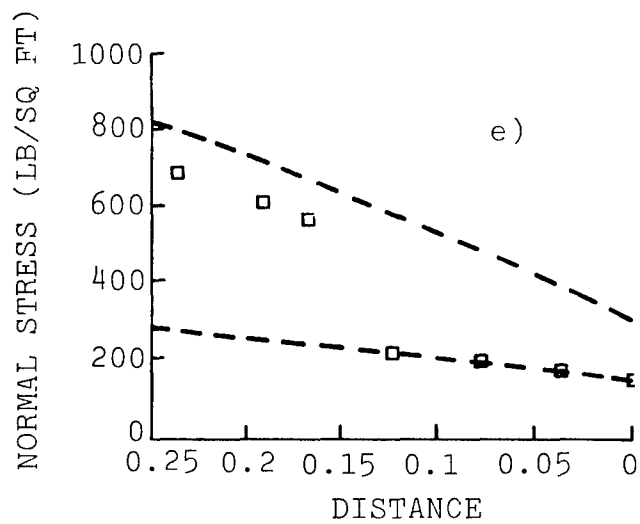
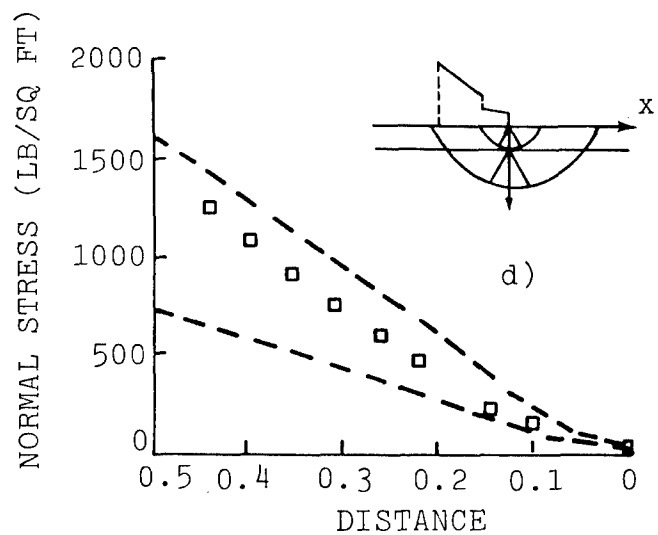


Fig. 17 Bearing Stresses Computed on the Basis of Composite Slip Line Fields for Two-Layer Systems, Sheet 2 of 2

hypothetical uniform soil conditions, assuming that the uniform soil has the strength properties of either the upper or the lower layer.

Figures 17a through 17e indicate that there is a jump in the normal stresses at the point where the lower layer starts to affect the slip line field in the upper layer. It is necessary to examine whether such a jump is permissible or not. One way to analyze this situation is to consider the normal stresses to the left of the jump as a surcharge and analyze whether a bearing failure due to the jump in the normal stresses is possible. In the cases shown the stress difference at the jump is not enough to cause such a failure, indicating that the upper layer is able to sustain the stress difference. Nevertheless, the slip line field associated with such stress differences is a different one from that of the composite field and one could speculate that the stress states in the soil would adjust to minimize the stress jump. Such an adjustment may take place by the development of opposing shear stresses beneath the footing. These shear stresses could increase the lower bearing stresses to the right of the jump and decrease the higher bearing stresses to the left. The effect of such shear stresses is illustrated in Fig. 17f, which shows the bearing stresses computed for an interface friction angle of $\delta = +5^\circ$ from the edge of the footing to the stress jump and for $\delta = -5^\circ$ past the jump. The figure shows that these opposite shear stresses tend to lessen the jump of the magnitude in the normal stresses and could conceivably completely eliminate the jump. The composite slip line field for these conditions is shown in Fig. 18.

This equalization of the normal stresses due to the development of shear stresses is very likely to occur in actuality. Unfortunately, there is neither a theoretical basis nor experimental

information that would allow to estimate these shear stresses or their distribution quantitatively. Because of this unknown factor, the bearing stresses computed without the consideration of shear stress developments are considered as limits only. Further theoretical and experimental research, including measurements of the shear stresses under various conditions, is needed for better understanding of the phenomena and the development of a theory to take these shear stresses properly into account.

SOLUTION METHOD FOR CASE 2

In Case 2 the upper layer is the stronger one. Consequently, the strength of the lower layer limits the shear stresses that are generated in an upper layer slip line field along the interface. The construction of an upper layer slip line field cannot be continued if at any location along the interface the following condition holds:

$$\tau \geq \tau_{\max} = (c_{\ell} + \sigma_n) \tan \varphi_{\ell} \quad (11)$$

If the limitation on the shear stresses is ignored and the construction of the slip line field continued, hypothetical shear stresses along the interface may be determined. These indicate that the shear stresses exceed the shear strength of the lower layer along some length of the interface. Thus, this length of the interface must be a slip line in a field in the lower layer, a basic feature of a failure mechanism that is intuitively recognized as correct. This feature has to be incorporated in a composite slip line field that comprises the plastic zones in both layers. Figure 19 shows schematically the various zones of such a composite slip line field.

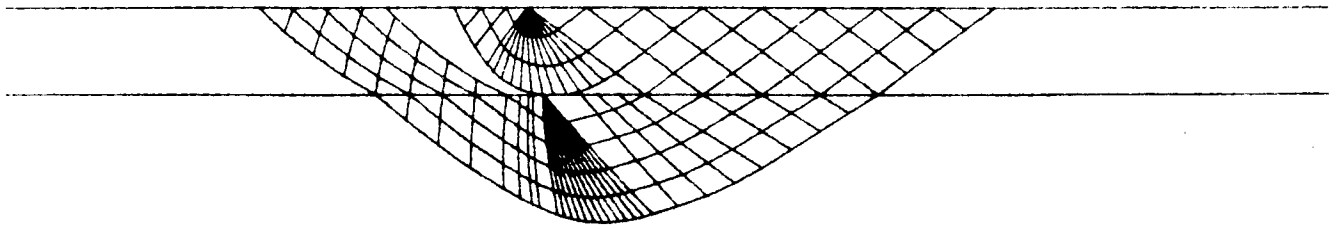
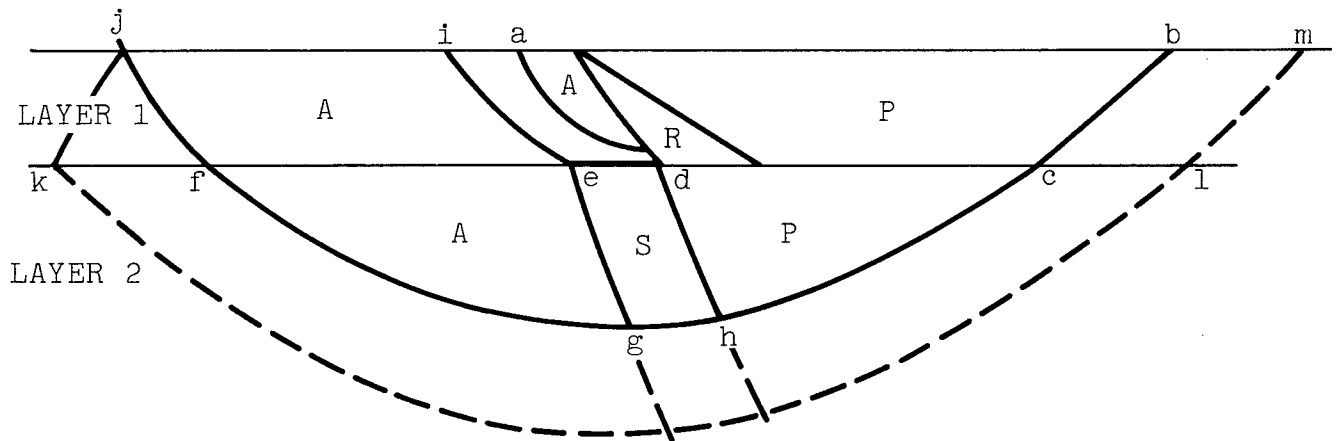


Fig. 18 Composite Slip Line Field With Base Friction



ZONES: A = ACTIVE, P = PASSIVE, R = RADIAL, S = SQUARE

Fig. 19 Scheme for Composition of Slip Line Fields for Case 2

In the upper layer, field (abed) is composed of the usual three zones (active, passive, and radial). The field is bounded at the left side by the "i" line, which at the crossover point at the interface produces shear stresses equal to the shear strength of the lower layer. In the lower layer, the field (cdefgh) is a special one, which, contrary to the usual fields, does not have a radial zone and a singular point. Instead, a "square" zone provides the transition from the active zone to the passive zone. The top line of this square zone is a "j" slip line. To construct this field, the δ values along (ef) are assumed to vary in a similar manner as they would in a field for uniform soil conditions. The field (efij) is similar to that in Case 1. Auxiliary points are needed (within the area indicated by dashed line) for the computation of this field.

The method of computation of each of these fields is essentially the same as in Case 1 except for the square field (degh), which requires special consideration.

The top j line in this field coincides with the interface where the interface friction angle δ equals φ and is constant along (de). The angle of inclination of the major principal stress (σ_1) is also constant and equals

$$\theta = \frac{1}{4} \pi - \frac{1}{2} \varphi \quad (12)$$

For the computation of this field, values of all four variables (x , z , σ , and θ) of the differential equations of plasticity must be given along (de). At point d the normal and shear stress transmitted from the upper layer are known, and the value of σ may be computed therefrom. The distance (de) is divided into equal intervals designating the end locations of i lines. For the determination of the σ values associated with these points, the following considerations apply.

The differential equation of plasticity that governs the σ variation is as follows (Ref. 3):

$$d\sigma + 2\sigma \tan \phi d\theta = \gamma(dz + \tan \phi dx) \quad (13)$$

As explained previously, along (de) $\theta = \text{constant}$, and for an interface parallel with the x-axis, $z = \text{constant}$. Consequently $d\theta = 0$ and $dz = 0$ and Eq. (13) is reduced to

$$d\sigma = \gamma \tan \phi dx \quad (14)$$

This allows the computation of σ along (de).

With the values of all four variables defined along (de), the slip line field in the square zone may be computed. The length of (de) is, however, not known and has to be estimated. The computation of the rest of the composite field is similar to that in Case 1.

Figures 20a and 20b show typical composite slip line fields for the following conditions:

Fig.	Upper Layer			Lower Layer		
	c (lb/sq ft)	ϕ (deg)	γ (lb/cu ft)	c (lb/sq ft)	ϕ (deg)	γ (lb/cu ft)
20a	10	35	100	10	30	100
20b	100	25	100	80	20	100

The computed bearing stresses for these cases are shown in Figs. 21a and 21b. The jump in the bearing stresses shown in these figures would be alleviated by opposite directed shear stresses developing at the base of the footing, just as it was shown for Case 1.

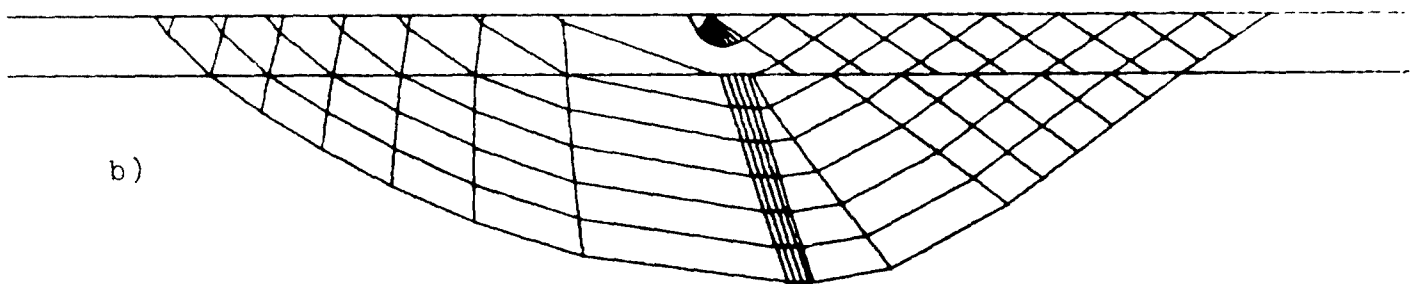
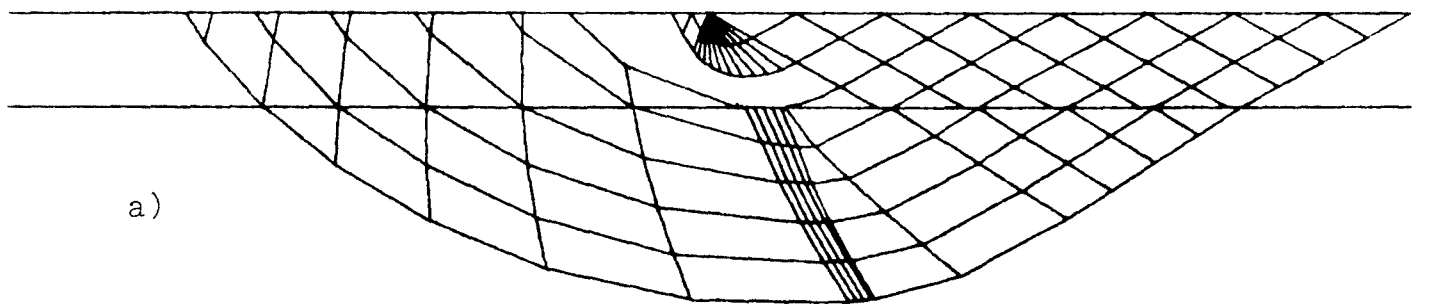


Fig. 20 Composite Slip Line Fields for Two-Layer Soils
in Case 2

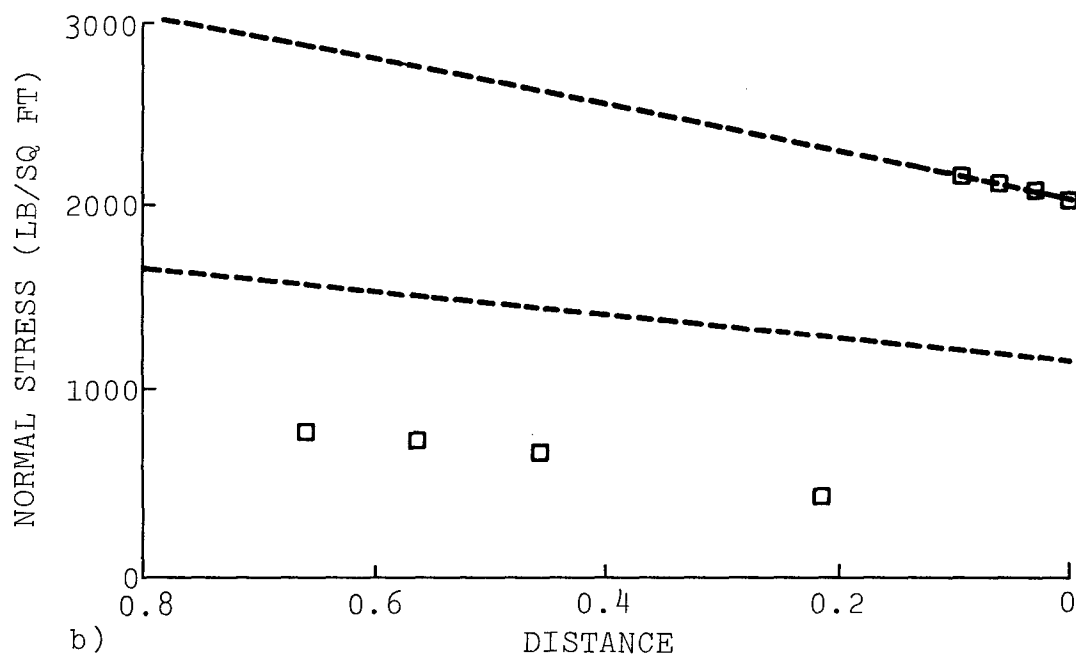
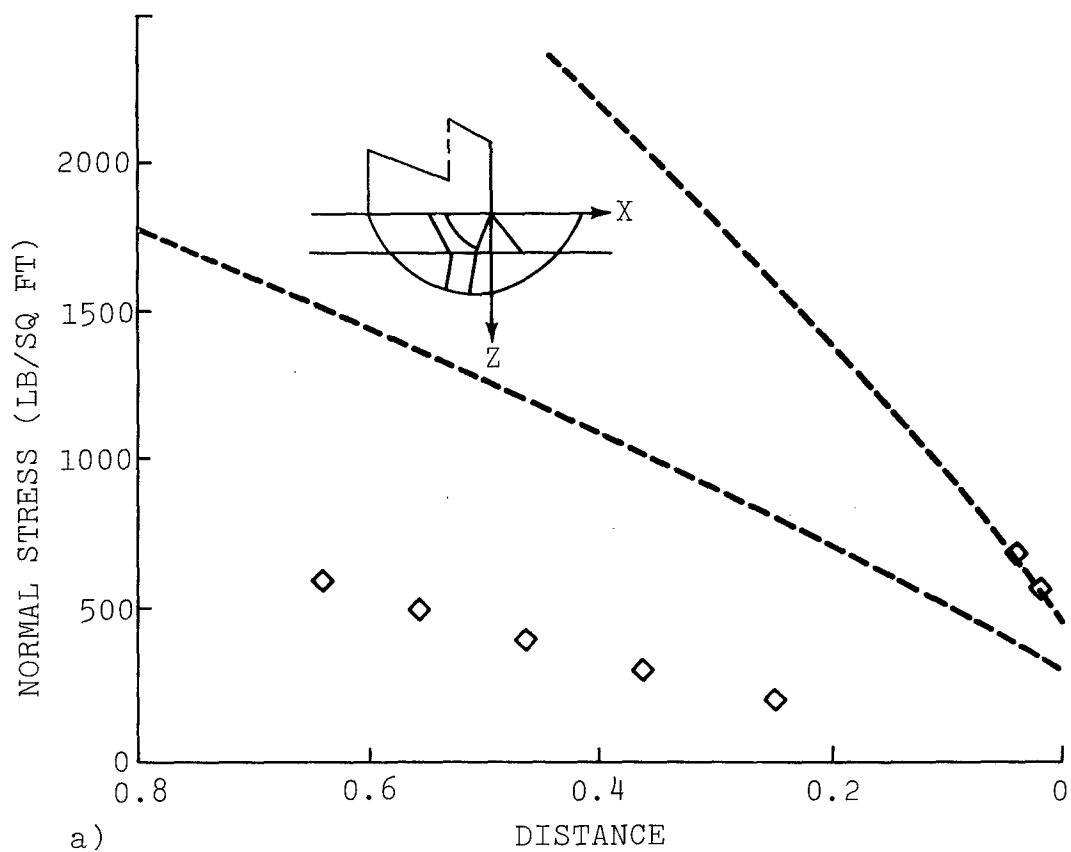


Fig. 21 Bearing Stresses Computed on the Basis of Composite Slip Line Fields, Case 2

EVALUATION OF THE EFFECTS OF DISCRETE LAYERING ON THE FAILURE NORMAL STRESSES

The distribution of bearing stresses obtained from the composite slip line fields for a two-layer system is characterized as consisting of two parts separated by a jump. The first part extends from the edge to a distance within which a slip line field for the upper layer can be constructed without interference from the lower layer. The second part extends from this point to the end of the composite slip line field. In the first part the bearing stresses are identical with that for uniform soil with the strength of the upper layer. In the second part the bearing stresses closely parallel that for uniform soil with the strength of the lower layer, but there is a shift in the magnitude of these stresses. For Case 1 this shift in the bearing stresses can be approximately determined, as shown in Fig. 22. The bearing stress at the point of interference ("A") (where the j slip line ending at this point touches the layer interface) equals that for the first layer, plus the difference between the edge bearing stress for upper layer strength and that for lower layer strength computed as if the soil were uniform.

In Case 2, the bearing stress at this point can be approximately calculated from the σ value at point "e" (Fig. 19), since the σ value is practically unchanged in the field (efij). The normal stresses at (\overline{ij}) are, however, affected by the δ value at (\overline{ij}) and can be calculated as follows:

$$q = \sigma \cos \delta (\cos \delta + \sqrt{\cos^2 \delta - \cos^2 \varphi}) - \psi \quad (15)$$

Thus, the bearing stresses in a two-layer system can be approximately calculated from the bearing stresses calculated for uniform soil with the strength of each of the layers and from the

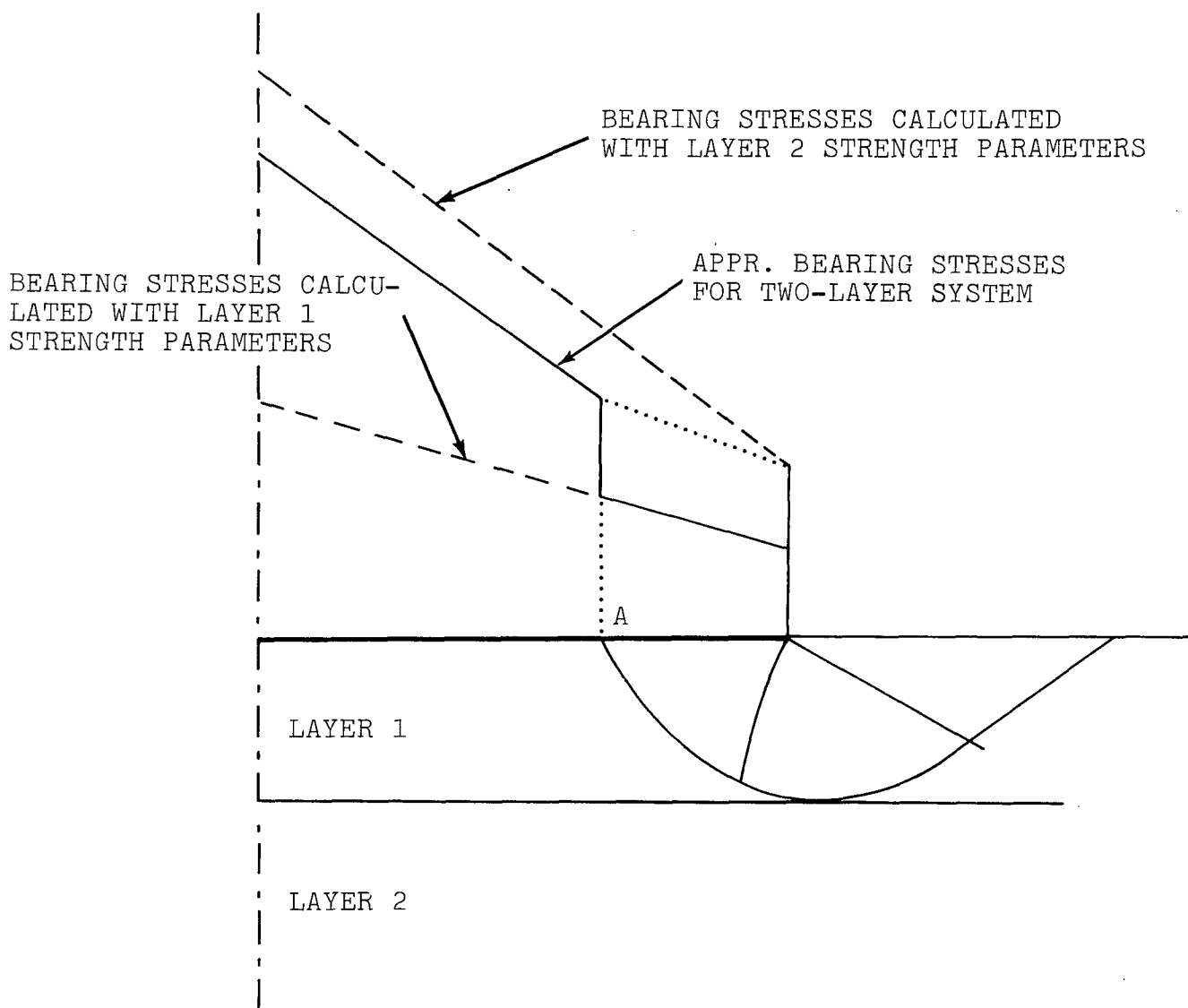


Fig. 22 Approximate Determination of Bearing Stresses
for Two-Layer Soils

magnitude of the shift at point A calculated by the methods discussed above. These bearing stresses, however, can be considered as limits only. The actual bearing stress depends on the development of oppositely directed shear stresses at the base. These shear stresses reduce the magnitude of the shift in the bearing stresses.

V. TIRE-SOIL MODEL FOR TWO-LAYER SOILS

The methods of constructing composite slip line fields (described in Section IV) for the bearing capacity problem in two-layer soils can be directly applied in the tire-soil model. However, the resulting discontinuous stress distribution would present serious problems in the various iteration schemes employed in that model. For example, the entry angle there is found by iteration on the condition that the normal stress at the angle of separation, q_m , computed from the slip line field, should match the limit pressure p_ℓ within an allowable tolerance limit. If the value of q_m falls within the magnitude of the jump of the normal stresses at the point of stress discontinuity, then this condition cannot be satisfied and some other means of finding the entry angle would have to be devised. At any rate, the more complex computations associated with the construction of composite slip line fields and the problems of iterations in the case of stress discontinuity would require a very elaborate computation scheme accompanied by a great increase in computing time.

The methods for estimating the interface normal stresses in a two-layer system on the basis of normal stresses computed for uniform soil conditions (described in Section IV) offer a more practical solution for the tire-soil interaction problem in two-layer soils. Instead of using composite slip line fields for the computation of interface stresses, the approximate method is applied for the estimation of these stresses. Accordingly, the interface stresses are computed first for the strength parameters of the upper layer. The locations where the lower layer causes a jump in the normal stresses are determined, and the approximate value of the jump is computed. In the second step the interface stresses are computed

with the strength parameters of the lower layer assuming the same centerline geometry as in the first step. The interface stress distribution for the two-layer soil is then determined by shifting the normal stresses computed with the strength parameters of the lower layer by the appropriate amount within the locations of the stress jumps determined earlier. The load, drawbar pull, and torque are determined for this interface stress distribution. The procedure is repeated, if necessary, for a new centerline geometry until the computed load is within the tolerance limits for the input load. The computation scheme is shown diagrammatically in Fig. 23. A more detailed flow diagram is given in the appendix.

An optional provision in the scheme allows the consideration of the equalization effect of opposite directed shear stresses (discussed in Section IV). A linearly varying value of the interface friction angle is superimposed on the uniform δ normally assumed in tire-soil interaction.

A typical interface normal stress distribution computed by this method for two-layer soils is shown in Fig. 24. The following limitations apply to the use of the model:

- The model applies only to cases where the deformed centerline of the tire is completely in the upper layer
- The strength conditions are such that both the cohesion and the friction angle of the upper layer is either higher or lower than that of the lower layer (Case 1 and Case 2)

The pull performances estimated by this tire-layered soil model were compared with experiments performed at WES (Ref. 13). Because of the difficulties involved with the preparation of layered soil

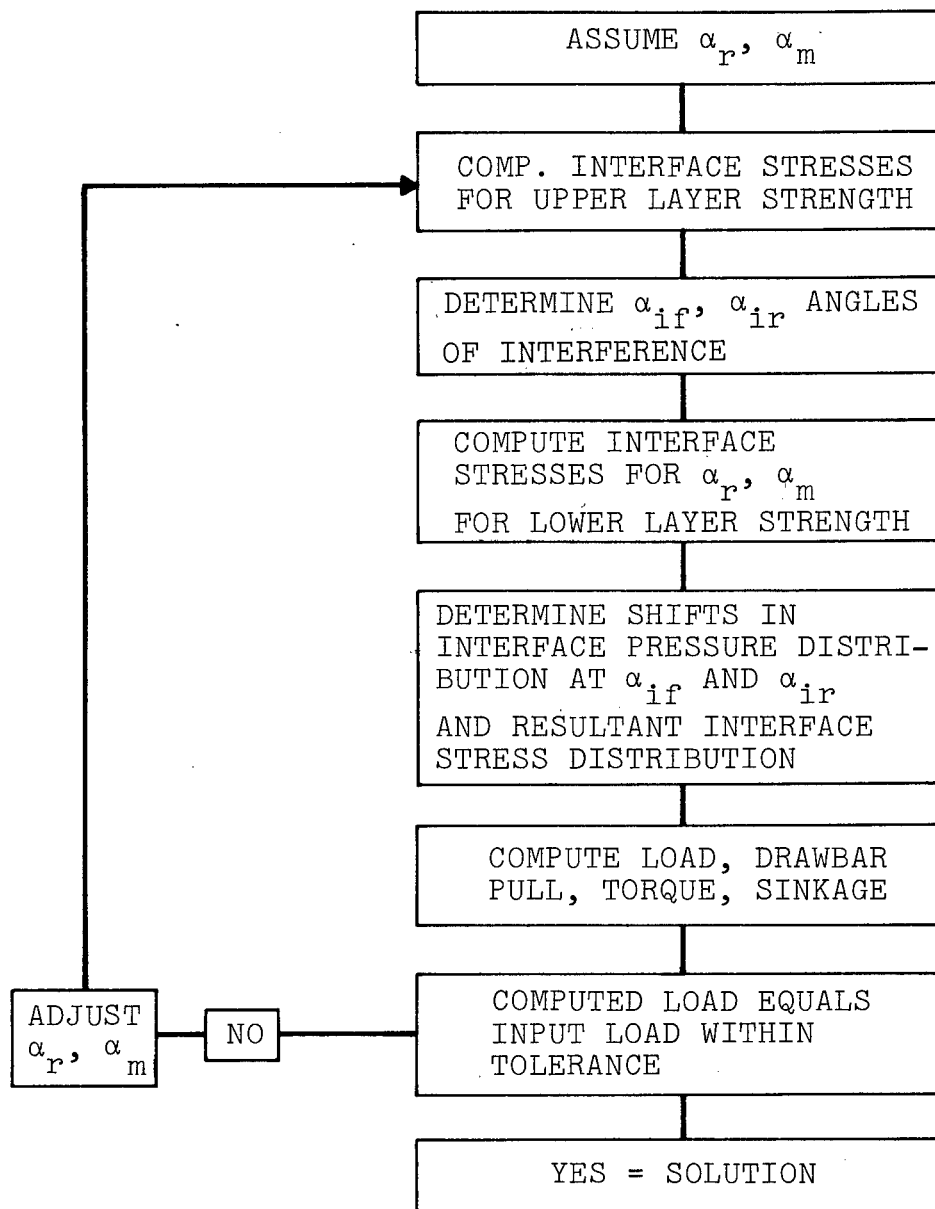


Fig. 23 Scheme of Computations for the Tire-Soil Model for Two-Layer Soils

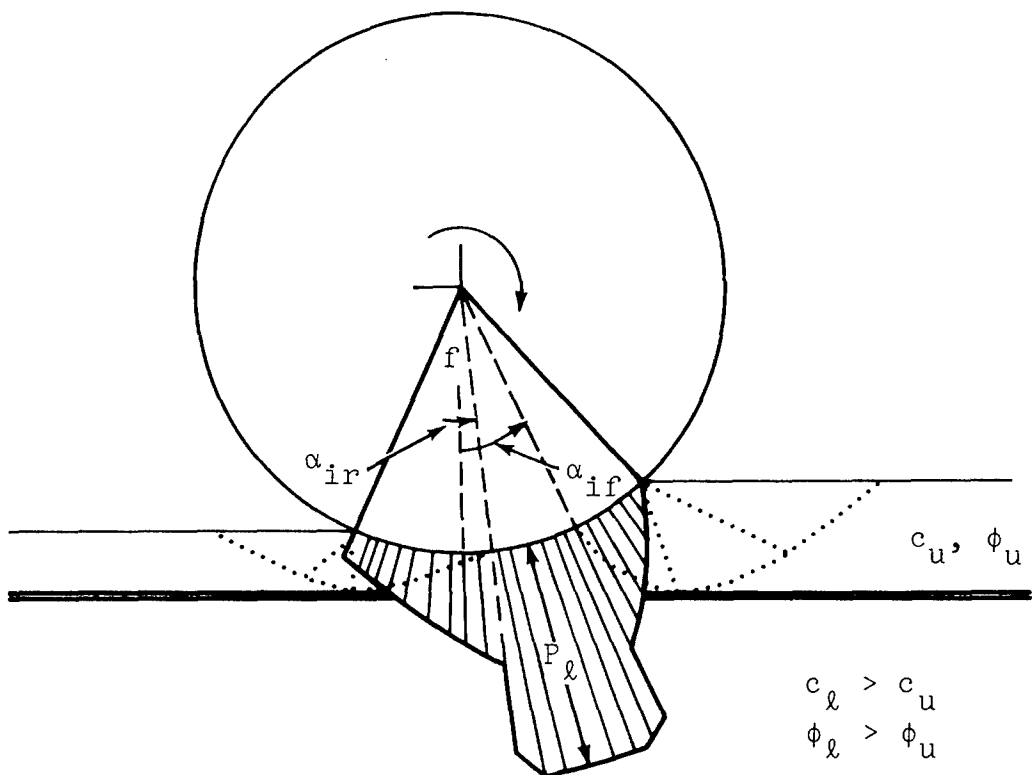


Fig. 24 Interface Normal Stress Distribution in the Case of Two-Layer Soils

beds where the strength of each layer is controlled, the experiments at WES were performed in a small soil bin with 2.50-4 tires. Even though great care was taken to prepare each layer with the specified strength, small deviations in the strength properties inevitably occurred, and all test data had to be normalized to allow a meaningful evaluation of the effects of layering. For that reason, the normalized test data, instead of individual test data, were used in the comparison with performance predictions by the model.

In the experiments, the differences in pull performances due to the lower layer were found to be relatively small. To predict such small differences, it was necessary to duplicate the pull performance of so-called "base line" tests closely. In the development of the tire-soil model (Ref. 7), various relationships that define the model parameters (limit pressure, deflection coefficients, slip coefficients) were developed from the analysis of tire performance tests conducted on tires 4.00-7 and larger. For the small 2.50-4 tire used in the experiments in two-layer soils, the model parameters estimated on the basis of these relationships yielded predictions generally acceptable, but not accurate enough for use in analyzing small differences in pull performances observed in the small scale mobility tests on layered soils. Thus it was desirable to make adjustments in these parameters so that the base line performances could be more closely duplicated. An uncertainty arose, however, with the shear-slip coefficients in the equation

$$\begin{aligned}\tan \delta &= \tan \delta_{\max} \left(1 - e^{-(j+j_o)/K} \right) \\ \tau &= \tau_{\max} \left(1 - e^{-(j+j_o)/K} \right)\end{aligned}\tag{16}$$

Since various combinations of the constants j_0 and K can yield the same δ value, it was not possible to establish firm values for these constants from the small scale mobility tests that were performed only for one value of the slip j , at approximately $j = 20$ percent. To avoid the problems associated with establishing the values of j_0 and K for the small scale mobility tests, it was found sufficient for the comparative analysis of these tests to establish the degree of shear mobilization defined as:

$$u = \frac{\tau}{\tau_{\max}} = \frac{\tan \delta}{\tan \delta_{\max}} \quad (17)$$

The degree of shear mobilization, as defined by Eq. (17), was established for the base line tests and retained in the performance simulation of two-layer conditions.

In the tests, the strength properties of the upper and lower layer were determined by cone penetration tests; the values of cone indices are shown in the respective columns. In the tire-layered soil model the strength properties of each layer are characterized by its Coulomb strength parameters. For the purpose of comparing the measured and predicted tire performances the cone index values have been converted to Coulomb strength parameters by the relationships established for the Buckshot clay in Ref. 7. These relationships are as follows:

$$\begin{aligned} c(\text{lb/sq ft}) &= 11.5 \text{ CI} \\ \phi(\text{deg}) &= 0.25 \text{ CI} \end{aligned} \quad (18)$$

The results of the small scale mobility tests performed in Buckshot clay on various combinations of upper and lower layer strength are summarized in Tables 1 and 2 together with the results of simulation by the tire-layered soil model.

TABLE 1 TIRE PERFORMANCE IN TWO-LAYER SOILS — SOFT OVER HARD LAYER

Tire, 2.50 x 4.00; Soil, Buckshot Clay

Group	Test No.	Normalized Test Conditions							Computed Tire Performance			
		Cone Index (psi)		Load (lb)	Tire		Thickness of Top Layer (ft)	Pull Coeff	Defl Coeff ϵ	Limit Press P_{ℓ} (psi)	Average Shear Mob (%)	Pull Coeff
		Upper Layer	Lower Layer		Defl (%)	Infl Press (psi)						
A	1	24	84	50	15	14.9	Inf	0.18	0.95	13.5	87	0.18
	2		83.8				0.328	0.21				
	3		84.4				0.197	0.23				
	4		65.8				0.131	0.24				
B	5	24	85	50	25	5.8	Inf	0.31	0.9	7.0	95	0.31
	6		85				0.197	0.33				
	7		84.2				0.131	0.35				
	8		81.2				0.098	0.36				
C	9	25	84	50	35	3.3	Inf	0.32	0.85	5.8	80	0.32
	10		84.2				0.197	0.32				0.32
	11		91.9				0.131	0.35				0.33
D	12	24	84	75	35	5.8	Inf	0.17	0.85	7.70	83	0.17
	13		83.8				0.328	0.19				0.17
	14		91.5				0.197	0.23				0.17
	15		91.9				0.131	0.24				0.21
	16		67.4				0.0625	0.24				0.23

TABLE 2 TIRE PERFORMANCE IN TWO-LAYER SOILS — HARD OVER HARD LAYER

Tire, 2.50 x 4.00; Soil, Buckshot Clay

Group	Test No.	Normalized Test Conditions						Computed Tire Performance				
		Cone Index (psi)		Load (lb)	Tire		Thickness of Top Layer (ft)	Pull Coeff	Defl Coeff ϵ	Limit Press P_{ℓ} (psi)	Average Shear Mob (%)	Pull Coeff
		Upper Layer	Lower Layer		Defl (%)	Infl Press (psi)						
A	1	84.8	28.2	25	15	4.9	Inf	1.15	0.95	8.0	45	1.23
	2	↓	↓	↓	↓	↓	0.0625	1.03	↓	↓	↓	1.00
B	3	79	28.7	75	15	25.2	Inf	0.65	0.95	20	48	0.64
	4	↓	28.4	↓	↓	↓	0.131	0.60	↓	↓	↓	0.63
	5	↓	28.7	↓	↓	↓	0.0625	0.56	↓	↓	↓	0.59
C	6	84	28.1	75	35	5.80	Inf	0.89	0.85	7.7	22	0.92
	7	↓	28.1	↓	↓	↓	0.131	0.89	↓	↓	↓	0.52
	8	↓	29.7	↓	↓	↓	0.0328	0.88	↓	↓	↓	0.28
D	9	74	25.6	150	35	17.5	Inf	0.44	0.85	17	40	0.50
	10	↓	25.6	↓	↓	↓	0.131	0.50	↓	↓	↓	0.42
	11	↓	24.7	↓	↓	↓	0.0625	0.44	↓	↓	↓	0.24

Table 1 shows the test results for Case 1, soft over hard layer. The base line test results are shown as for infinite top layer thickness. The gain in pull performances due to a stronger lower layer was minimal in all these tests. The simulation by the tire-layered soil showed no increase in the pull performance in Group A (tests 1 through 4) and Group B (tests 5 through 8). The reason for the stronger lower layer having no influence on the pull coefficient in these simulations is that neither the forward nor the rear slip line field computed in the model intersected the layer interface in these cases. The question arises whether the actual failure zones, contrary to the simulation, intersected the layer interface, or whether the increase in pull coefficient was due to some interaction in that portion of the upper layer where the limit pressure governs the stresses and the soil is not in failure conditions. An explanation for the tire-layered soil model not showing the increase in pull coefficient obtained in the tests is that the actual friction angle might have been higher than that estimated by Eqs. (18). While the over-all performance is not sensitive to small deviations in the friction angle, the depth of the slip line field changes appreciably with the friction angle and could thereby affect the simulation of the interaction in two-layer soils. These questions can only be clarified by an experimental program conducted for this purpose. At any rate, a modification of the model on account of the marginal increases in the pull coefficients in these tests does not appear justified. The simulation of the pull performance in Group C (tests 9 through 11) and Group D (tests 12 through 16) is satisfactory, even though the simulation was not sensitive in the case of the largest top layer thickness — probably for the same reasons as cited for Groups A and B.

Table 2 shows the test results for Case 2, hard over soft layer. In this case the tire-layered soil model tended to over-predict the decrease of pull coefficient due to the lower strength of the bottom layer. A look at the test results, for example in Group D, casts doubts whether the tests or the simulation gives the right answer. Attention may be called to the significance of shear stresses at the layer interface. The studies performed in connection with the development of methods for constructing composite slip line fields showed that shear stresses at the layer interface strongly influence the bearing stresses, especially in Case 2. Such shear stresses are generated by the stress field in the upper layer, but they may also be generated and "locked in" in the process of the preparation of layered beds. Locked in shear stresses may be an explanation for the insensitiveness of the tests to the weak bottom layer. An experimental program with normal and shear stress measurements at both the tire-soil and layer interfaces could clarify the problems.

VI. THE TIRE-LAYERED SOIL MODEL AND THE PROBLEM OF SLIPPERINESS

In connection with the development of methods for the construction of composite slip line fields (discussed in Section IV), it was pointed out that the construction of such slip line fields may not be feasible if the strength of the upper layer is low compared to that of the lower layer. Although slippery conditions have not been defined in terms of strength, it is reasonable to assume that they can be identified with the condition when the construction of composite slip line fields, as proposed in Section IV, is not feasible. At this point it is useful to recall that these slip line fields represent the solution of the differential equations of plasticity for soils. Along the slip lines, the Mohr-Coulomb yield criterion as well as the differential equations of equilibrium are satisfied. In plasticity theory such solutions are labeled as "lower bound" solutions that become true solutions if the slip lines are compatible with certain kinematic conditions.

When stress solutions do not exist for the given boundary conditions, as under slippery conditions, the upper bound theorem of the theory of plasticity may be used for the estimation of failure stresses. According to this theorem, slip line fields are constructed on the basis of kinematics, and the stresses are integrated along the given slip lines. Such procedure yields a so-called upper bound solution. Figure 16 shows such a kinematic slip line field for the simple bearing capacity case. If the friction angle of the slippery layer is assumed as zero, then the bearing stress can be calculated from the following formula (Ref. 11):

$$p = c \left(\frac{1}{2} \pi + \frac{B}{2h} \right) + m2c \quad (19)$$

where

B = width of footing

h = thickness of upper layer

m = factor $0 \leq m \leq 1$

An inspection of Eq. (19) indicates that with decreasing thickness of the upper layer the interface pressure p tends to go to infinity. In the case of slipperiness, the slushy upper layer may be squeezed out from beneath the tread to some extent, but never completely, since that would require an infinitely large pressure. According to the concept of tire-soil interaction there is a limit to the pressures that soil can develop under the tire load. One may assume that under slippery conditions the upper slushy layer would be squeezed out from underneath the tire tread as long as the pressure is smaller than that indicated by Eq. (19). The pressure will rise due to the gradual decreasing of the thickness of the upper layer as the slushy material is squeezed out, but will stabilize at the limit pressure. Thus, under slippery conditions the interface normal stress may be assumed as p_ℓ , and the interface itself flat, paralleling the lower hard layer. The pull coefficient may be approximately computed as:

$$u = \frac{s}{p_\ell} \quad (20)$$

where s is the strength of the slush. The pull coefficient predicted by the tire-layered soil model for slippery conditions will be approximately that computed from Eq. (20).

Equation (20) denotes the pull coefficient for slippery conditions when there is no traction component from the lower hard

layer. The lower hard layer can be engaged in traction only if p_l is high enough to cause failure and penetration in the lower hard layer. This explains why tires with high inflation pressures work better under slippery conditions than low inflation pressure tires. Slippery conditions may occur for a wide range of bottom layer strength; therefore, the use of higher inflation pressure would be advantageous only for a specific range of bottom layer strength.

VII. FIELD DETERMINATION OF PROPERTIES OF LAYERED SOILS

To account for layered soil conditions in the evaluation of mobility over a terrain that exhibits such conditions, it is necessary to determine in the field the variation of the strength properties of soil with depth. The suitability of the present field techniques for this purpose has been reviewed and the possibilities of improvements investigated. The results of this review are summarized in this section.

PLATE SINKAGE TEST

Although the plate sinkage tests in their present form are used primarily for the establishment of pressure-sinkage curves, a sharp break in these curves indicates the point at which plastic yielding starts in the soil. The total load on the plate at this point may be computed from the failure stresses that produce plastic zones in the soil. The plate sinkage test differs from the simple bearing capacity case analyzed in Section IV in that it is an axially symmetric case. The effects of layering in the two dimensional and axially symmetric case are essentially the same. In a plate sinkage test in a two-layer system the bottom layer affects the bearing stresses as soon as the plastic zone intersects the lower layer. Thus there is no distinct change in the pressure-sinkage curve that would be indicative of the strength properties of the lower layer, but rather a continuous transition in the pressure that would be exceedingly difficult to evaluate. Thus, in principle, the plate sinkage test is unsuitable for the evaluation of the strength properties of discrete individual layers.

CONE PENETRATION TESTS

Cone penetration tests are intended to measure strength properties of soil for mobility evaluation. In layered soils, not only the plastic zones created by the cone but the cone itself intersects the layer interface, thereby making the distinction of strength properties of individual layers impractical. A few cone penetration tests were conducted in the laboratory in layered soils to demonstrate the problem and see whether the use of a right angle, instead of a 30° cone, would alleviate the situation. Typical results of these tests are shown in Figs. 25, 26, and 27. Figure 25 shows the variation of cone penetration with depths for a 30° and a 90° cone in two layers of Buckshot clay. With the 30° cone the reading for the 1-in. (2.5 cm) thick top layer ($CI = 11$) is completely obscured by the presence of the stronger bottom layer. This is understandable since the more than 3 cm long cone penetrates the bottom layer even when its base is at the surface. The 90° cone showed momentarily a reading corresponding to the strength of the upper layer. Nevertheless, from the signature itself one could not evaluate the strength of the upper layer even if the thickness of the layer were known. Figure 26 shows the variation of the cone penetration resistance in a Buckshot clay with alternating layers of different strengths. The changes in cone penetration resistance indicate that layering is present, but the signature in itself is insufficient to establish depths of layer interfaces or the strength properties of individual layers.

Figure 27 shows the results of cone penetration tests in a two-layer sand. The change in the gradient of the resistance appears to occur at the layer interface. Another change in the gradient, at point "A", may be the result of the slip zones reaching the upper loose layer, as shown by dashed lines in the figure.

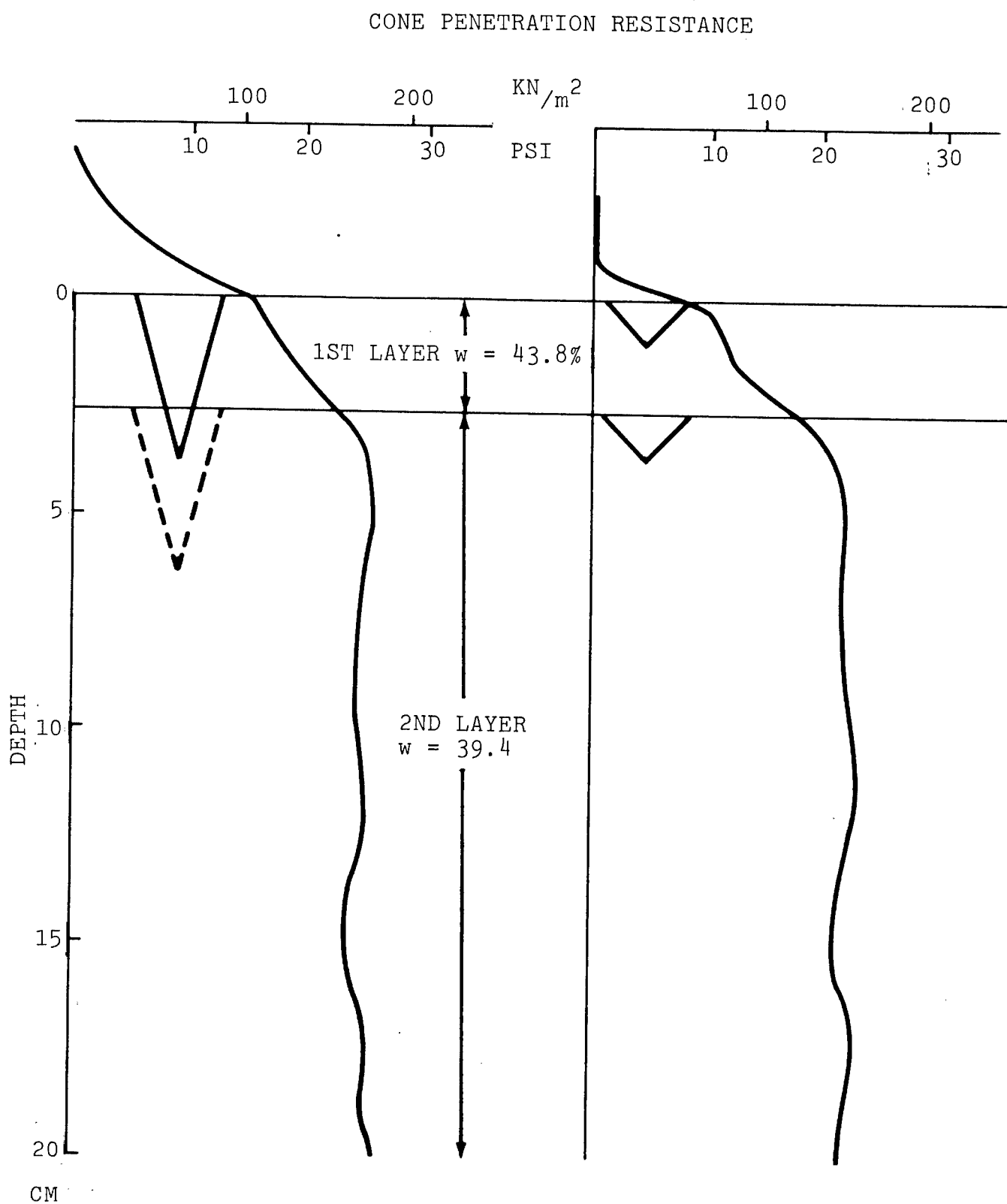


Fig. 25 Results of Cone Penetration Tests in Two-Layer Clay Soil

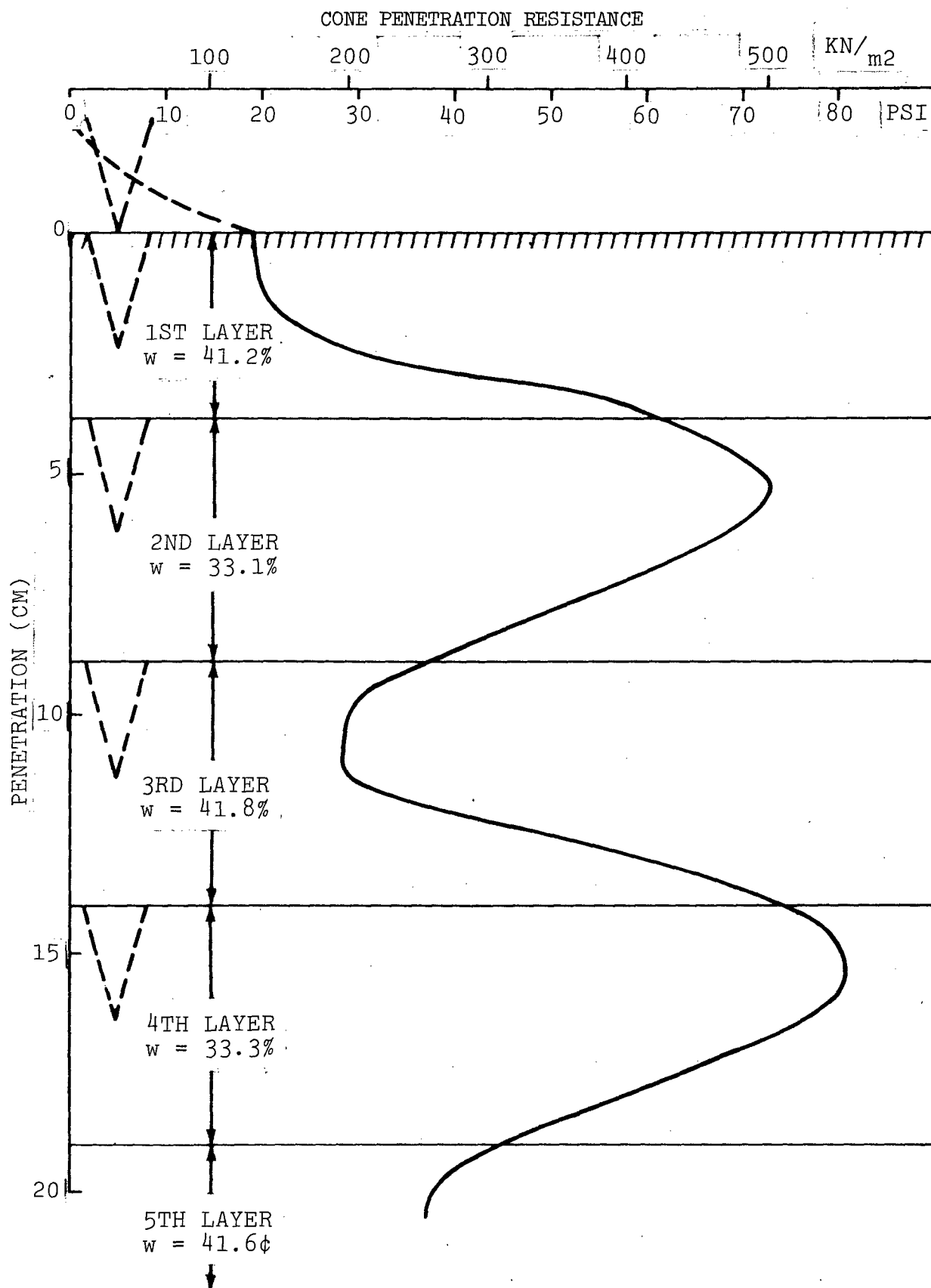


Fig. 26 Results of Cone Penetration Tests in Multilayered Clay Soils

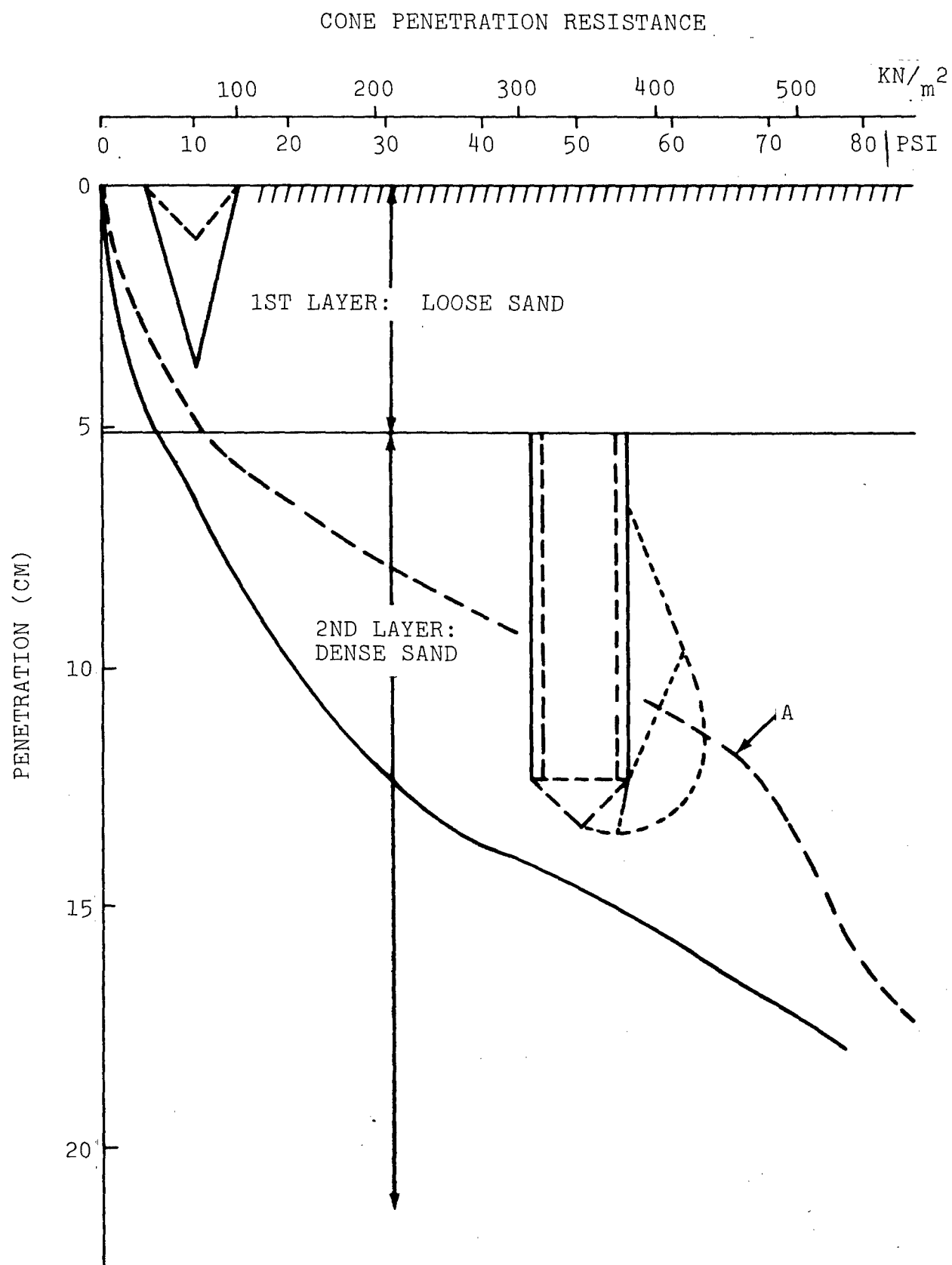


Fig. 27 Results of Cone Penetration Tests in Two-Layer Sand

RING SHEAR TESTS

From the preceding discussions it is obvious that field techniques that engage both layers either directly or indirectly through the creation of plastic zones at some distance from the layer interface are unsuitable for the measurement of strength properties of individual layers. The ring shear test that has been used in mobility technology for some time engages only a horizon of the soil fully; it therefore appears better suited for determining strengths of individual layers than do the other techniques.

The drawback of the ring shear test technique is that the peak shear stress measured at an applied normal stress equals the shear strength of the material only if the base of the annulus is the failure plane. Observations and theoretical considerations indicate that in many instances this condition is not met. The failure plane in soils is perpendicular to the plane of the major and minor principal stress. If the lateral stresses in the soil are low, then the minor principal stress is in the lateral direction and the major principal stress is in the plane tangent to the rotation and inclined to the vertical due to the application of shear stresses. The failure plane is an oblique one, perpendicular to the plane that includes the minor principal stress inclined to the vertical. The development of such an oblique failure plane manifests itself by an excessive sinkage or "digging in" of the ring shear apparatus, since plastic flow from along the inclined failure plane moves soil out from underneath the annulus. A detailed discussion of this problem is given by Liston in Refs. 14 and 15. He proposes an evaluation procedure that takes failure along the oblique plane into account.

The development of an oblique failure plane nullifies the advantage of the ring shear test in that it engages only a horizon

of the soil. Thus, for the purpose of measuring the shear strengths of individual layers, failure along oblique planes would have to be prevented rather than the evaluation procedures modified for this condition. Theoretical considerations indicate that failure along oblique planes could be prevented by placing a surcharge (metal plates) around the shear ring and possibly in the open area in the center. Preliminary calculations indicate that a surcharge equal to the vertical stresses applied to the shear ring would be sufficient for this purpose. The schematic arrangement of a ring shear test with surcharge is shown in Fig. 28.

The application of surcharge would prevent any appreciable sinking of the ring shear device during a test. To reach deeper horizons, a cylindrical bottom split scooper would have to be attached to the device to remove the soil to the desired depth. The ring shear test would then be carried out at this depth to determine the strength properties of soil at this horizon.

Ring shear devices, portable and track mounted, are already available. The concept of surcharge application could be implemented with minor modifications to the existing equipment. It is strongly recommended that a program be initiated for detailed development of the modified techniques of the application of ring shear devices and the performance of laboratory tests for the validation of the concept. The development of this improved technique would solve not only the problem of determining the strength properties of layered soils but could also be used to determine strength properties of cohesive-frictioned soils and, therefore, fill a gap in the area of applicability of cone penetration tests.

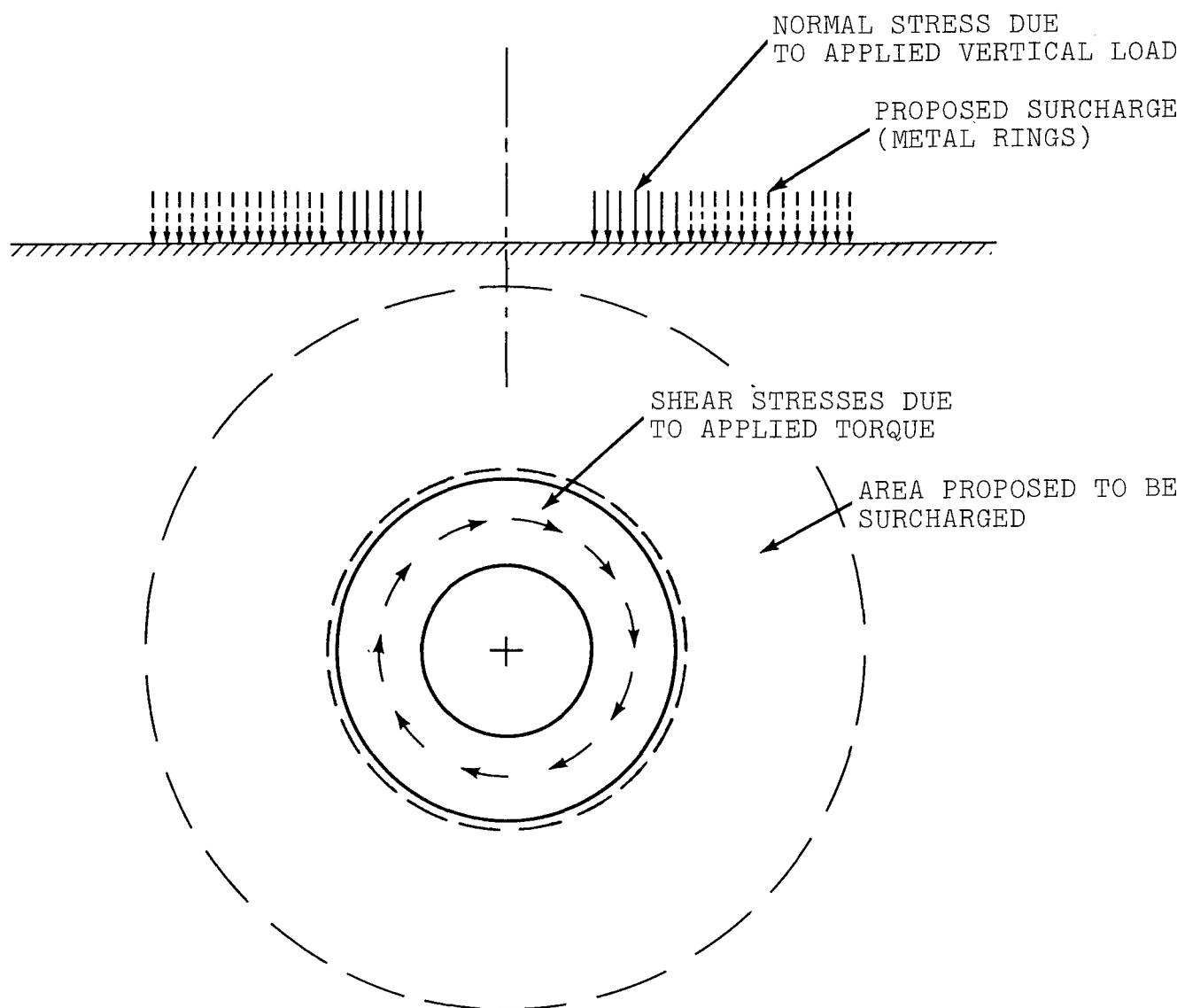


Fig. 28 Schematic Arrangement of Ring Shear Test with Surcharge

VIII. CONCLUSIONS AND RECOMMENDATIONS

The variation of strength properties of soil with depth, frequently occurring in the field, and its effect on tire-soil interaction have been investigated theoretically. One method for the consideration of a continuous variation of strength and another for the consideration of discrete layering have been developed and applied in an expanded tire-soil model.

In the tire-soil model expanded for continuously varying soil strength a linear variation of soil strength with depth is considered. Analyses performed by this model indicate that the pull performance depends more on the strength of the surface than at depth as long as the rate of decrease of soil strength is less than a certain limit. At this limit a no go situation occurs quite abruptly. It is recommended that the "constant strength" concept requiring an averaging of the soil properties within a certain depth be changed to a "linearly varying strength" concept and that a constant plus a rate of variation be used for the characterization of soils in conjunction with the variable strength tire-soil model. The accuracy of performance prediction could be significantly improved thereby with little additional effort in field data processing.

The consideration of discrete layer interfaces in plasticity theory solutions required both extensive theoretical research and the development of new numerical techniques. These applied to the simple bearing capacity case resulted in a new method of constructing composite slip line fields and obtaining bearing stresses for two-layer soils. An approximate method for estimating these stresses was applied in the tire-soil model for the consideration of two-layer soils. The simulation by the model of small scale tire tests

performed in two-layer soils was acceptable, but some assumptions in this two-layer model require further experimental research. It is recommended that an experimental program be initiated in which both tire-soil and layer interface stresses are measured. Such a program would be not only useful for the validation of the concepts adopted in the tire-layered soils model but would also contribute to the understanding of the basic phenomena in tire-soil interaction in layered soils.

The techniques employed for the determination of soil properties in the field were examined with respect to their suitability for distinguishing the strength of individual layers. Neither the plate sinkage nor the cone penetration tests are suitable for this purpose. The ring shear test is best suited, but the application of a surcharge is required to prevent lateral failure. It is strongly recommended that the existing ring shear devices be adapted for the accommodation of surcharge plates and the procedure be validated in an experimental program. The proposed procedure is expected to be applicable not only in layered soil conditions but also for determining strength properties of frictional-cohesive soils for which present procedures are inapplicable.

IX. REFERENCES

1. Froehlich, O. K., Druckverteilung im Baugrunde, Springer, 1934.
2. Burmister, D. M., "The General Theory of Stresses and Displacements in Layered Systems," Journal of Applied Physics, Vol. 16, February 1945.
3. Sokolovskii, V. V., Statics of Granular Media, Pergamon Press, 1965.
4. Karafiath, L. L., Nowatzki, E. A., Ehrlich, I. R., and Capin, J., "An Application of Plasticity Theory to the Solution of the Rigid Wheel-Soil Interaction Problem," U.S. Army Tank Automotive Command Mobility Systems Laboratory Technical Report No. 11758(LL141), March 1973.
5. Karafiath, L. L. and Sobierajski, F. S., "Effect of Speed on Tire-Soil Interaction and Development of Towed Pneumatic Tire-Soil Model," U.S. Army Laboratory Technical Report No. 11997 (LL151), October 1974.
6. Nowatzki, E. A. and Karafiath, L. L., "General Field Conditions in a Plasticity Analysis of Soil-Wheel Interaction," Journal of Terramechanics, Vol. 11, No. 1, 1974.
7. Karafiath, L. L., "Development of Mathematical Model for Pneumatic Tire-Soil Interaction," U.S. Army Tank Automotive Command Mobility Systems Laboratory Tech. Report No. 11900(LL147), July 1974.
8. Tcheng, Y., "Pouvoir Portant d'un Solide Composé de Deux Couches Plastiques Differentes," Cahiers de Recherche, Ass. Francaise de Recherchers et d'Essais sur les Materiaux et les Constructions, Cahier No. 5, 1958.

9. Brown, J. D. and Meyerhof, G. G., "Experimental Study of Bearing Capacity in Layered Clays," Proc. 7th Int. Conf. on SMFE, Mexico City, Vol. 2, 1969.
10. Salencon, J., "Bearing Capacity of a Footing on a $\phi = 0$ Soil with Linearly Varying Strength," Geotechnique, 1974.
11. Yamaguchi and Terashi, "Ultimate Bearing Capacity of the Multi-layered Ground," Proceedings of the 4th Asian Regional Conference on Soil Mech. and Gound. Eng., Bangkok, Thailand, Vol. 1, 1971.
12. Harr, M. E., Foundations of Theoretical Soil Mechanics, McGraw-Hill Book Company, 1966.
13. Swanson, G. D. and Patin, T. R., "Small Scale Mobility Tests in Fine-Grained Layered Soils," Technical Report M-75-1, Mobility and Environmental Systems Laboratory, U.S. Army Engineer Waterways Experiment Station, June 1975.
14. Liston, R. A., "A Strip Load Approximation for a Track," ASAE Paper 73-1507.
15. Liston, R. A., "The Combined Normal and Tangential Loading of Soil," Ph.D. Thesis, Michigan Technological University, 1973.

APPENDIX
FLOWCHARTS

FLOWCHART FOR THE COMPUTATION OF SLIP LINE FIELDS
FOR SOIL STRENGTH VARYING WITH DEPTH

CHART TITLE - NON-PROCEDURAL STATEMENTS

```

COMMON RO,GO,COH,PHI,D1,A0,AH,A1,VK,UK,PL,DF,XX,
OF,AF,VA,UA,J1,H(36),Q(36),E(36),U(36),Y(36)
COMMON DEPHI,DECOH,ARC,ENOB,IH1
COMMON F1MAX,F1MIN,COMAX,COMIN
COMMON X(43,15),Z(43,15)
DIMENSION P(43,15)
DIMENSION S(43,15),T(43,15),
A(36),B(36),C(36),D(36)
INTEGER XX,XXX
REAL L,L1,L2
STATEMENT FUNCTION DEFINITION: DEL(D9,F9)=ATAN((SIN(D9)/SIN(F9)) /
      SORT(1-(SIN(D9)/SIN(F9))**2))
STATEMENT FUNCTION DEFINITION: QUA(D9,F9)=COS(D9)+SORT(COS(D9)**2-COS(F9)**2)
STATEMENT FUNCTION DEFINITION: QUP(D9,F9)=COS(D9)-SORT(COS(D9)**2-COS(F9)**2)
STATEMENT FUNCTION DEFINITION: EP0(F9,T9,T8)=EXP(2*(T9-T8)*SIN(F9)/COS(F9))
STATEMENT FUNCTION DEFINITION: D1S(R9,D9,T9,T8,F9)=R0*(R9-D9)*EXP((T9-T8)*
      SIN(F9)/COS(F9))
FORMAT(1H-,'CANT COMPUTE CASE : CHECK INPUT')
FORMAT(1H,'PHI LT.0 IN XX= ',I4,'I= ',I3,'J= ',I3,'Z= ',F7.3)
FORMAT(1P3E(5.7,2I9,1PE15.7)
FORMAT(1H,'COH LT.0 IN XX= ',I4,'I= ',I3,'J= ',I3,'Z= ',F7.3)

```

112

242

8899

248

CHART TITLE - SUBROUTINE SLFI

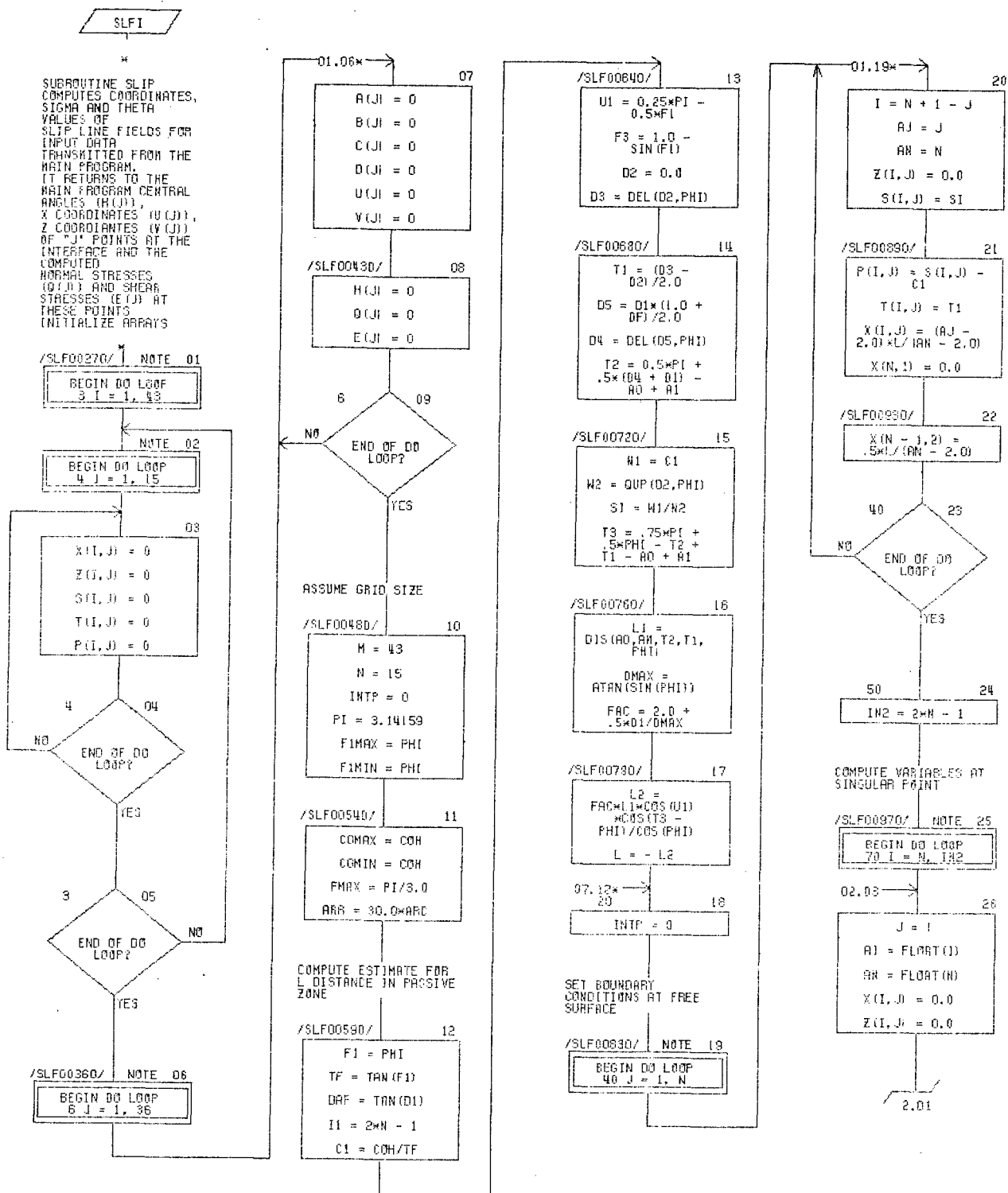


CHART TITLE - SUBROUTINE SLF1

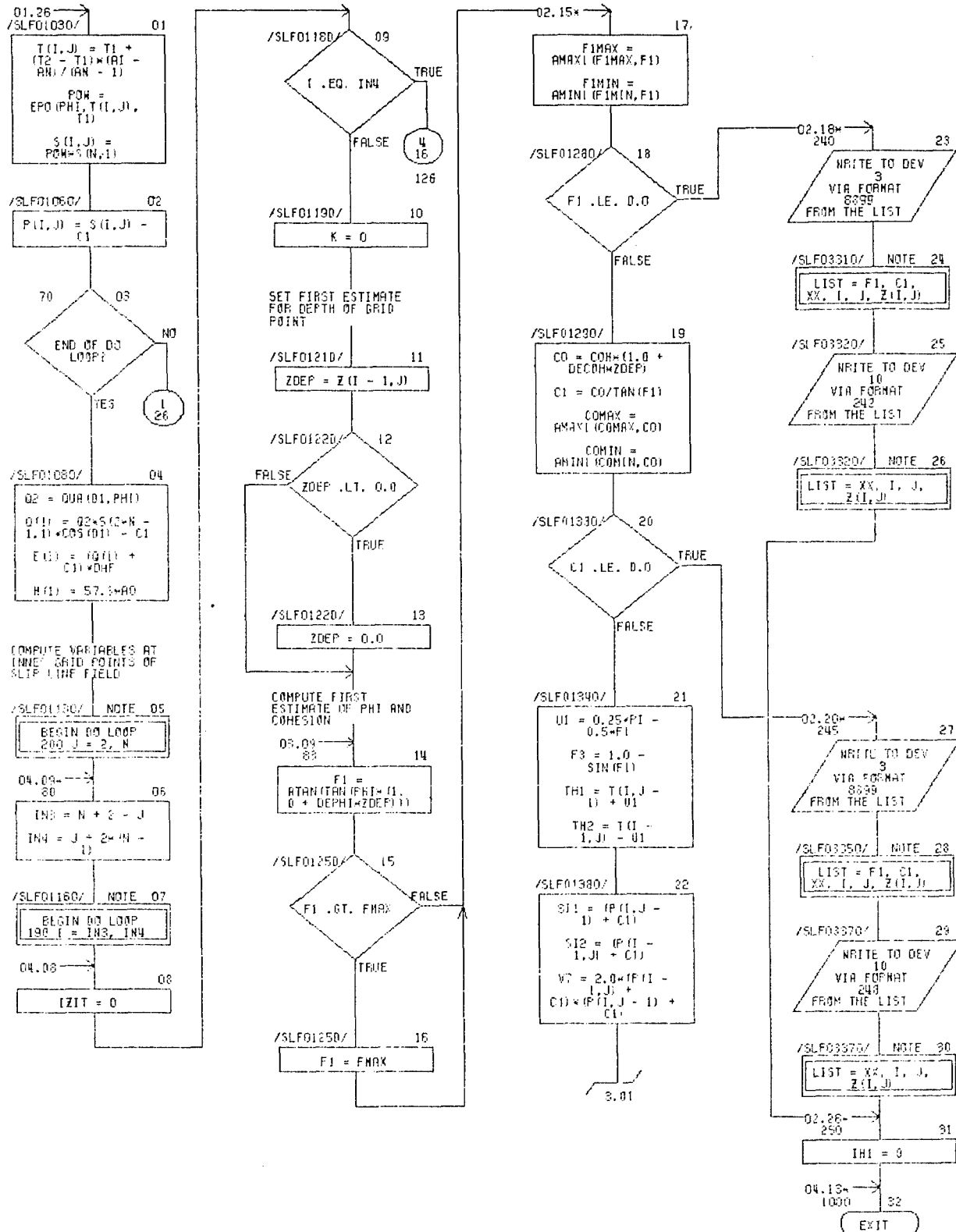


CHART TITLE - SUBROUTINE SLF0

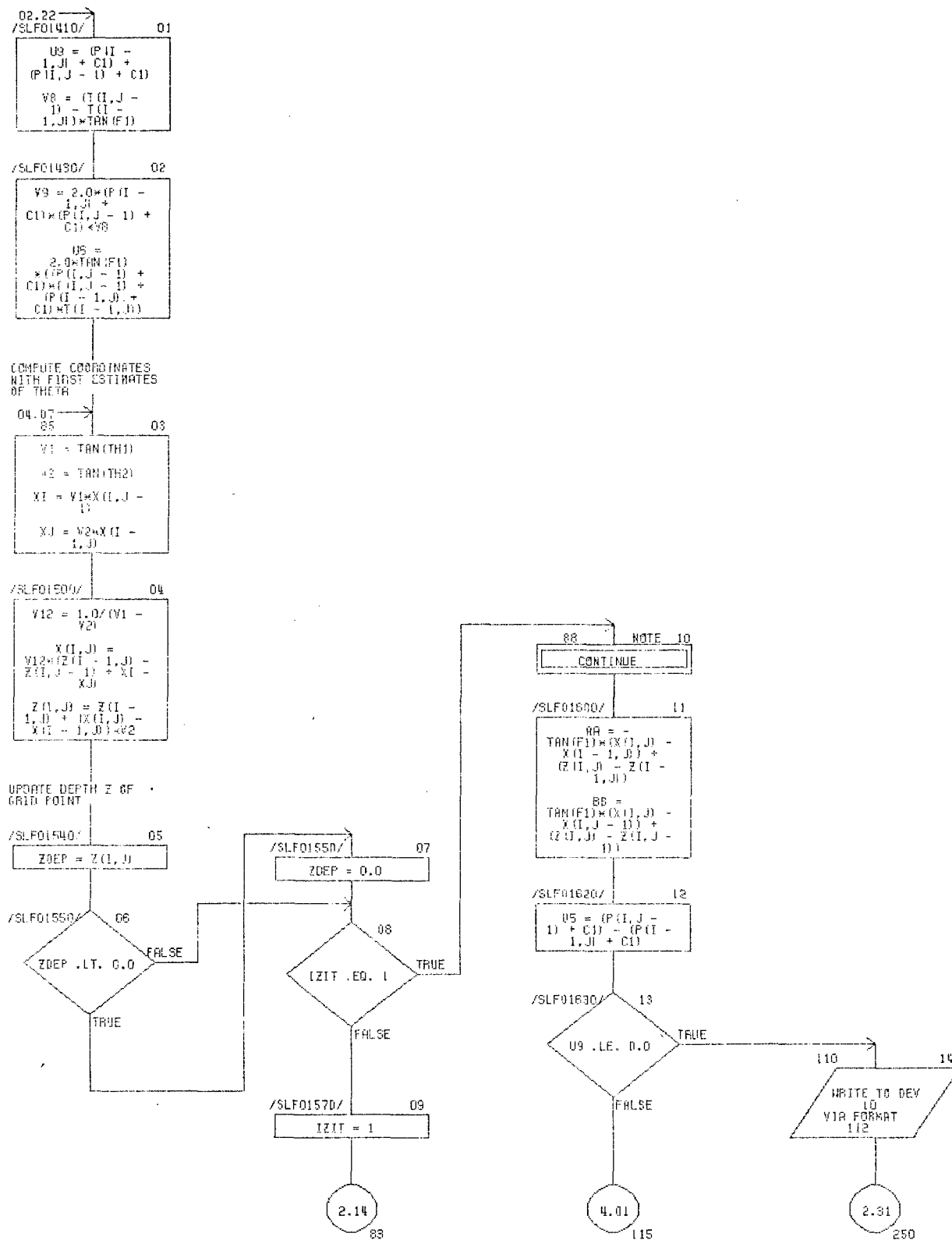


CHART TITLE - SUBROUTINE SLF1

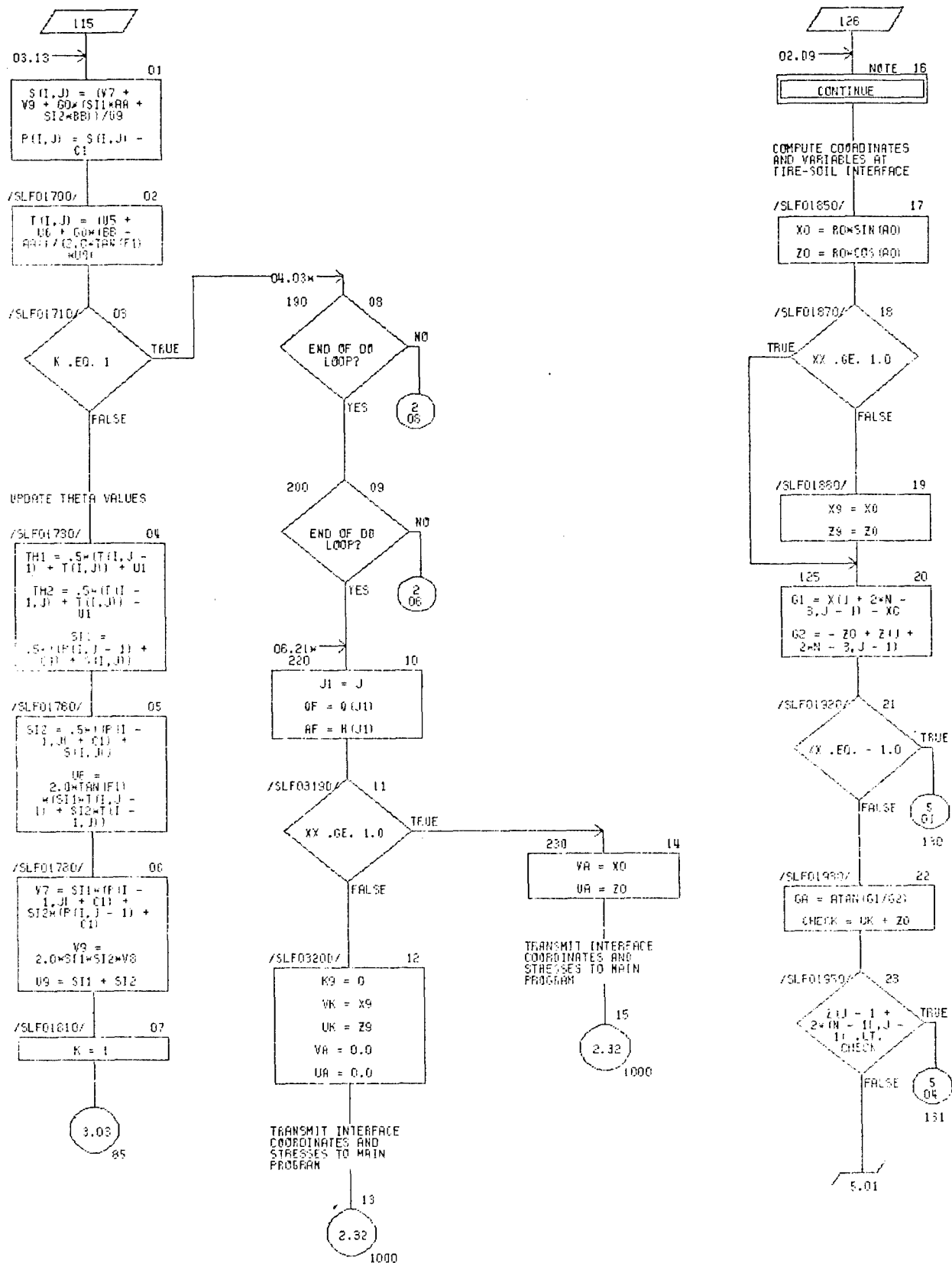


CHART TITLE - SUBROUTINE SLF0

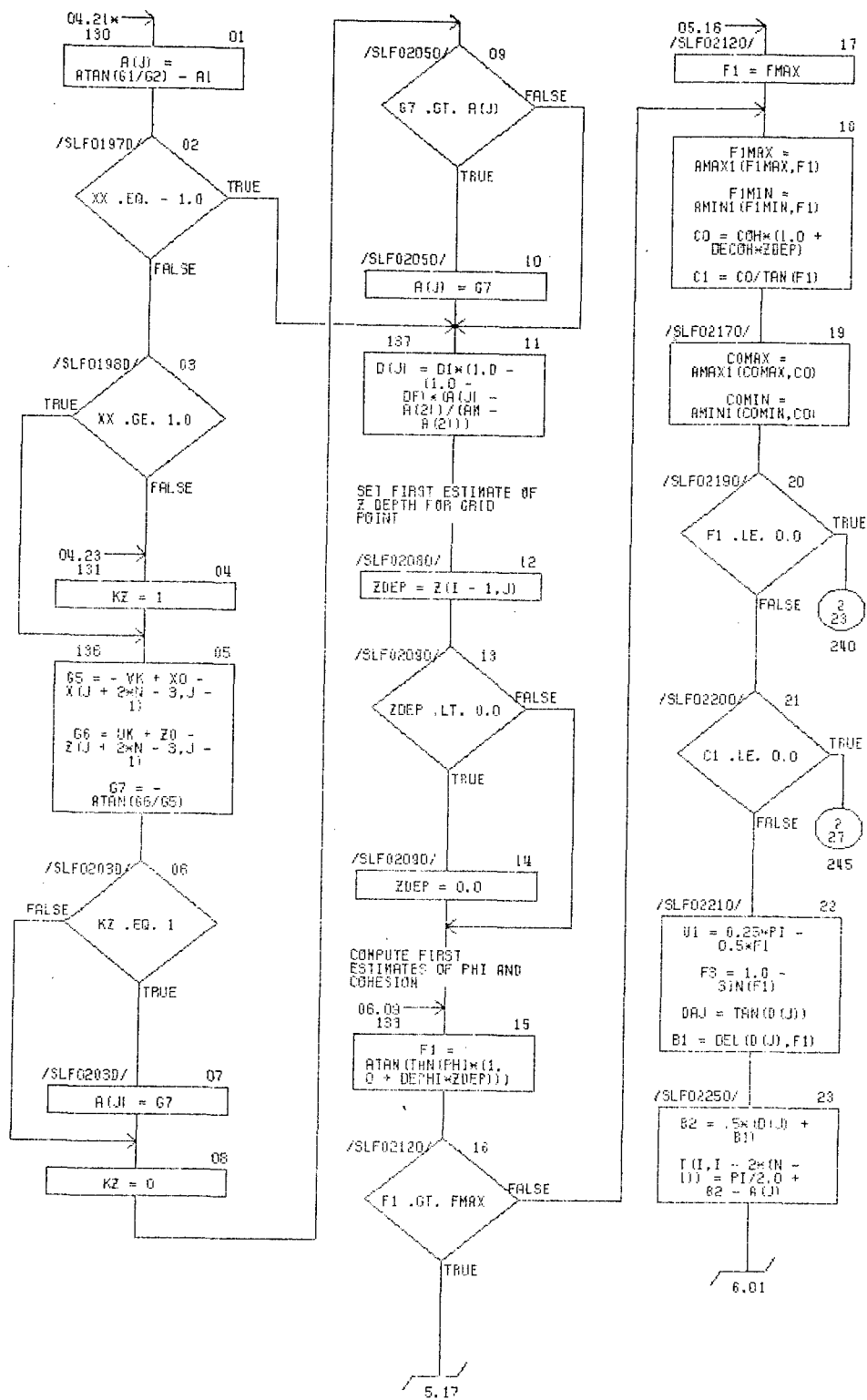


CHART TITLE - SUBROUTINE SLF1

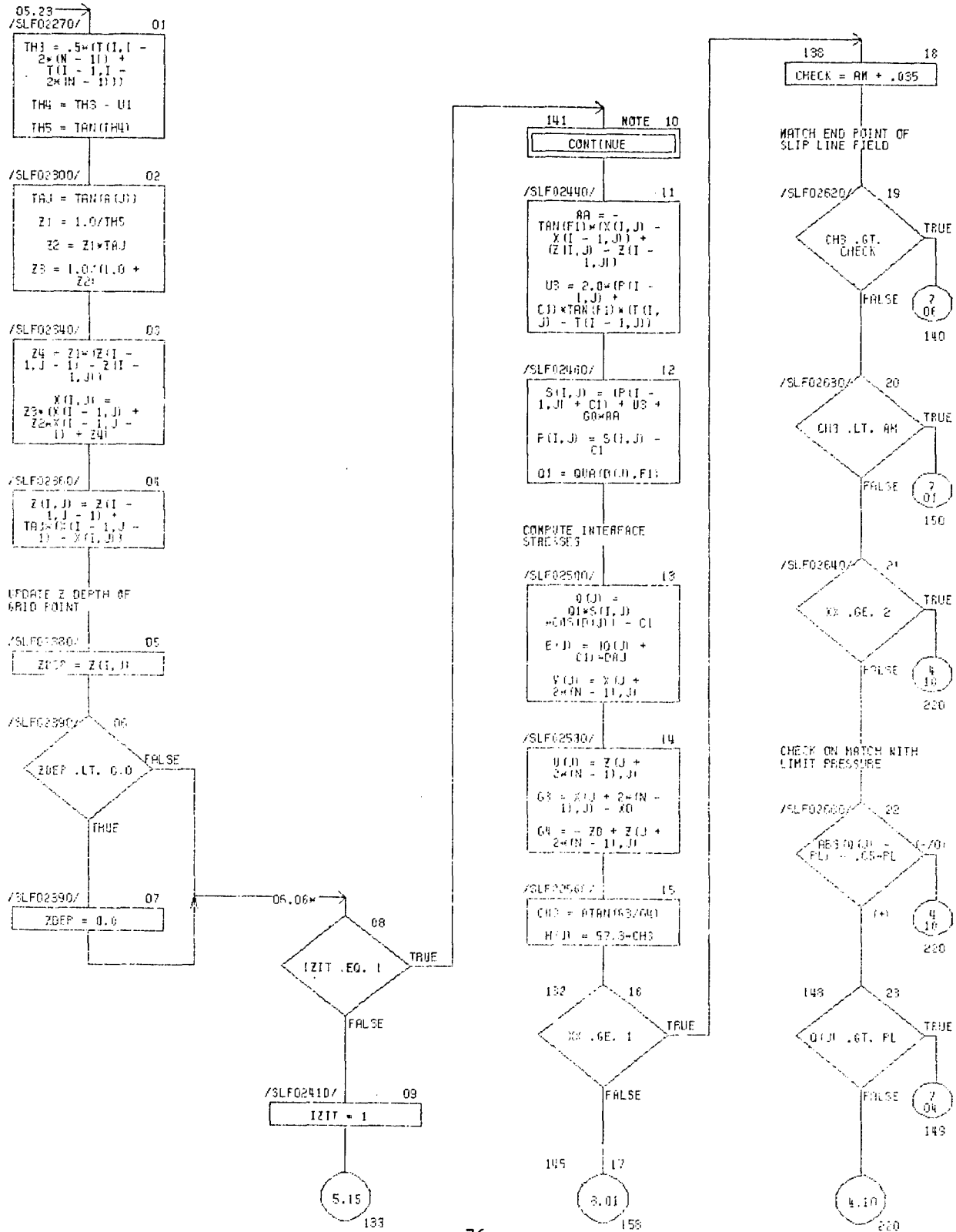
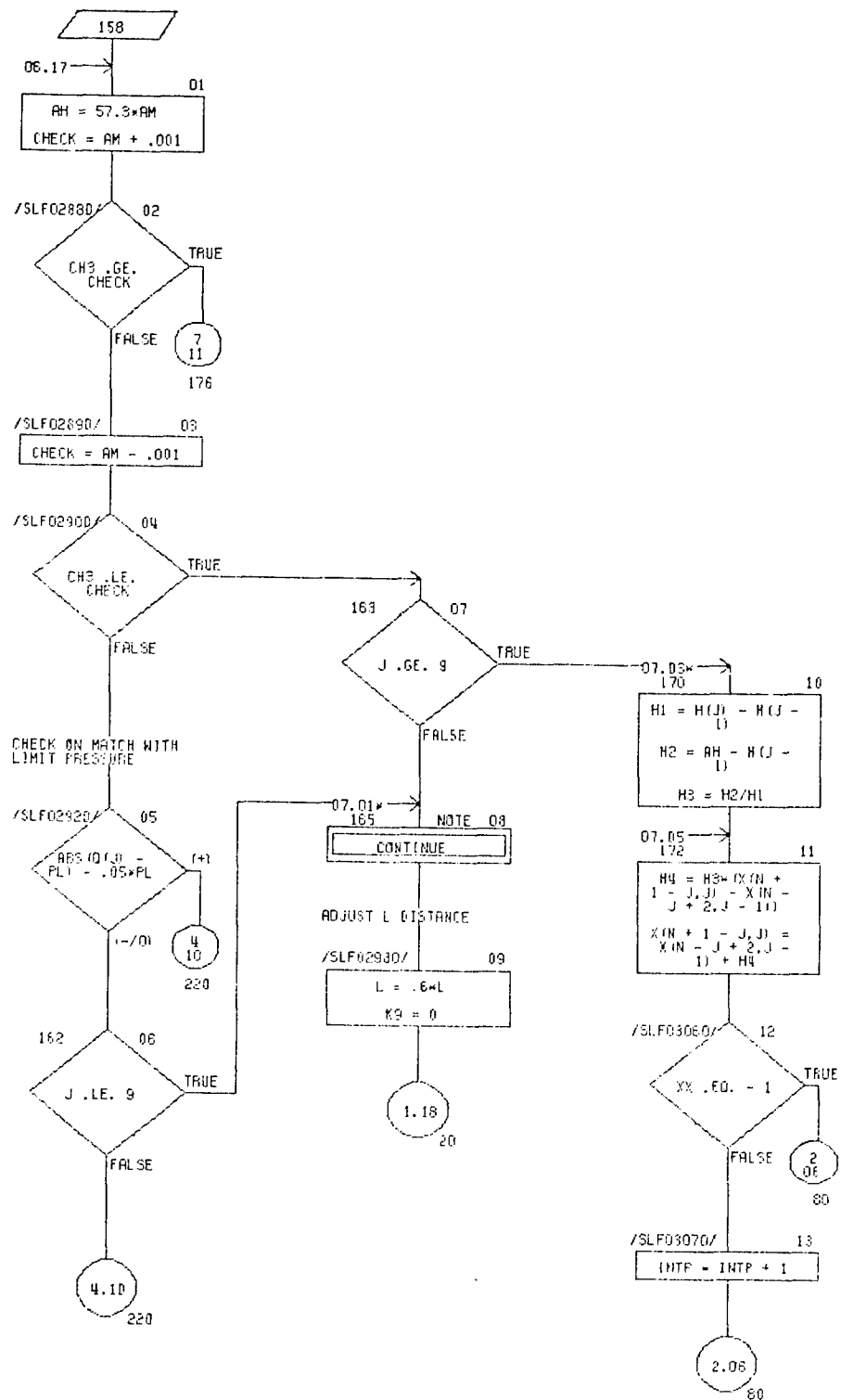


CHART TITLE - SUBROUTINE SLFI



CHART TITLE - SUBROUTINE SLF1



FLOWCHART FOR COMPUTATION OF
TIRE PERFORMANCE IN TWO-LAYER SOILS

11/05/75

AUTOFLOW CHART SET - FLOCHART LES00010

PAGE 01

CHART TITLE - INTRODUCTORY COMMENTS

CONTROL USLIMIT, LABEL, MAP

THIS PROGRAM COMPUTES OFF-ROAD TIRE PERFORMANCE IN TWO LAYER
SOILS FROM THE FOLLOWING INPUTS

TIRE RADIUS (FT) , WIDTH (FT)

TIRE LOAD (LBS) , LIMIT PRESSURE PSUBL (LBS/SQ IN)

DEFLECTION COEFF. EPSILON, SLIP (DECIMAL)

SLIP PARAMETER JZERO, SLIP PARAMETER K

DELTA DISTRIBUTION COEFF (=1 FOR UNIFORM DISTR.)

UPPER LAYER COHESION(LBS/SQ FT), FRICTION A. (DEG), GAMMA (LBS/CU FT)

LOWER LAYER COHESION(LBS/SQ FT), FRICTION A. (DEG), GAMMA(LBS/ CU FT)

THE PROGRAM IS APPLICABLE ONLY IF BOTH STRENGTH
COMPONENTS(C AND PHI) ARE EITHER GREATER OR
SMALLER IN THE UPPER LAYER THAN IN THE LOWER ONE
AND THE DEFLECTED TIRE IS COMPLETELY IN THE UPPER
LAYER.

THE LIMIT PRESSURE PSUBL MAY BE ASSUMED AS
PSUBL=0.64*INFLATION PR. +4 (PSI)

FOR DEFLECTION AND SLIP PARAMETERS SEE REPORT

CHART TITLE - PROCEDURES

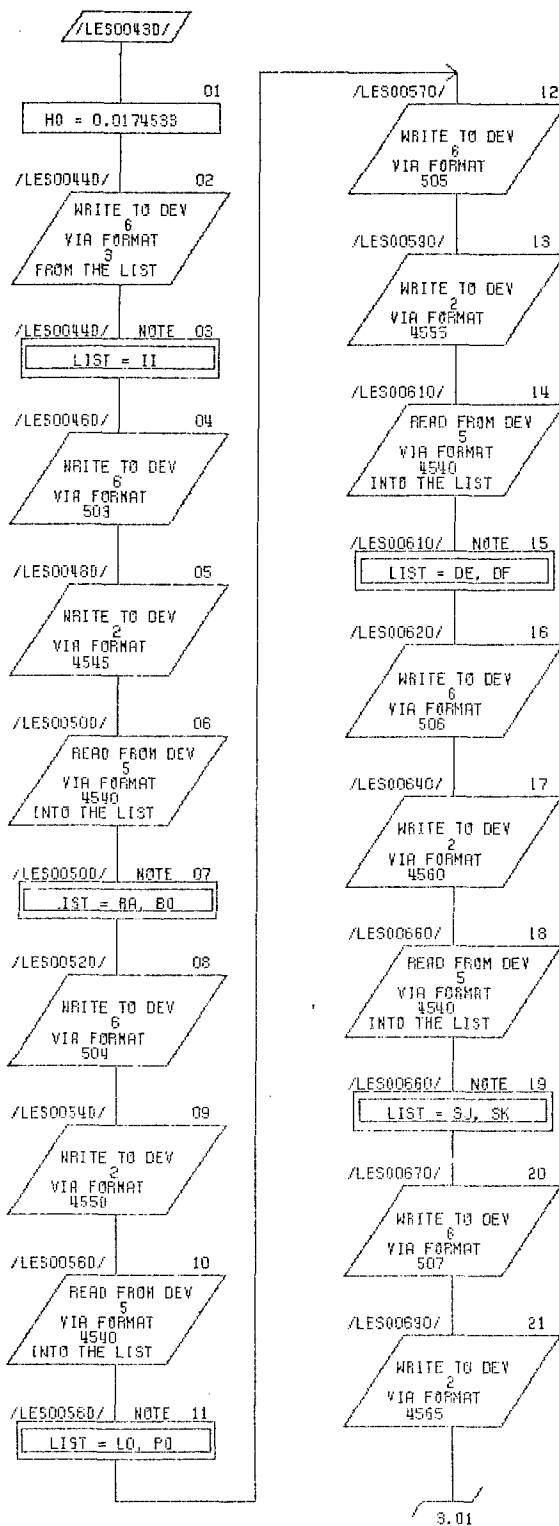


CHART TITLE - PROCEDURES

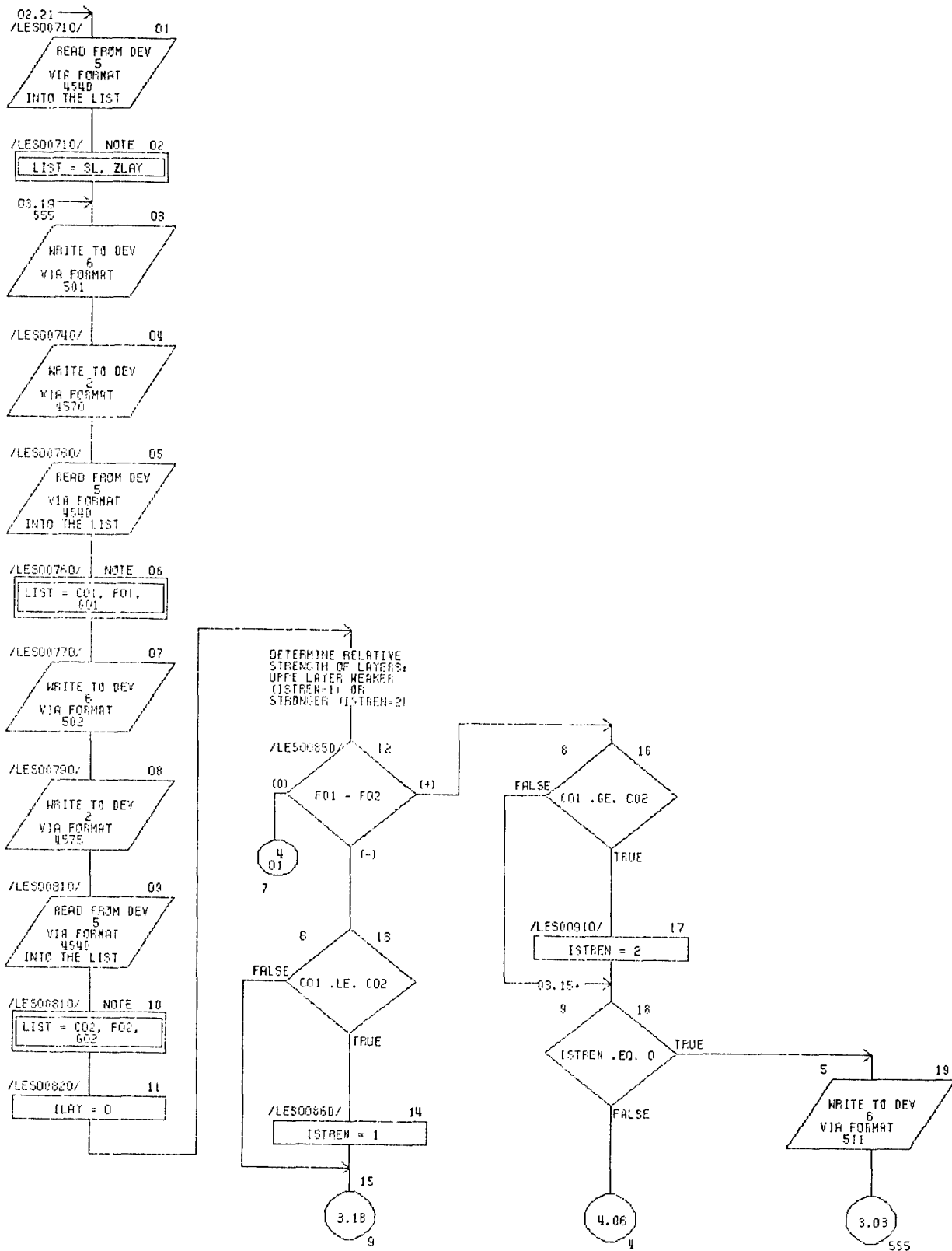


CHART TITLE - PROCEDURES

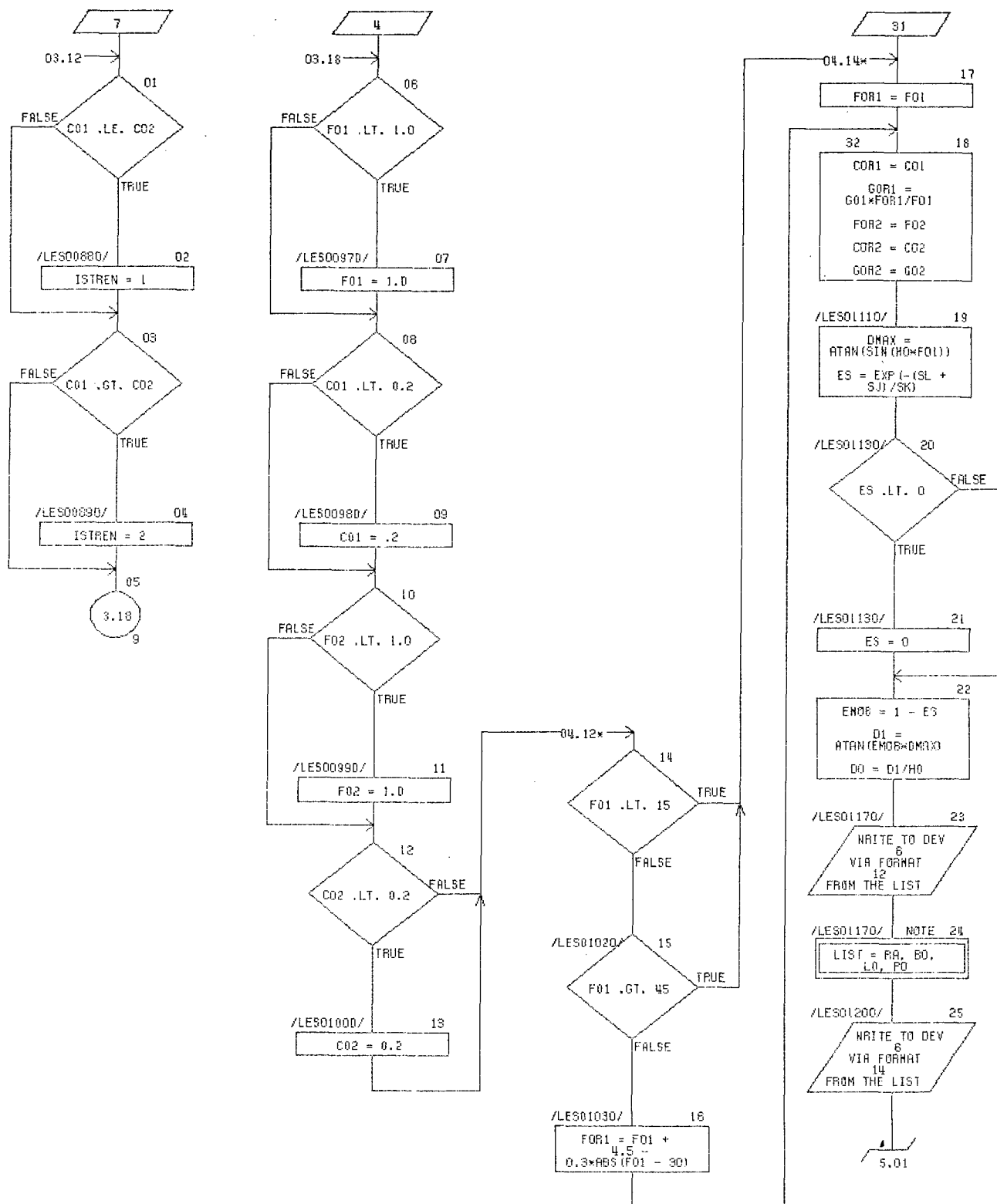


CHART TITLE - PROCEDURES

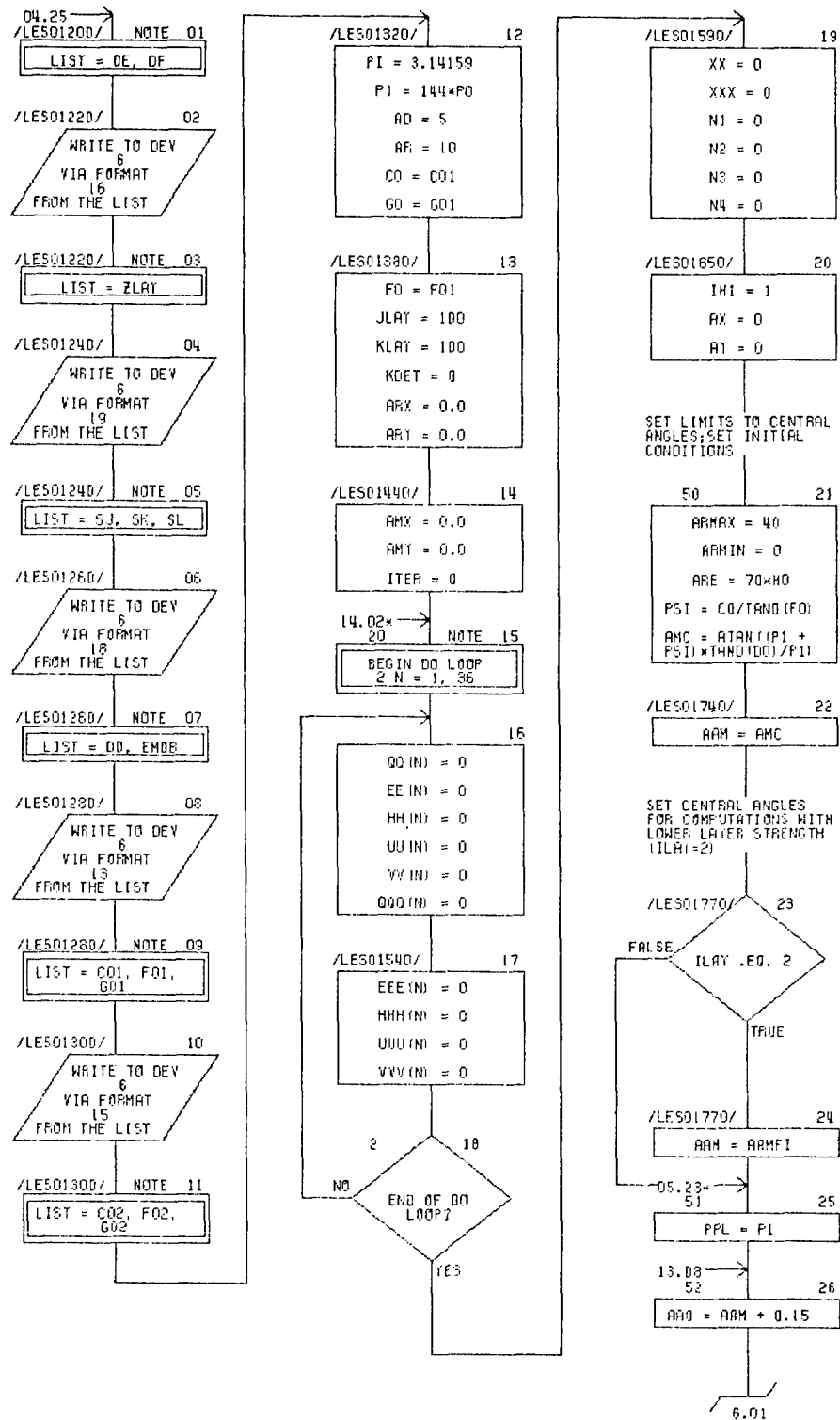


CHART TITLE - PROCEDURES

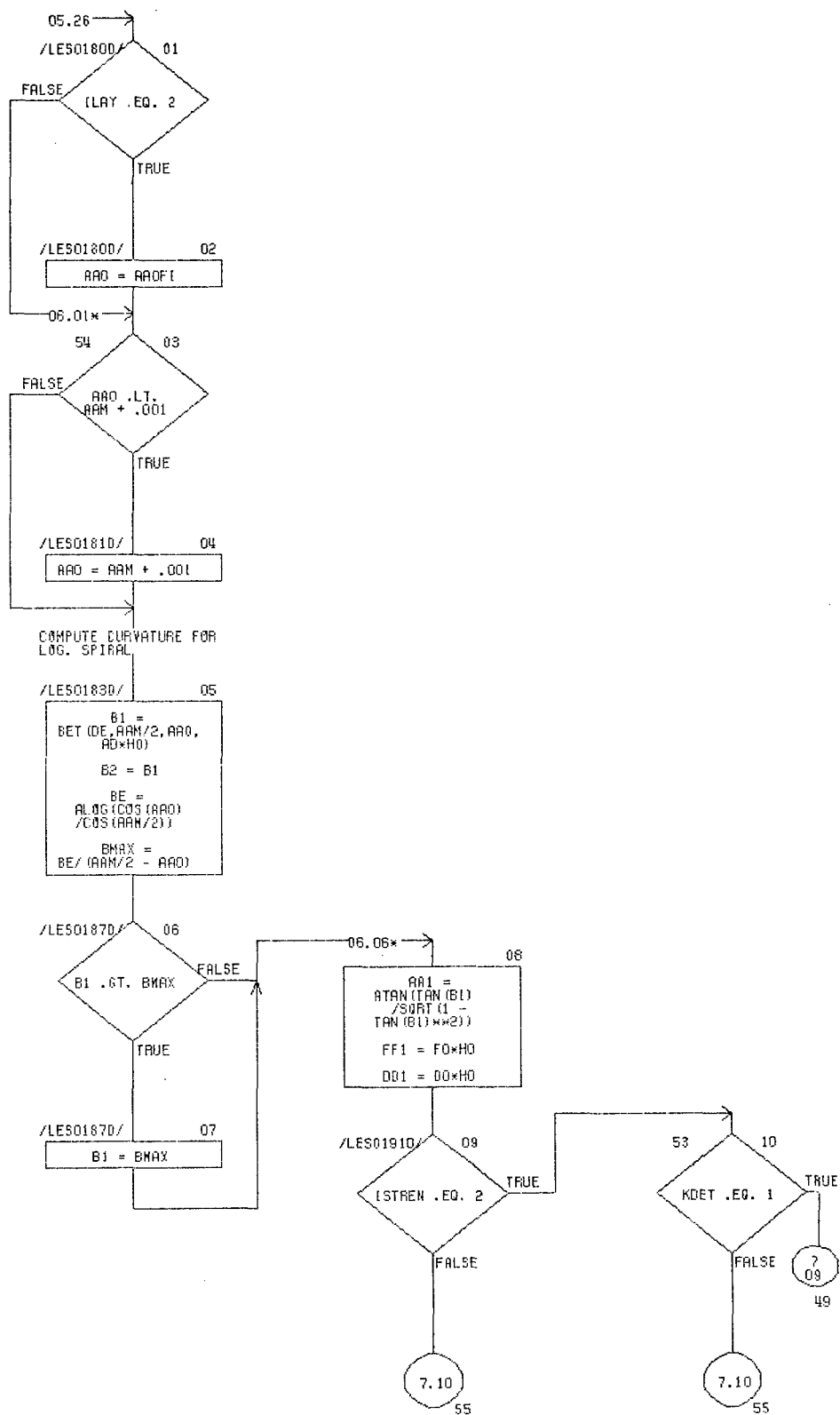
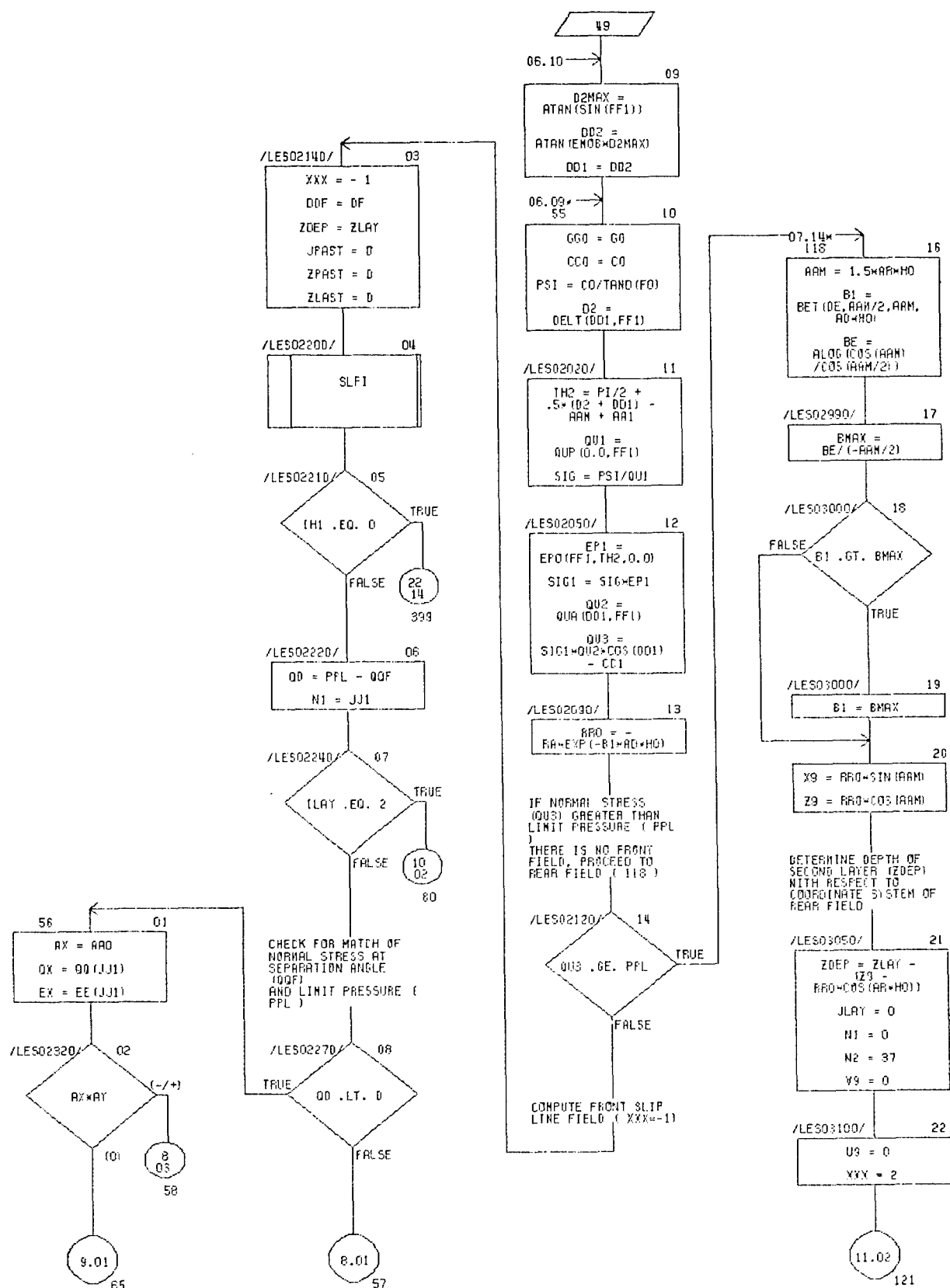


CHART TITLE - PROCEDURES



WART TITLE - PROCEDURES

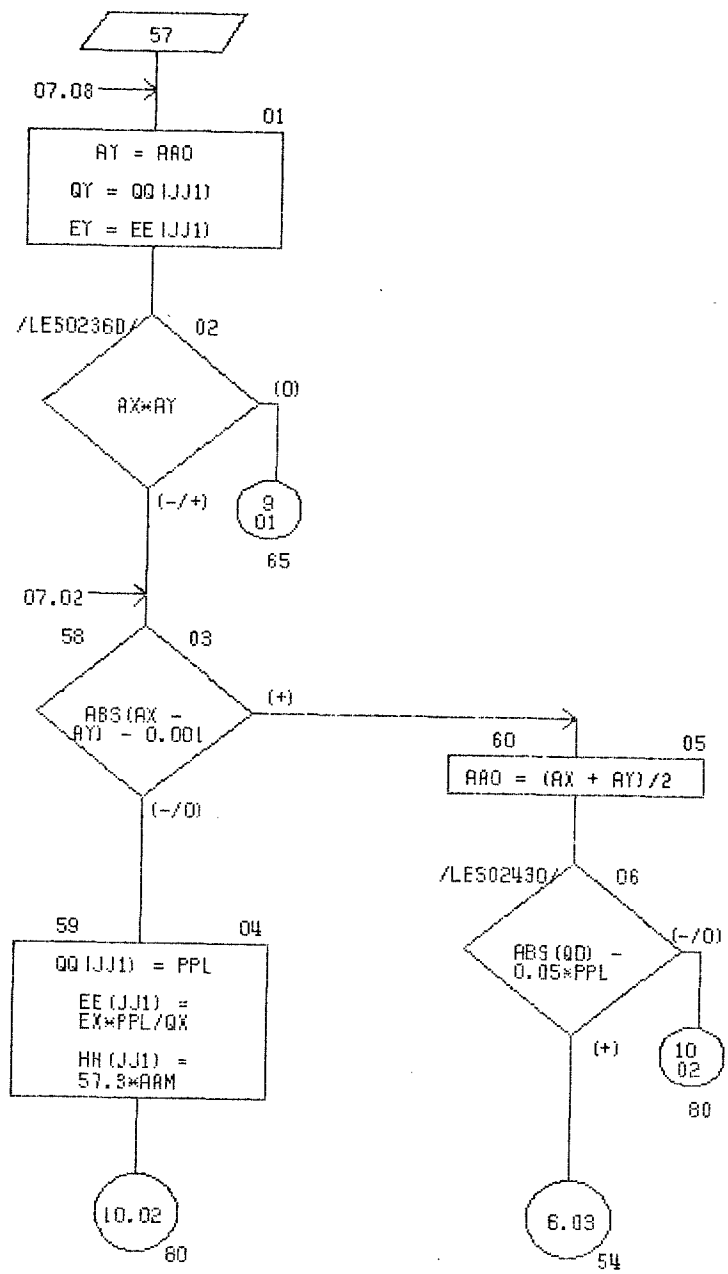


CHART TITLE - PROCEDURES

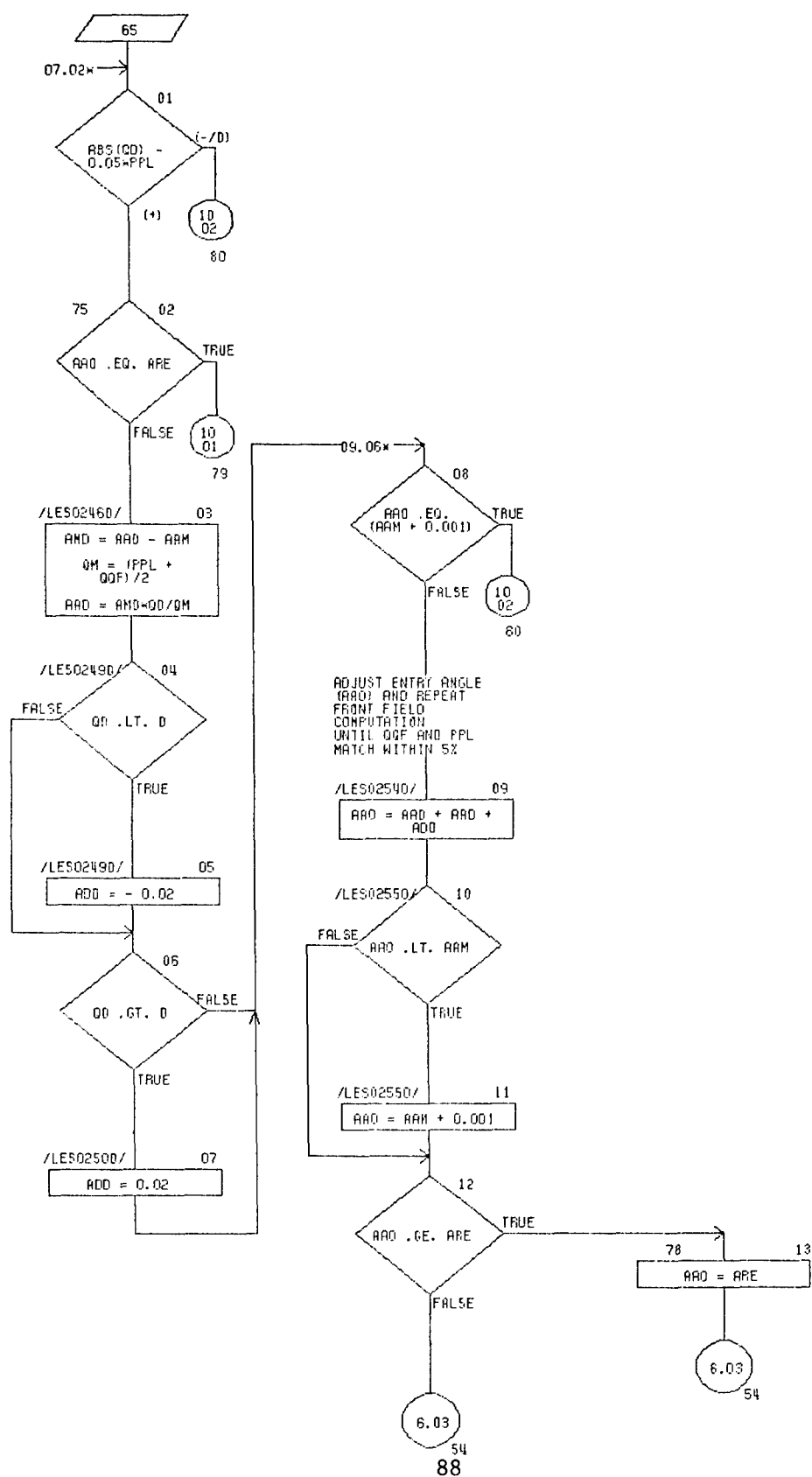


CHART TITLE - PROCEDURES

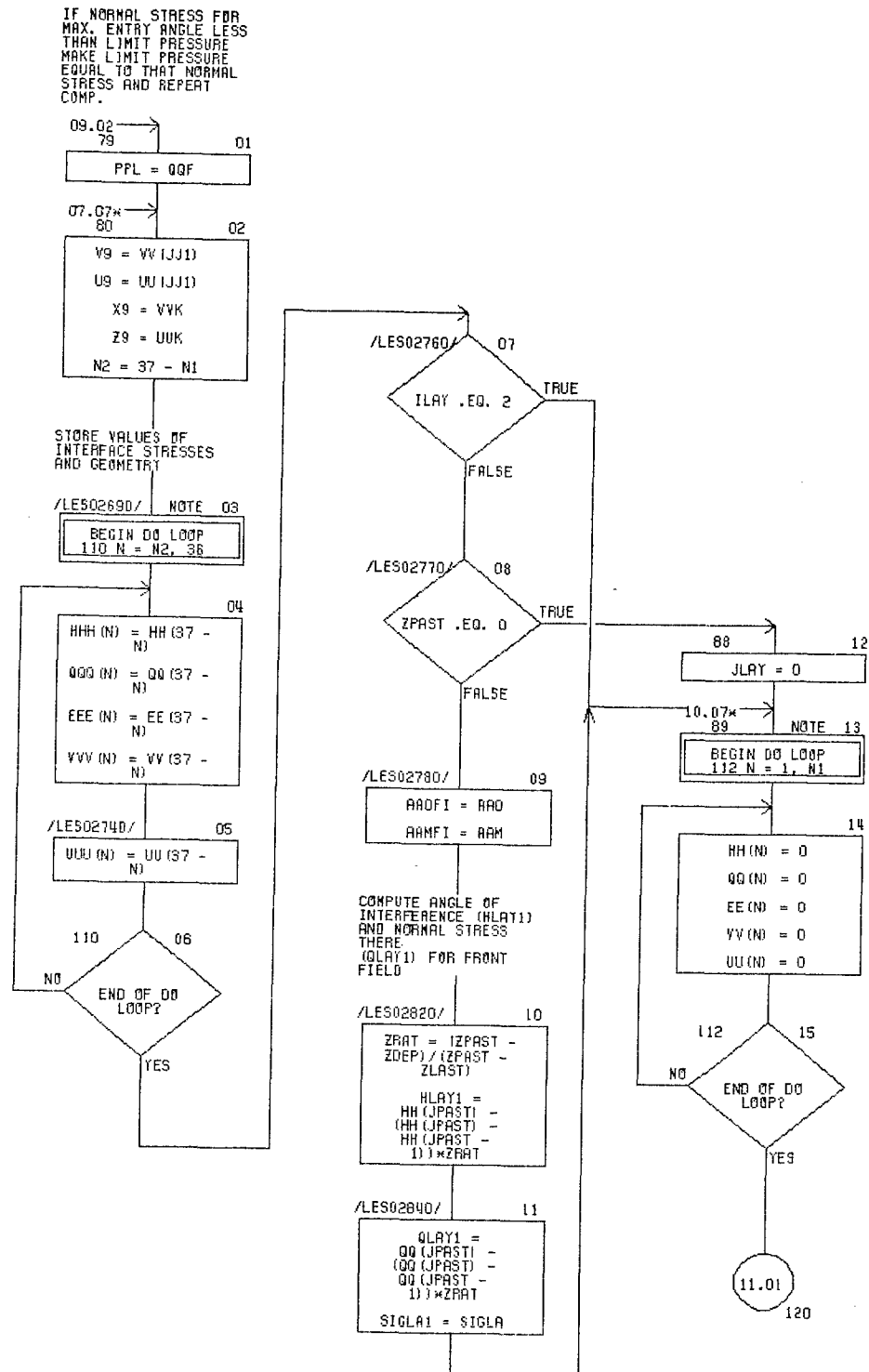


CHART TITLE - PROCEDURES

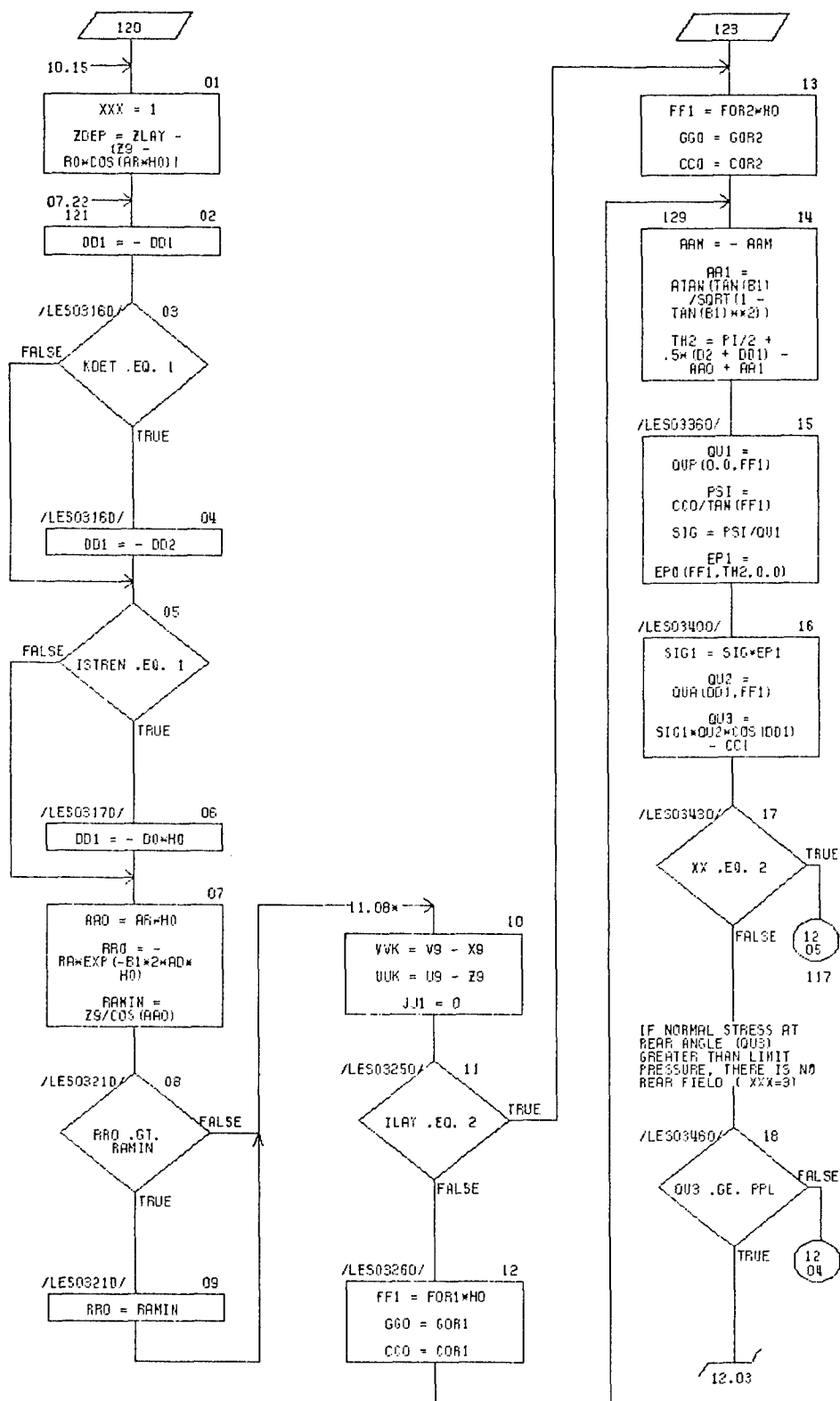


CHART TITLE - PROCEDURES

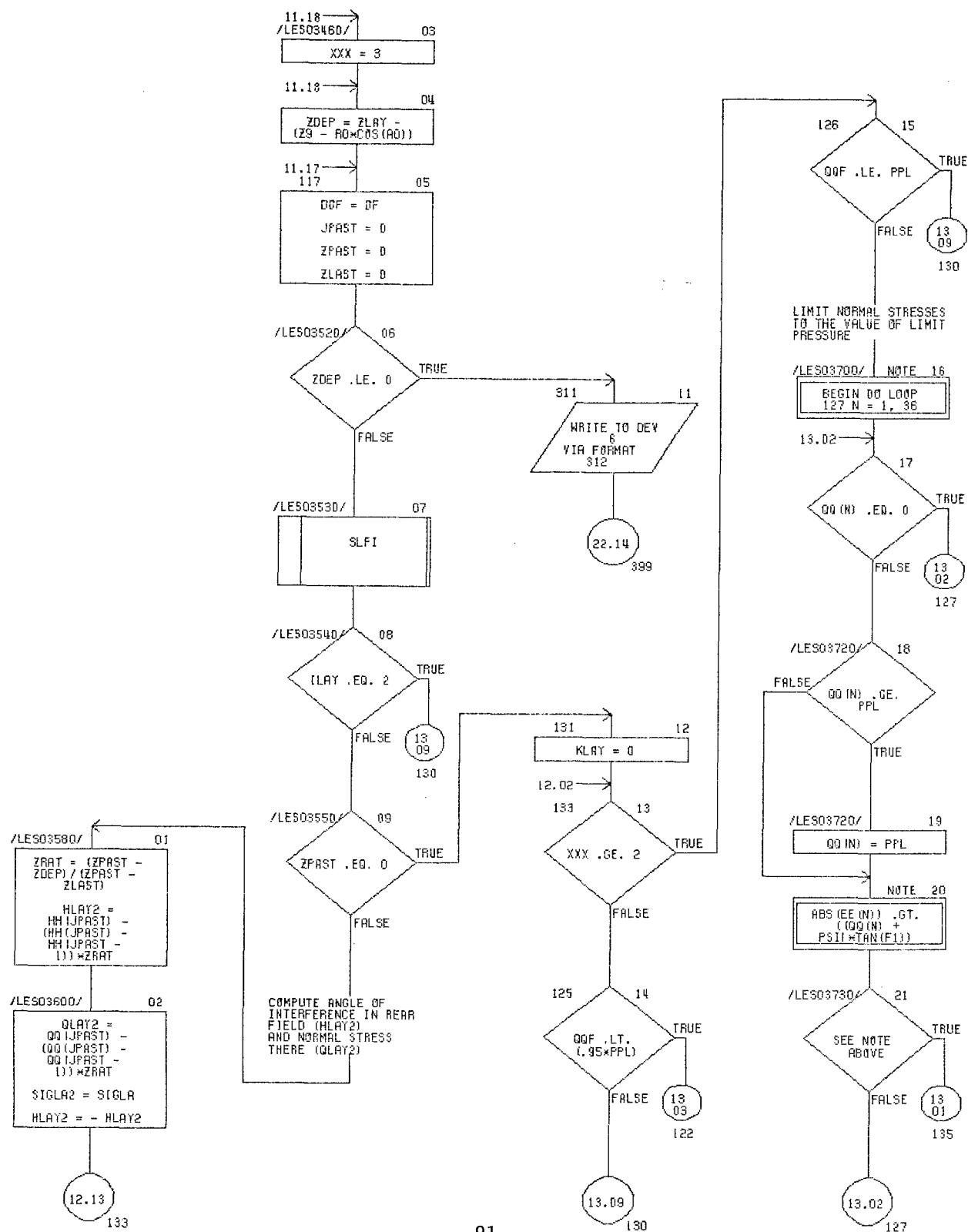


CHART TITLE - PROCEDURES

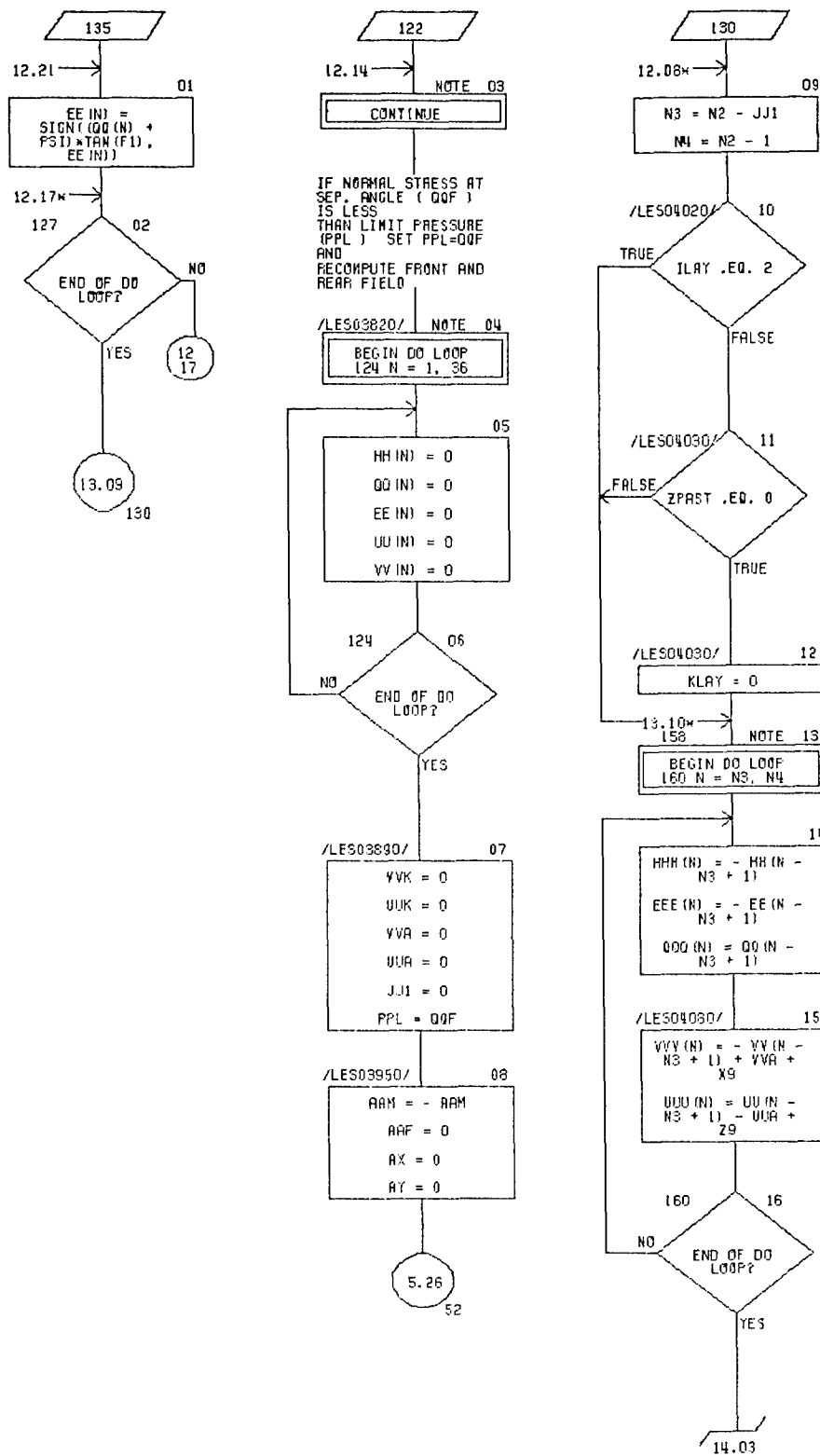


CHART TITLE - PROCEDURES

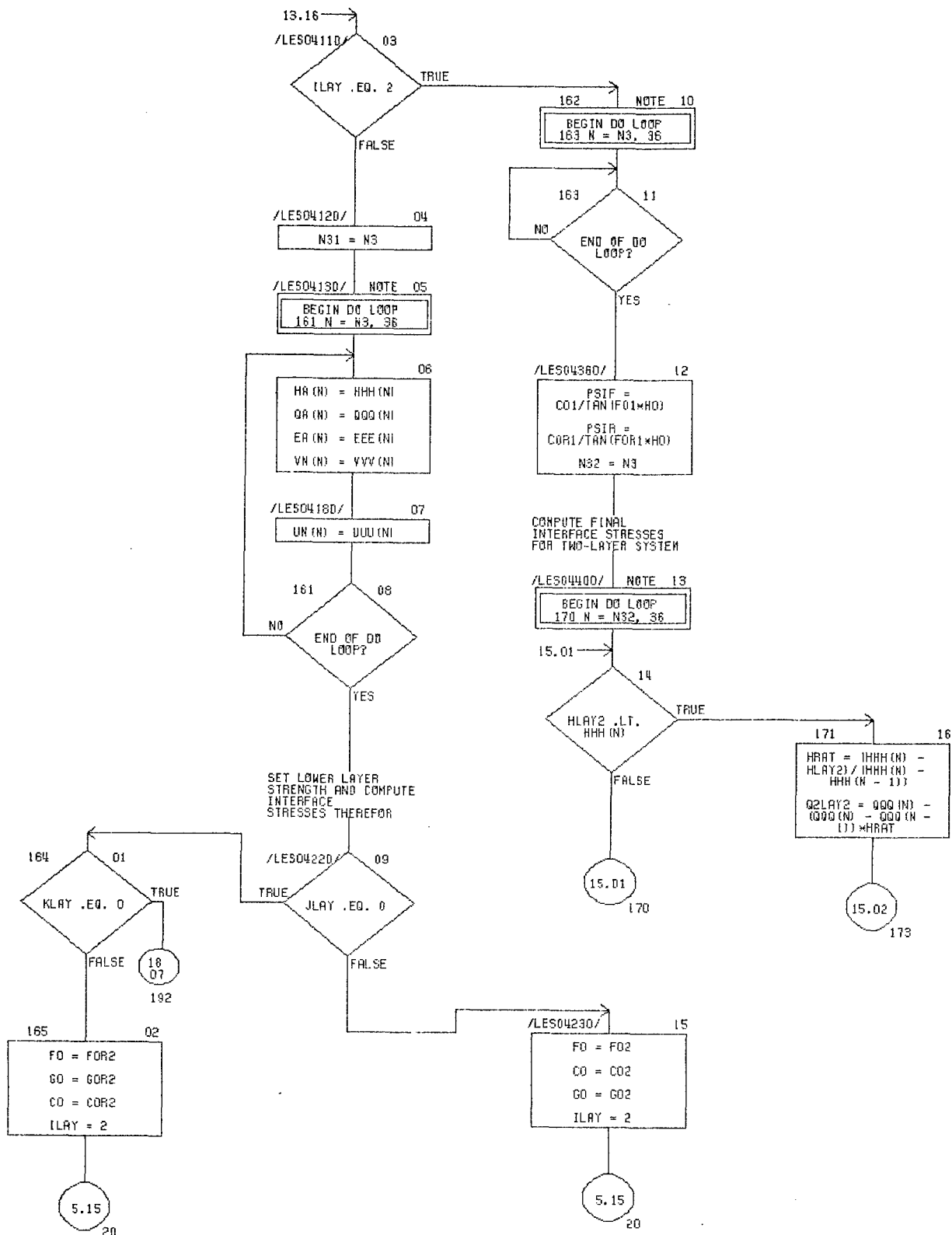


CHART TITLE - PROCEDURES

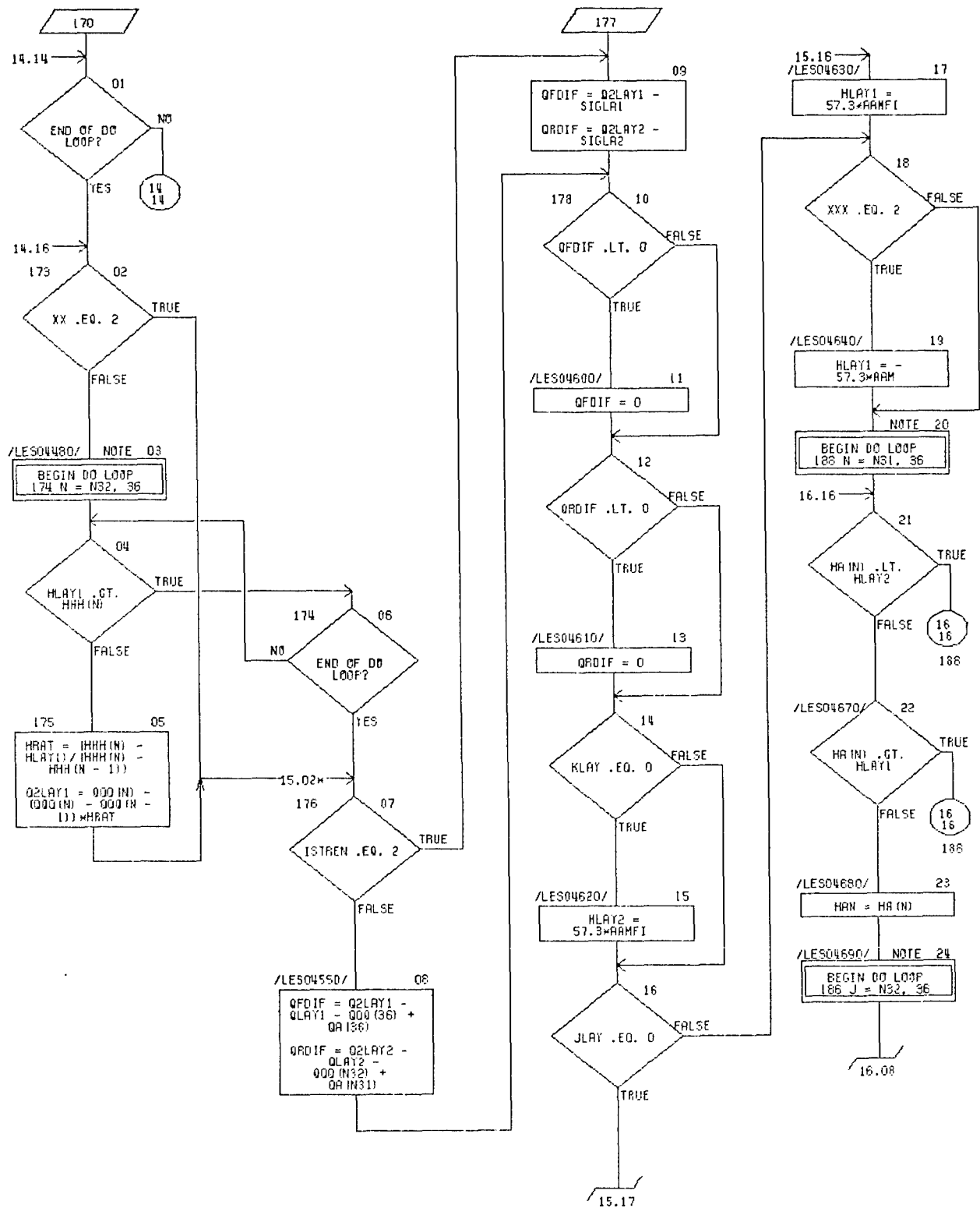


CHART TITLE - PROCEDURES

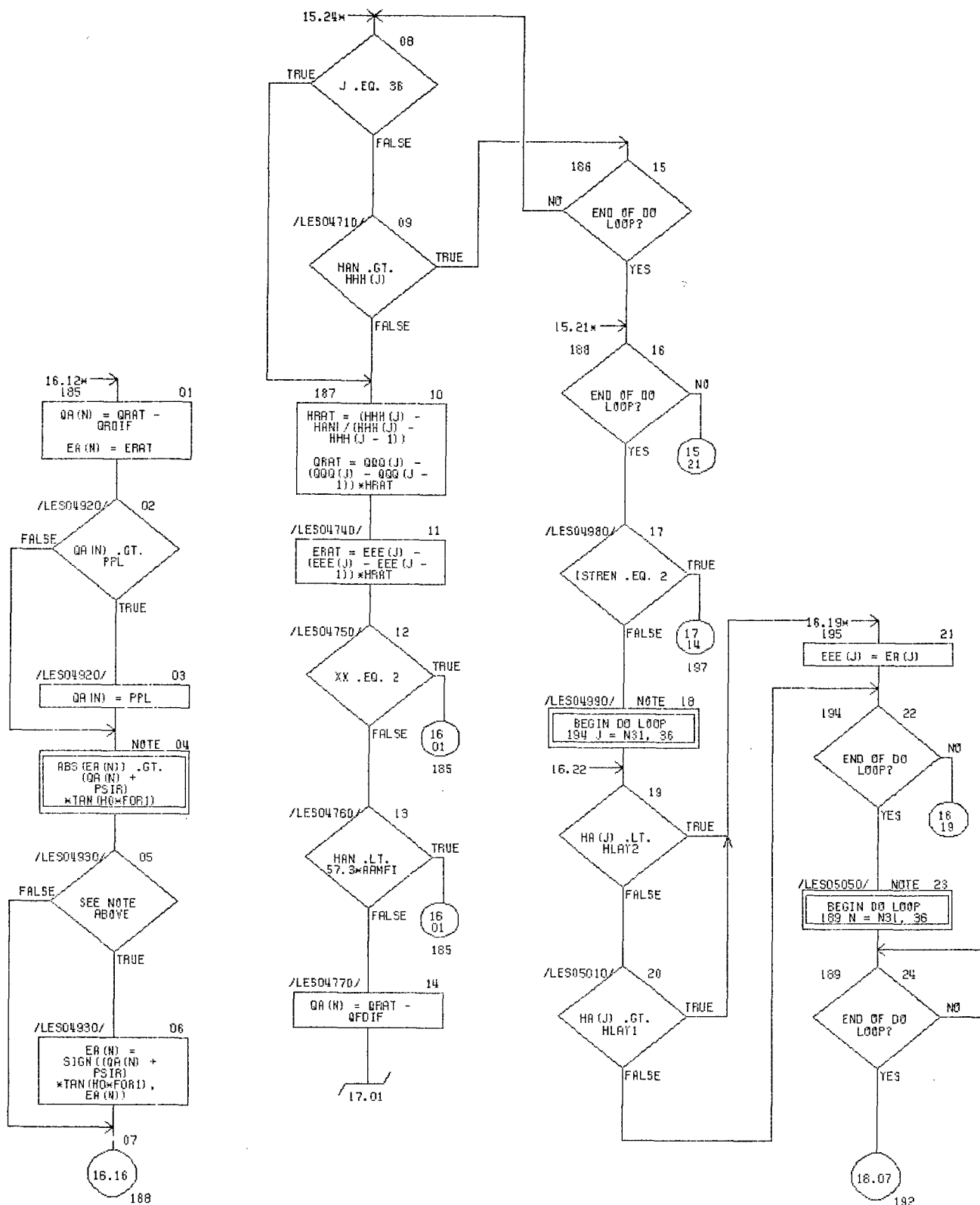


CHART TITLE - PROCEDURES

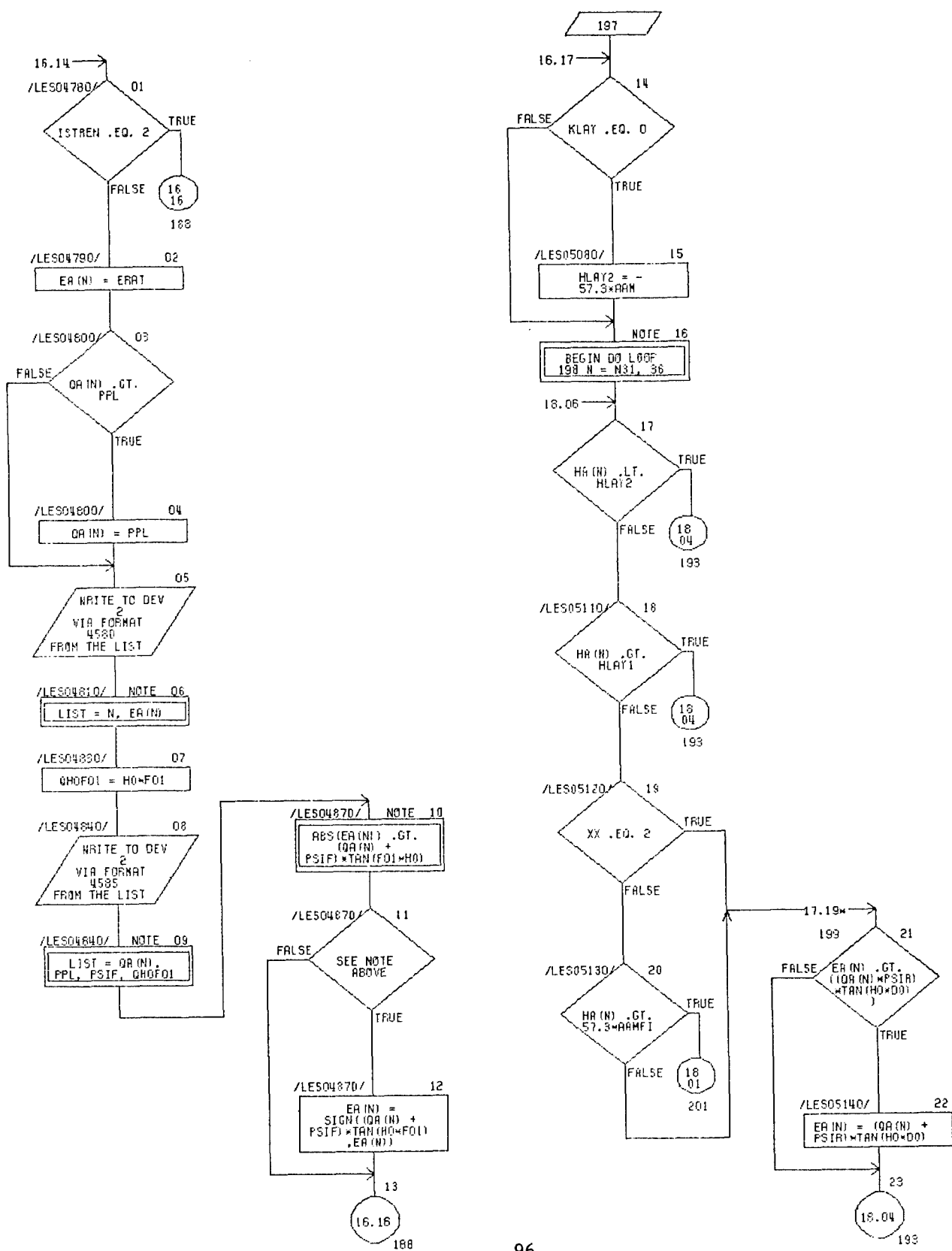


CHART TITLE - PROCEDURES

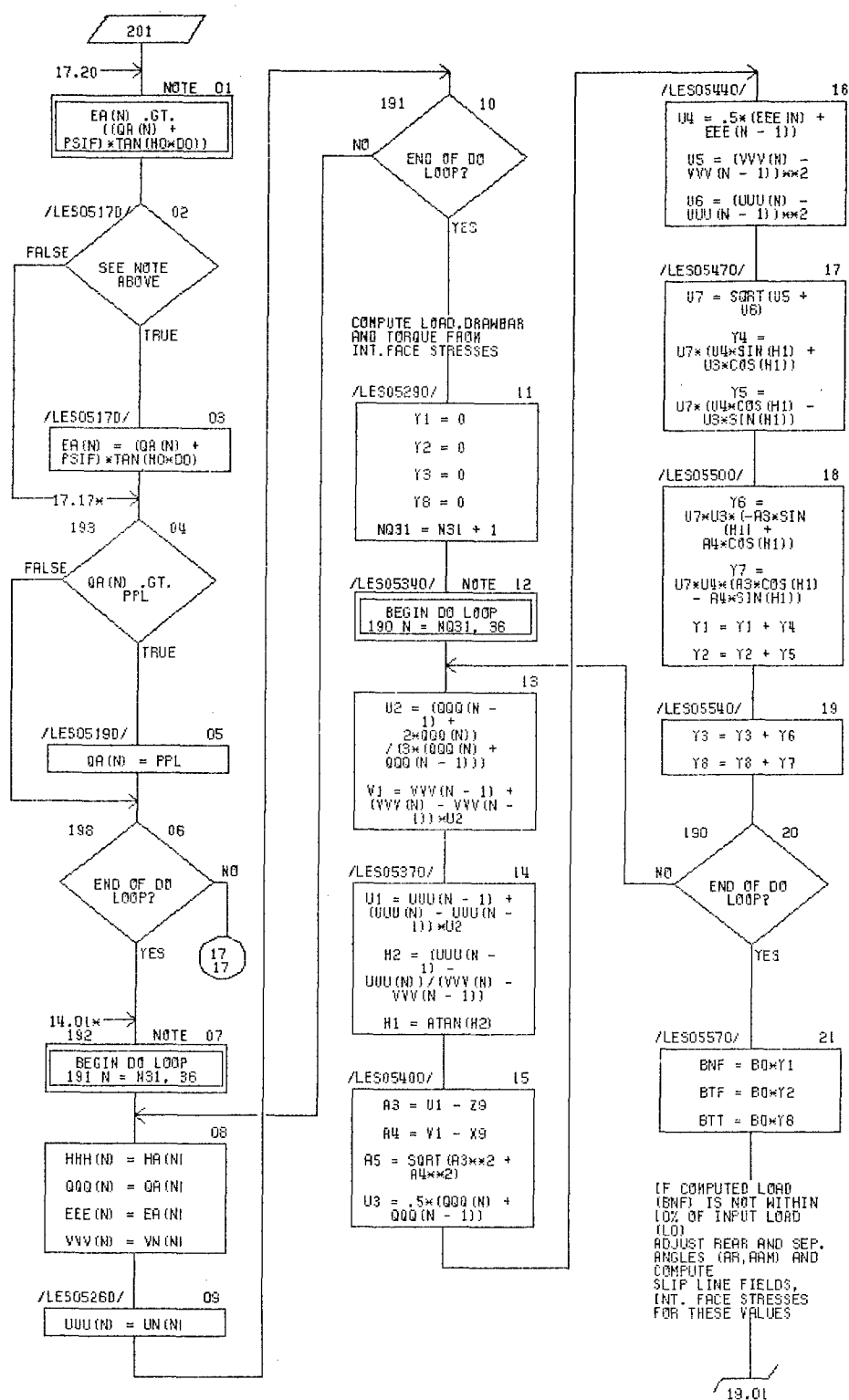


CHART TITLE - PROCEDURES

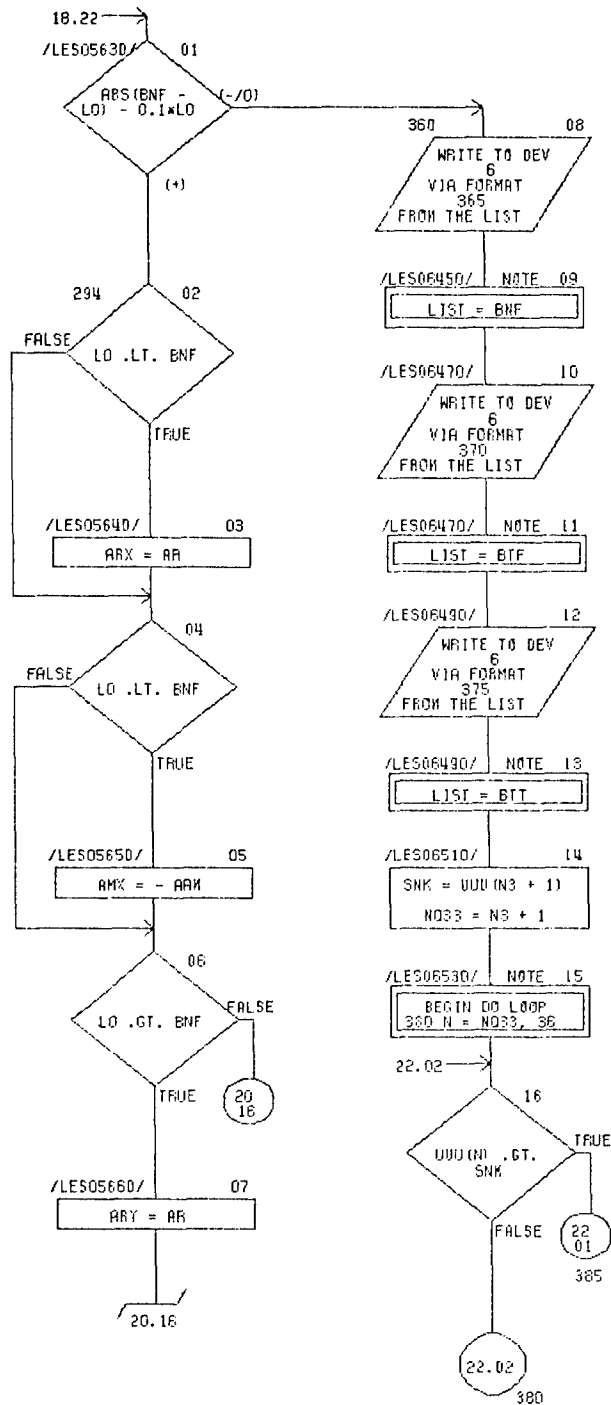


CHART TITLE - PROCEDURES

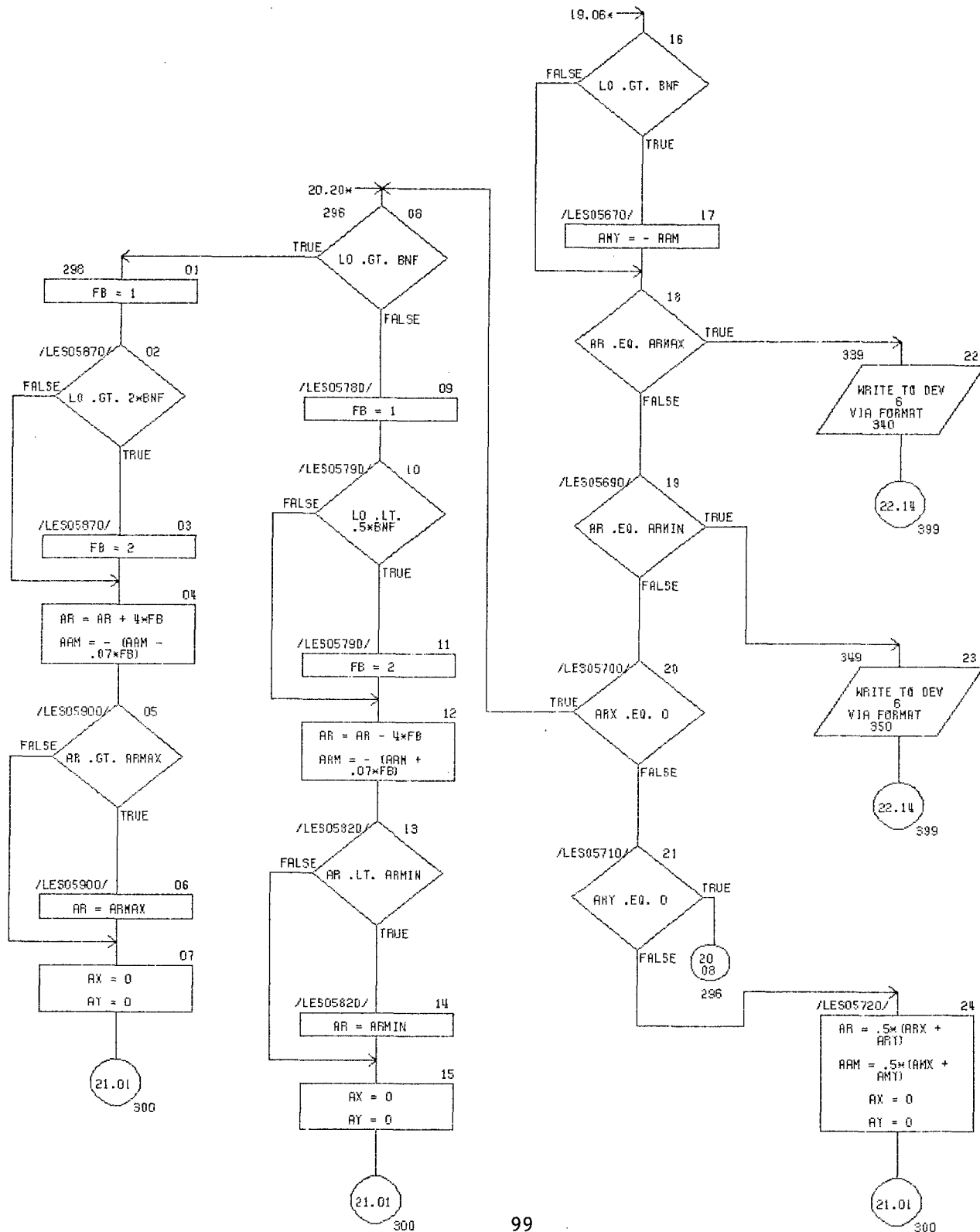


CHART TITLE - PROCEDURES

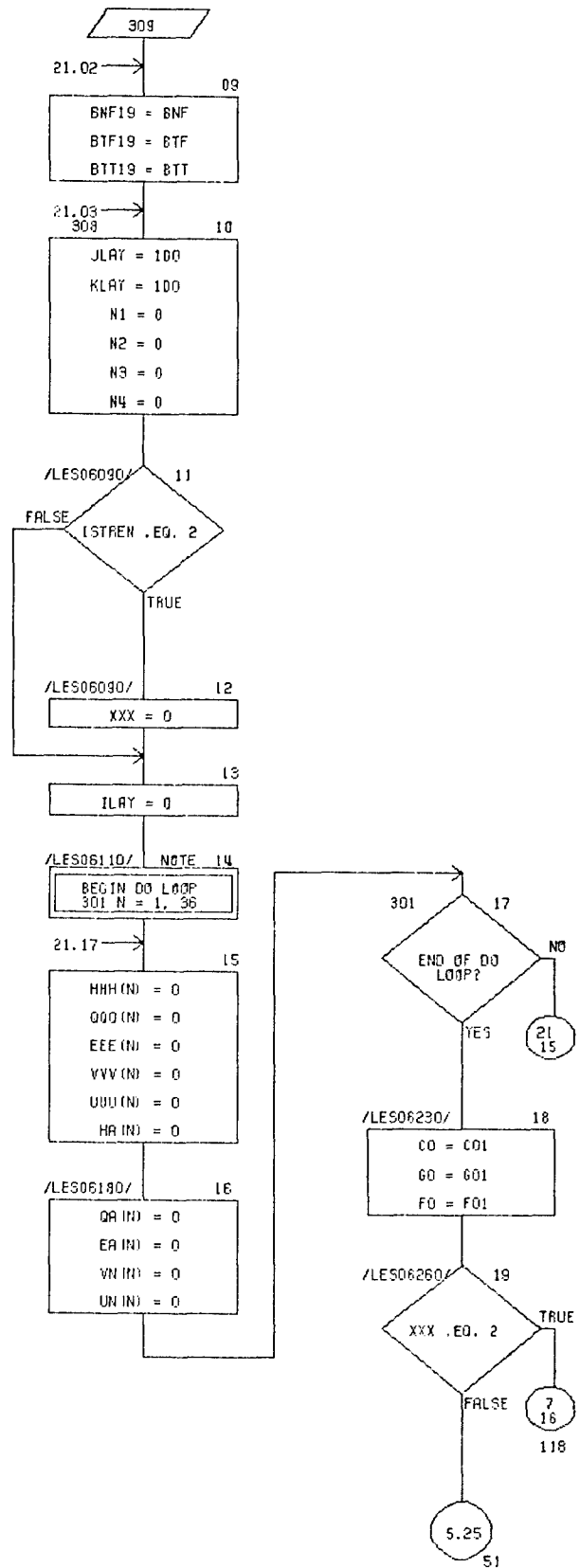
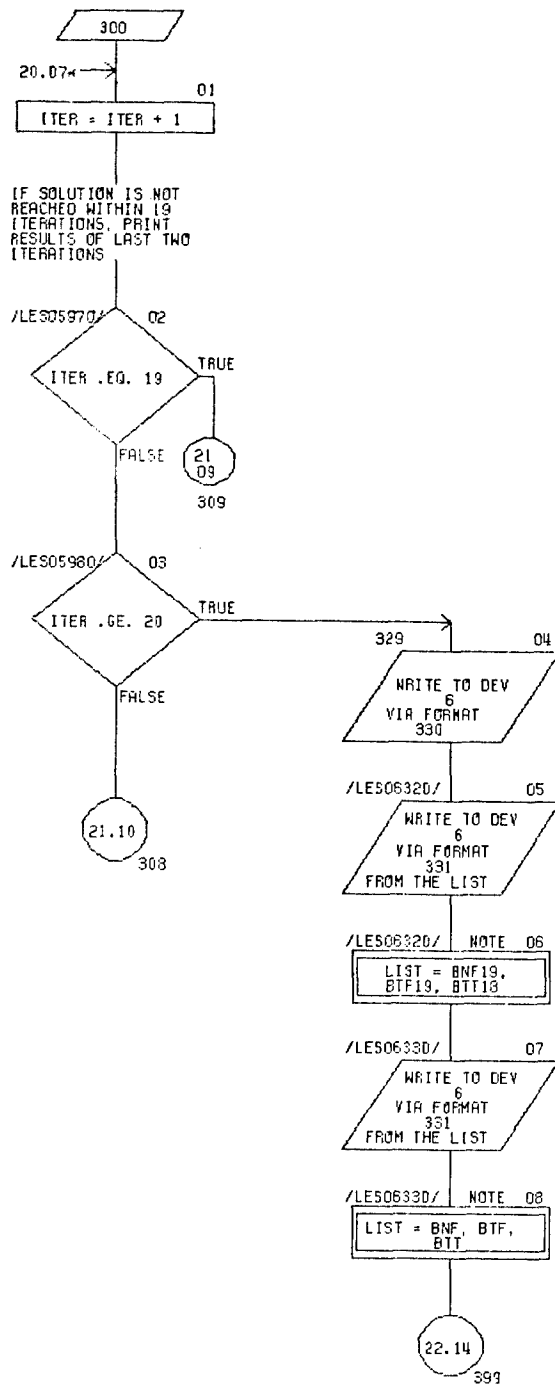
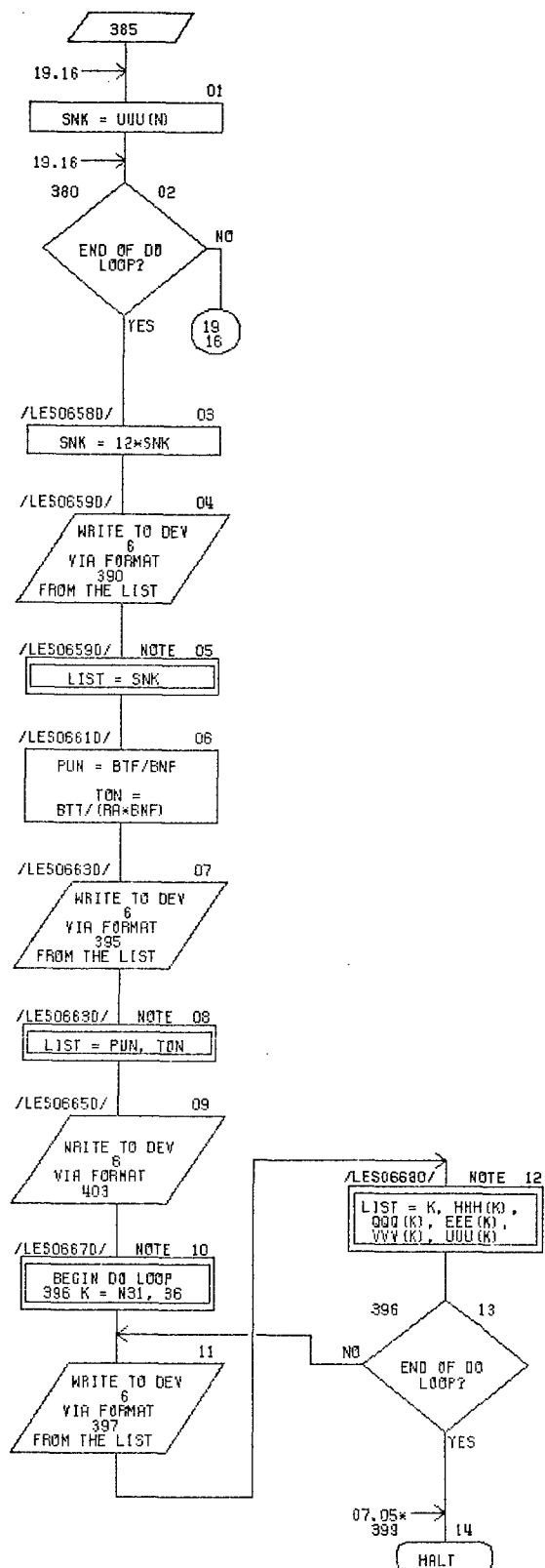


CHART TITLE - PROCEDURES



101 RETURN TO SYSTEM

CHART TITLE - NON-PROCEDURAL STATEMENTS

```

      IMPLICIT REAL (L)
      COMMON RO,GO,CO,F1,D1,AO,AM,A1,VK,UK,PL,DF,XX,
             QF,RF,VA,UA,J1,H(36),Q(36),E(36),U(36),V(36)
      COMMON ZDEP,ZPAST,ZLAST,JPAST,I(STREN,IH)
      COMMON F02,F0R2,C02,C0R2,H0,SIGLA,KDET
      EQUIVALENCE (RA0,RO), (G00,GO), (C00,CO), (FF1,F1),
             (D01,D1), (AA0,AO), (AAM,AM), (AA1,A1), (VVK,VK),
             (UUK,UK), (PPL,PL), (DOF,DF), (XXX,XX), (QQF,QF),
             (AAF,AF), (VVA,VA), (UUA,UA), (JJ1,J1), (HH(1),H(1)),
             (QQ(1),Q(1)), (EE(1),E(1)), (UU(1),U(1)), (VV(1),V(1))
      DIMENSION QQ(36),EE(36),HH(36)
      DIMENSION UU(36),VV(36)
      DIMENSION QQQ(36),EEE(36),HHH(36)
      DIMENSION UUU(36),VVV(36)
      DIMENSION QA(36),EA(36),HA(36)
      DIMENSION VN(36),UN(36)
      STATEMENT FUNCTION DEFINITION: DELT(D,F)=ATAN(SIN(SIN(D)/SIN(F))/SQRT(1-(SIN(D)/SIN(F))**2))
      STATEMENT FUNCTION DEFINITION: QUA(D9,F9)=COS(D9)+SQRT(COS(D9)**2-COS(F9)**2)
      STATEMENT FUNCTION DEFINITION: QUP(D9,F9)=COS(D9)-SQRT(COS(D9)**2-COS(F9)**2)
      STATEMENT FUNCTION DEFINITION: EPO(F9,T9,T8)=EXP(2*(T9-T8)*SIN(F9)/COS(F9))
      STATEMENT FUNCTION DEFINITION: TAN(F9)=SIN(F9)/COS(F9)
      STATEMENT FUNCTION DEFINITION: TAND(F9)=SIN(2*PI*(F9)/360)/COS(2*PI*(F9)/360)
      STATEMENT FUNCTION DEFINITION: BET(E9,D9,A8,A9)=ALOG(E9)/(D9-A8-A9)
3      FORMAT(1H0,'TIME= ',I6)
503     FORMAT(1H,' INPUT RADIUS,WIDTH IN FT ')
4545    FORMAT(' RA,B0')
4540    FORMAT(3F10.3)
504     FORMAT(1H,' INPUT LOAD (LBS), PSUBL (PSI) ')
4550    FORMAT(' LO,PO')
505     FORMAT(1H,' INPUT DEFL. COEFF, DELTA COEFF ')
4555    FORMAT(' DE,DF')
506     FORMAT(1H,' INPUT SLIP PARAMETERS JZERO AND K ')
4560    FORMAT(' SJ,SK')
507     FORMAT(1H,' INPUT SLIP, DEPTH OF SECOND LAYER')
4565    FORMAT(' SL,ZLAY')
501     FORMAT(1H,' INPUT UPPER LAYER COHESION,FR.ANGLE,GAMMA ')
4570    FORMAT(' C01,F01,G01')
502     FORMAT(1H,' INPUT LOWER LAYER COHESION,FR.ANGLE,GAMMA ')
4575    FORMAT(' C02,F02,G02')
511     FORMAT(1H,' RELATIVE STRENGTH OF LAYER INCONSISTENT,TRY AGAIN')
12      FORMAT(1H,'RAD.=',F9.2,' WIDTH=',F9.2,' LOAD=',F9.2,'
             PSUBL=',F9.2)
14      FORMAT(1H,'DEFL. COEF.=',F8.3,' DELTA COEFF. =',F8.3)
16      FORMAT(1H,'DEPTH OF 2ND LAYER= ',F10.3)
19      FORMAT(1H,' J ZERO = ',F8.4,' K = ',F8.4,' SLIP = ',F8.4)
18      FORMAT(1H,' DELTA = ',F9.3,' DEG. OF SHEAR MOD= ',F9.3)
13      FORMAT(1H,'1ST L. COH= ',F10.3,' PHI= ',F8.3,' GAMMA= ',F8.2)
15      FORMAT(1H,'2ND L. COH= ',F10.3,' PHI= ',F8.3,' GAMMA= ',F8.2)

```

11/05/75

AUTOFLOW CHART SET - FLOCHART LES00010

PAGE 24

CHART TITLE - NON-PROCEDURAL STATEMENTS

```

4580      FORMAT(' N = ',I6.2X,' EA(N) = ',F12.4)
4585      FORMAT(' Qa(N) = ',F12.4,' PPL= ',F12.4,' PSIF =',F12.4,
        ' H0*F01 = ',F12.4)
312      FORMAT(1H,' TIRE IN LOWER LAYER, MODEL NOT APPLICABLE')
330      FORMAT(1H,' PROBLEM SOLUTION REQUIRES FINER GRID. TRY SLIGHTLY
        DIFFERENT DEPTH OR ESTIMATE SOLUTION FROM THE RESULTS OF THE
        LAST TWO ITERATIONS AS FOLLOWS : ')
331      FORMAT(1H,' LOAD= ',F9.2,' DRAGB.= ',F9.2,' TORQUE= ',F9.2)
340      FORMAT(1H,' NO GO')
350      FORMAT(1H,' USE HARD SURFACE FORMULA')
365      FORMAT(1H,' NORMAL FORCE=',F10.2)
370      FORMAT(1H,' TANG. FORCE=',F10.2)
375      FORMAT(1H,' TORQUE=',F10.2)
390      FORMAT(1H,' SINKAGE=',F10.3,' (N')
395      FORMAT(1H,' PULLCOEFF=',F10.4,' TORQCOEFF=',F10.4)
403      FORMAT(1H,' I ALPHA NORMAL STR. SHEAR STR. X Z')
397      FORMAT(1H,' [4,F7.2,2F10.1,2F11.4)

```

CHART TITLE - SUBROUTINE SLFI

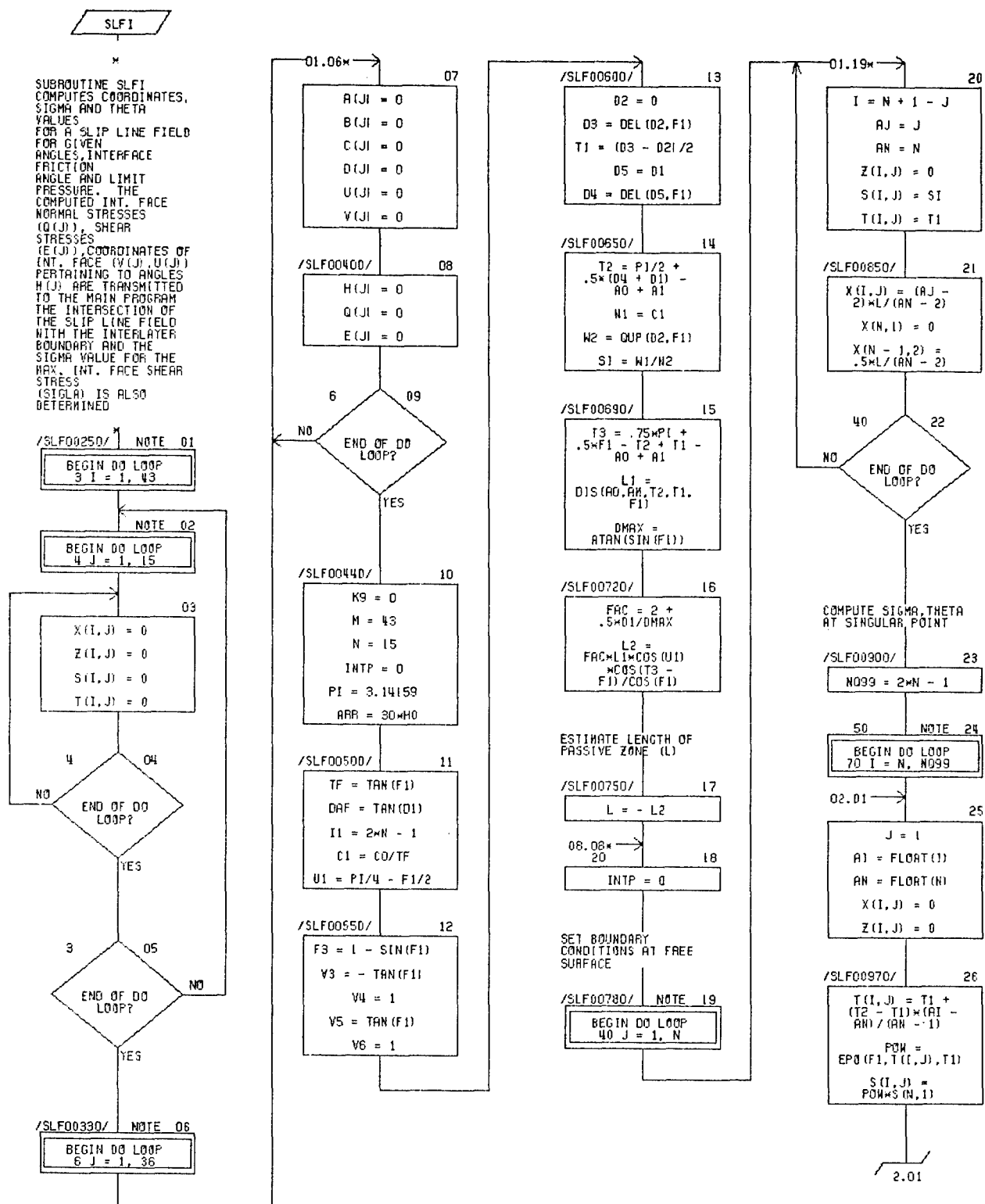


CHART TITLE - SUBROUTINE SLF0

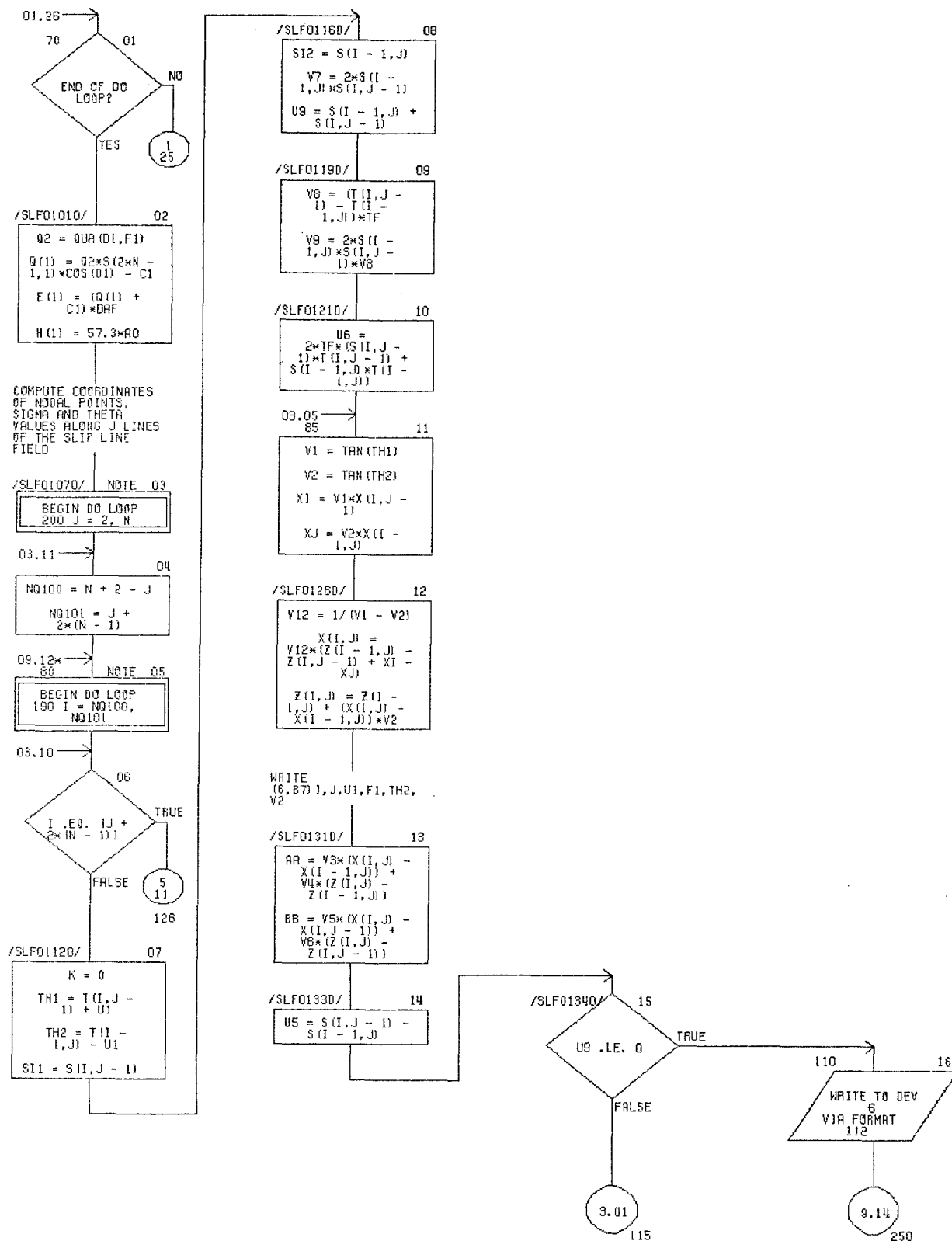


CHART TITLE - SUBROUTINE SLF1

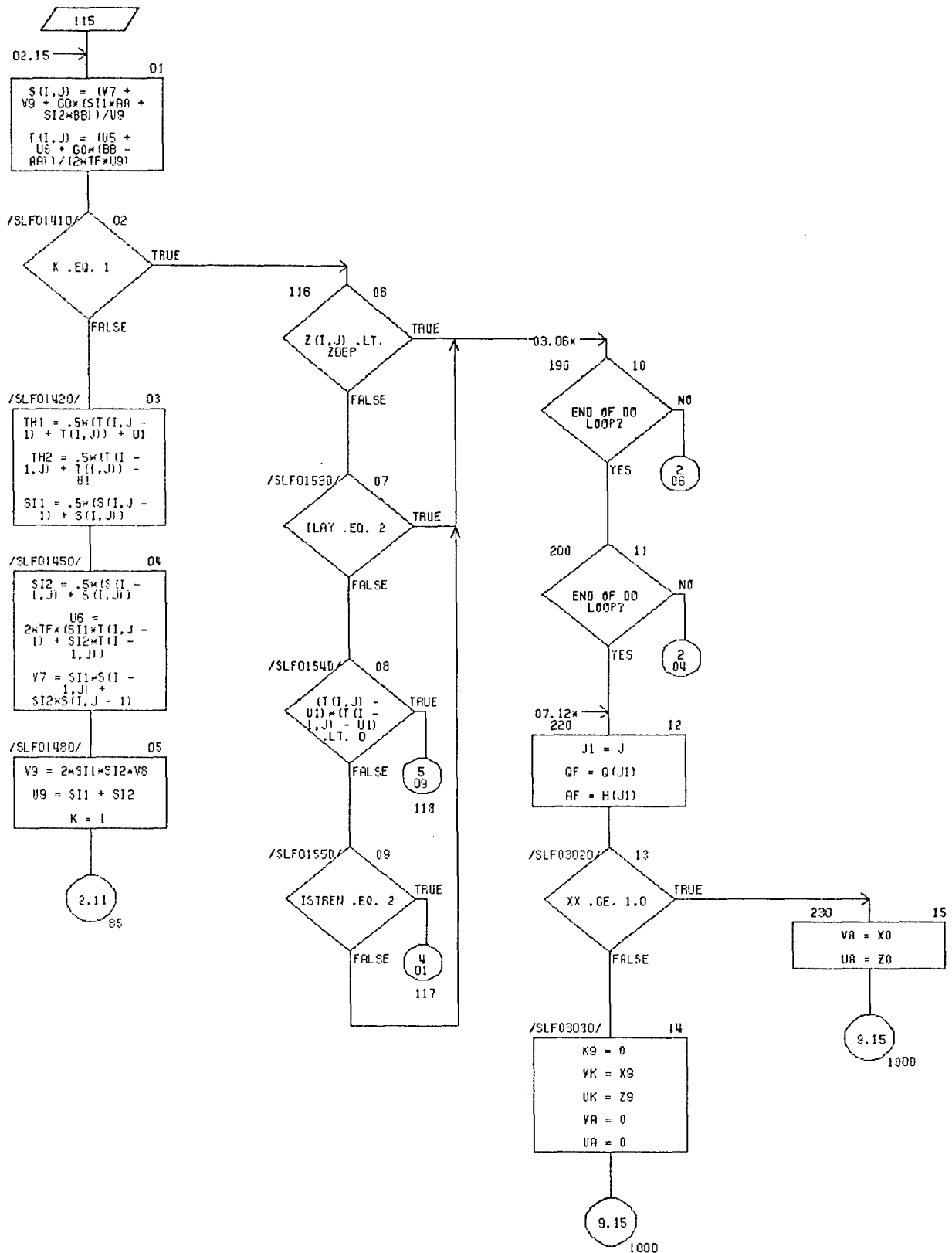


CHART TITLE - SUBROUTINE SLF1

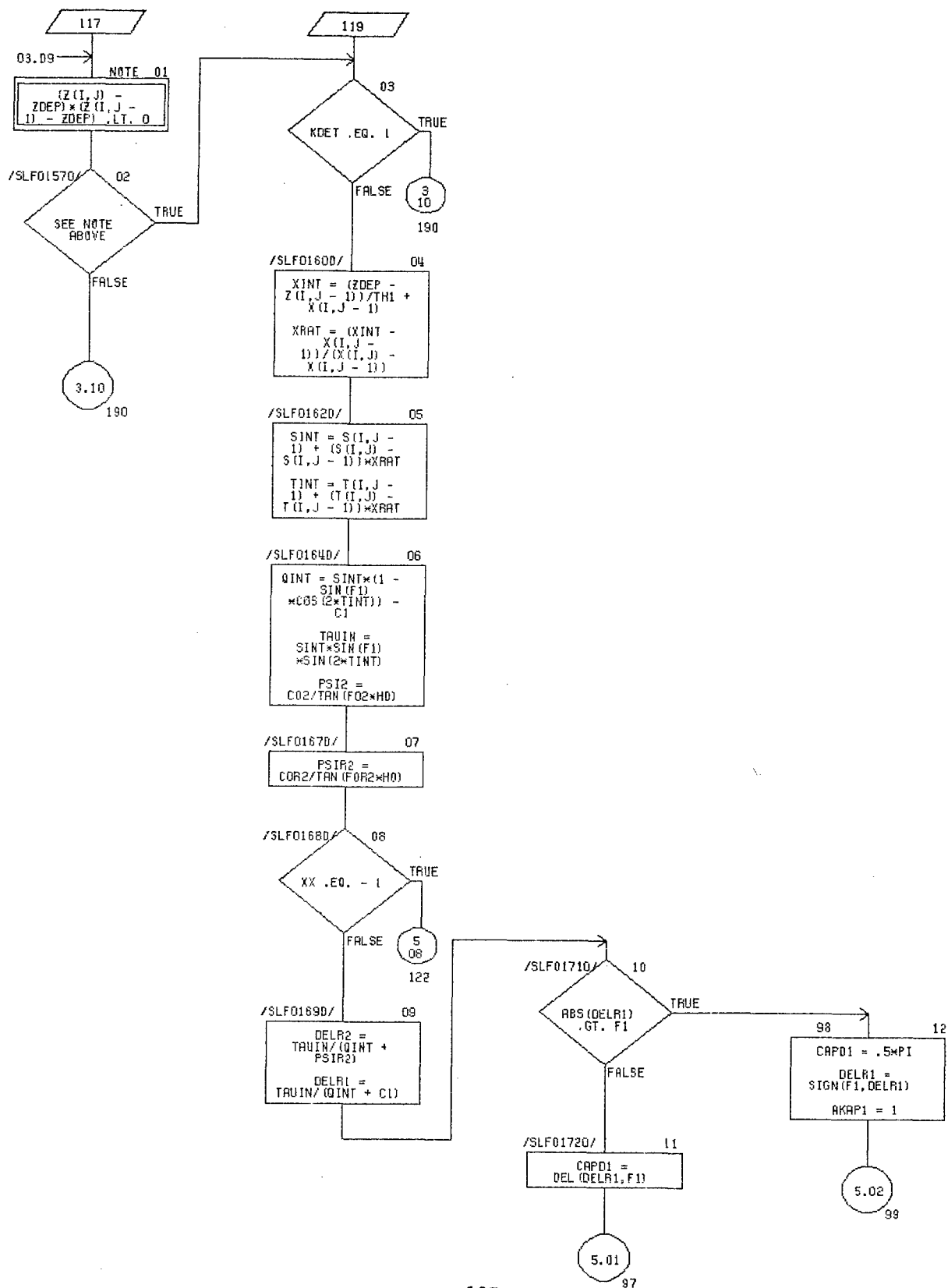


CHART TITLE - SUBROUTINE SLF0

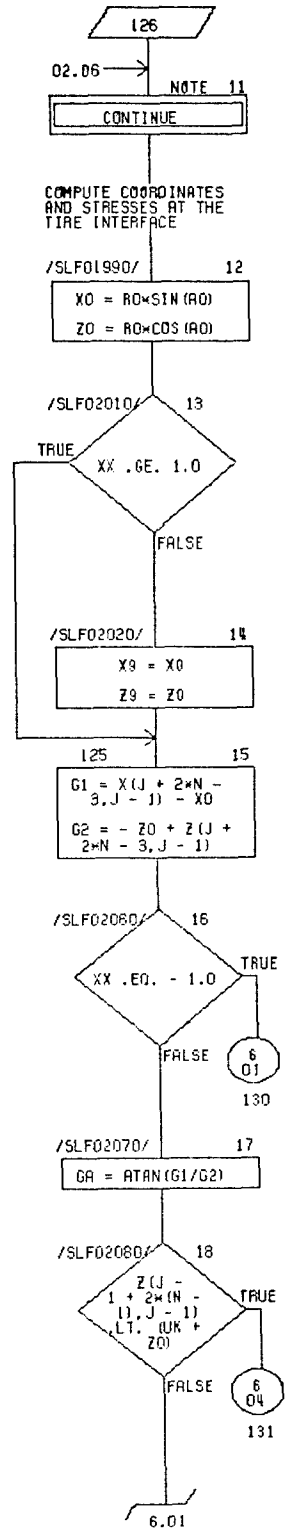
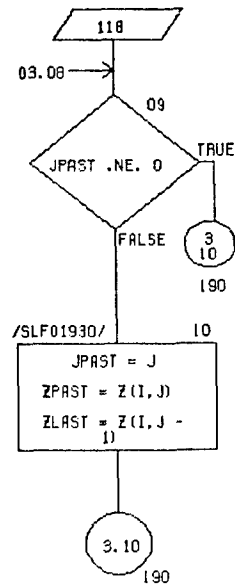
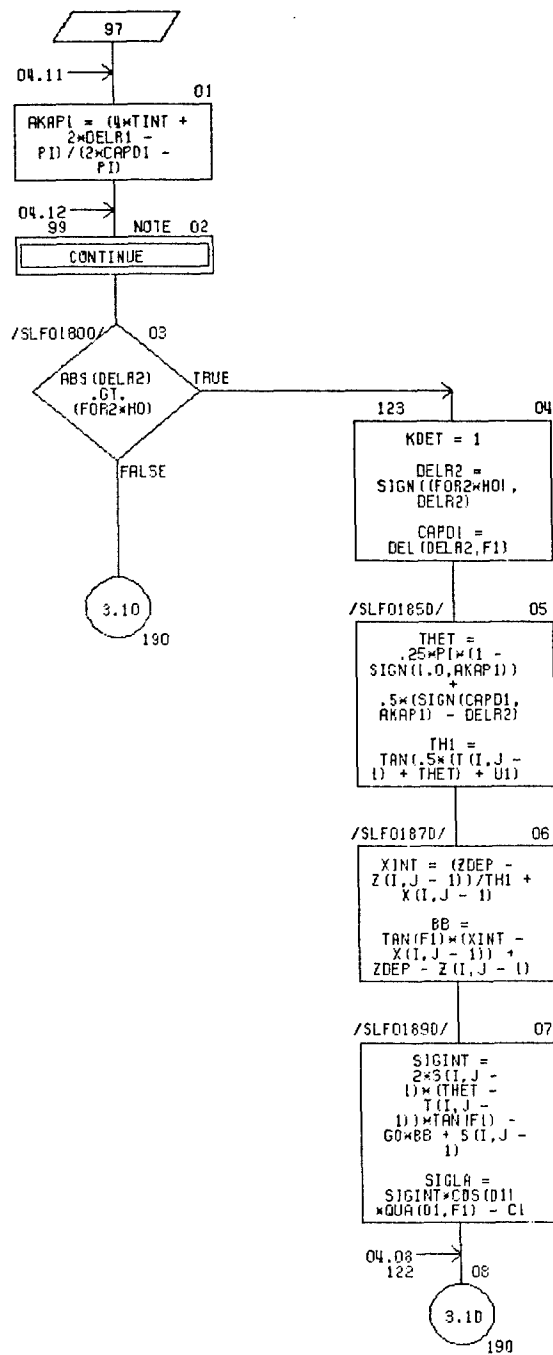


CHART TITLE - SUBROUTINE SLF0

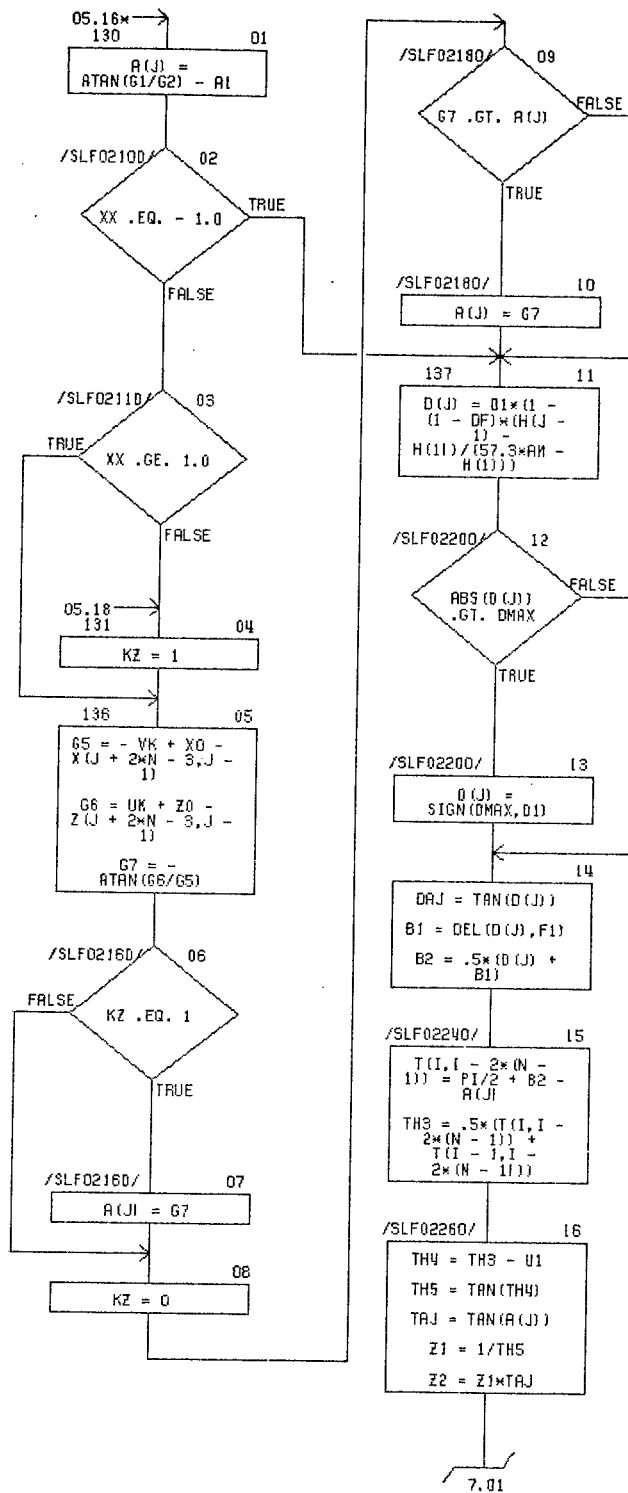


CHART TITLE - SUBROUTINE SLF1

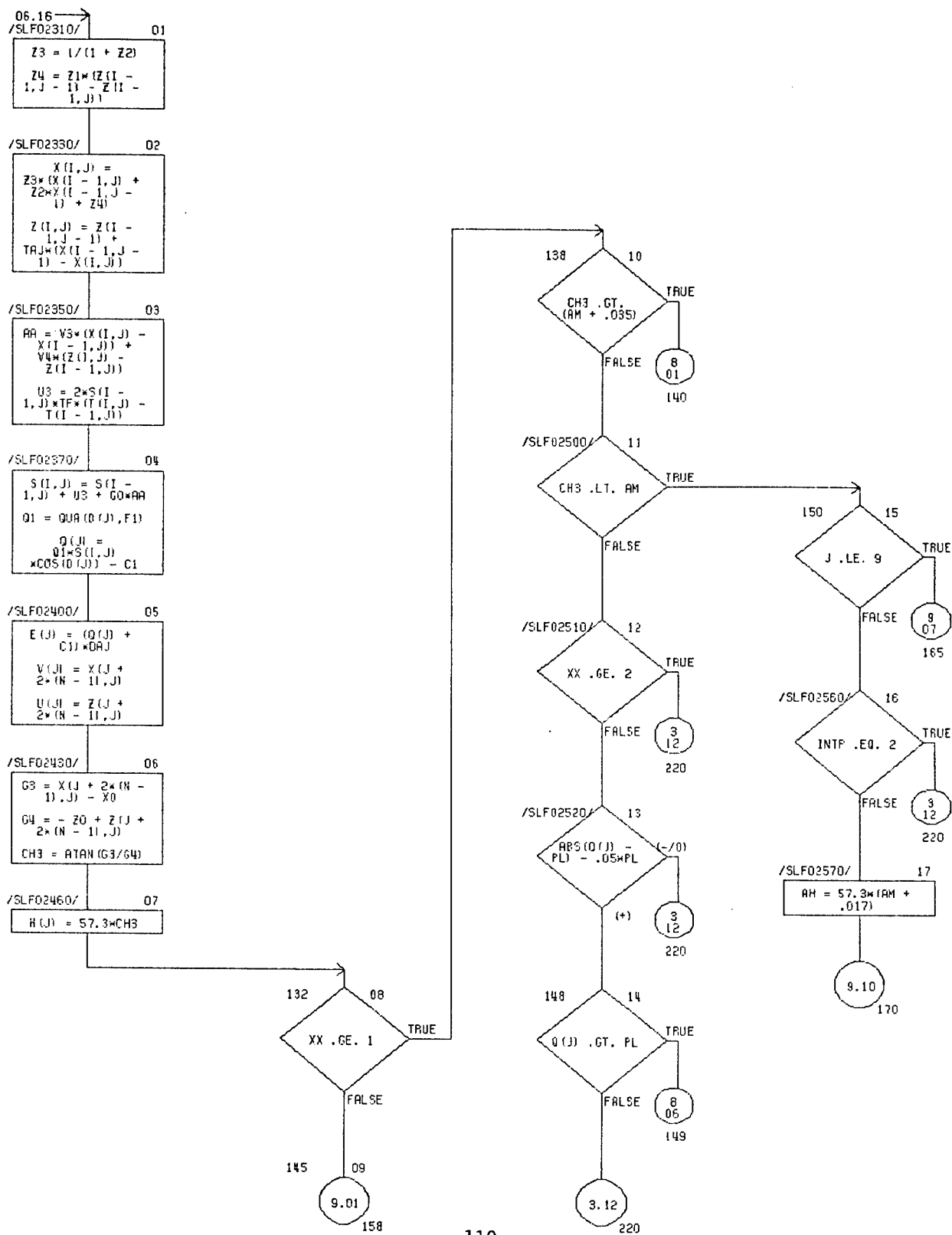


CHART TITLE - SUBROUTINE SLF1

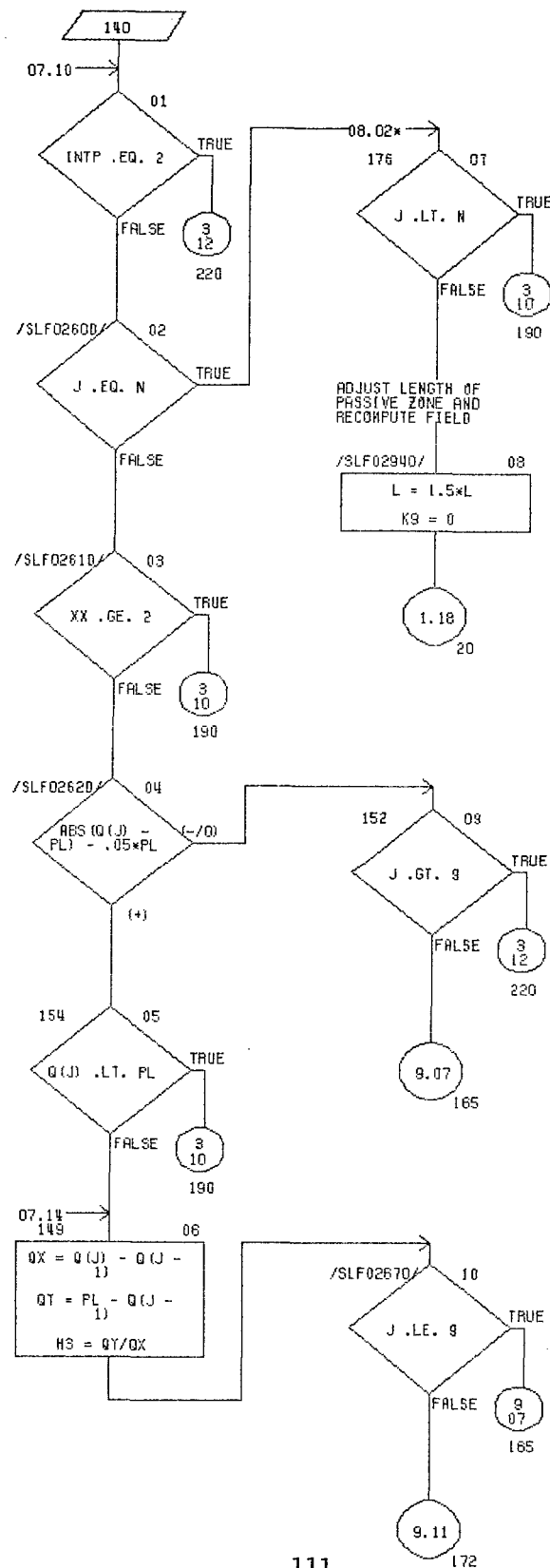
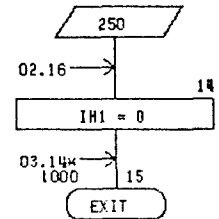
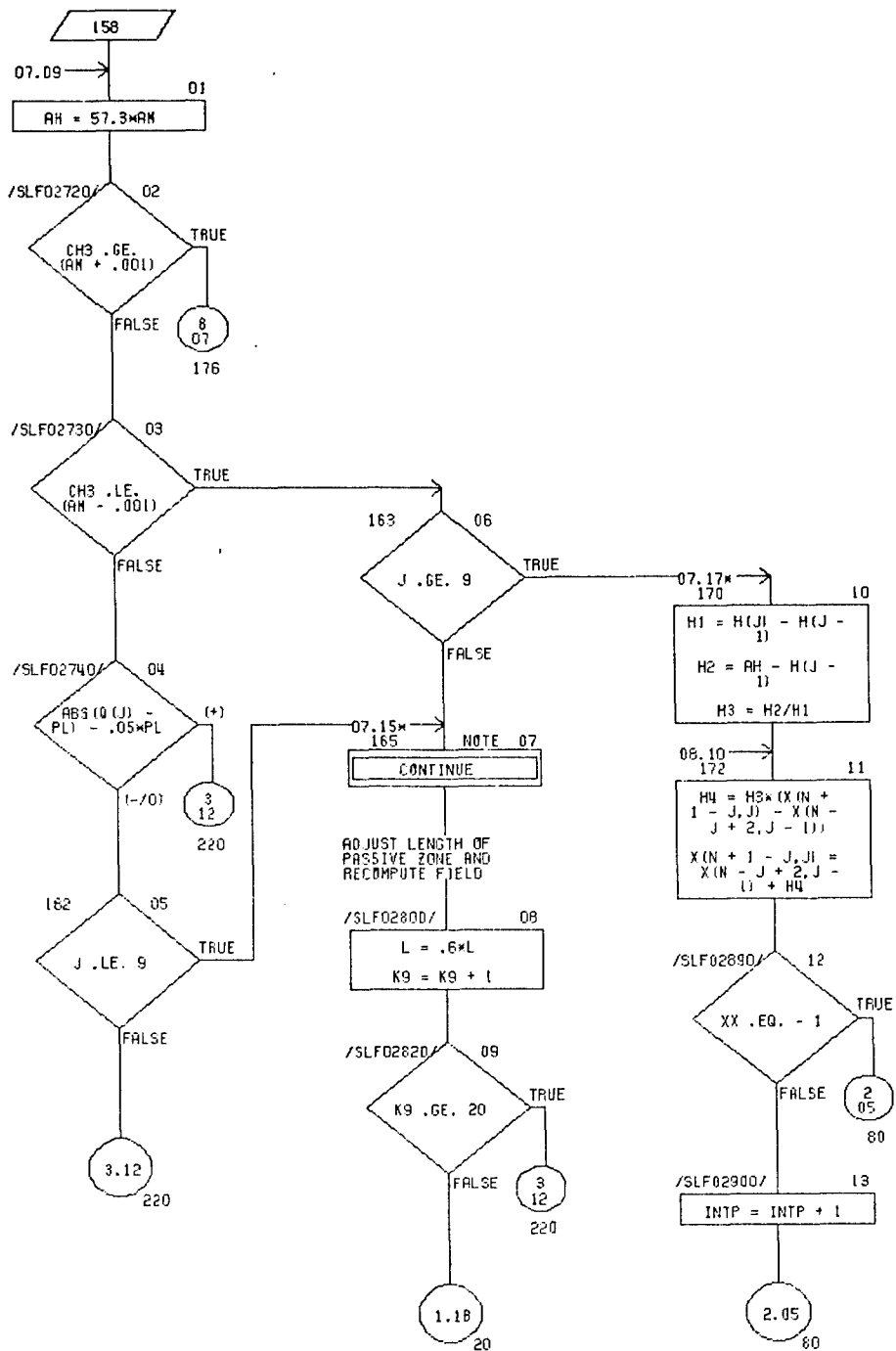


CHART TITLE - SUBROUTINE SLF1



DISTRIBUTION LIST
(As of March 1975)

DRDTA -
Please notify USATACOM, ~~AMSTA~~-RHM, Warren, Michigan 48090,
of corrections and/or changes in address.

No. of
Copies

50

Commander
U.S. Army Tank-Automotive Command
Warren, MI 48090

ATTENTION:

Chief Scientist, AMSTA-CL (230)	(1)
Director of RD&E, AMSTA-R (200)	(1)
Deputy Director of RD&E, AMSTA-R (200)	(1)
Foreign Intelligence Ofc, AMSTA-RI (200)	(1)
Systems Development Division, AMSTA-RE (200)	(4)
System Engineering Division, AMSTA-RB (200)	(2)
Engineering Science Division, AMSTA-RH (200)	(6)
Armor & Components Division, AMSTA-RK (215)	(4)
Methodology Function, AMSTA-RHM (215)	(10)
Propulsion Systems Division, AMSTA-RG (212)	(3)
Canadian Forces Liaison Office, CDLS-D (200)	(1)
US Marine Corps Liaison Ofc, USMC-LNO (200)	(3)
Project Manager MICV, AMCPM-MCV (Dqr)	(2)
Product Manager XM861, AMCPM-CT (Dqr)	(2)
Project Manager, M60 Tank Dev (AMCPP-M60TD)Dqr	(2)
Project Manager XM-1, AMCPM-GCM (dqr)	(2)
Technical Library, AMSTA-RWL (200)	(3)
TRADOC Liaison Ofc, TRADOC-LNO (200)	(3)

2

Chief, Research Development and Acquisition
Department of the Army
Washington, DC 20310

1

Superintendent
US Military Academy
ATTN: Professor of Ordnance
West Point, NY 10996

1

Commander
US Army Logistic Center
ATTN: ATCL-CC (Mr. J. McClure)
Ft. Lee, VA 23801

- 1 Commander
US Army Concept Analysis Agency
Long Range Studies
8120 Woodmont Avenue
Bethesda, MD 20014
- 1 Dept of the Army
Office Chief of Engineers
Chief Military Programs Team
Rsch & Dev Office
ATTN: DAEM-RDM
Washington, DC 20314
- 2 Director
US Army Corps of Engineers
Waterways Experiment Station
P.O. Box 631
Vicksburg, MS 39180
- 3 Director
US Army Corps of Engineers
Waterways Experiment Station
ATTN: Mobility & Environmental Laboratory
P.O. Box 631
Vicksburg, MS 39180
- 3 Director
US Army Cold Regions Research & Engineering Lab
ATTN: Dr. Freitag, Dr. W. Harrison, Library
P.O. Box 282
Hanover, NH 03755 *to diston*
- 3 Commander
US Army Materiel Command
AMC Building, Room 8S56
ATTN: Mr. R. Navarin, AMCRD-TV
5001 Eisenhower Avenue
Alexandria, VA 22333
- 2 President
Army Armor and Engineer Board
Ft. Knox, KY 40121
- 1 Commander
US Army Arctic Test Center
APO 409
Seattle, Washington 98733

2 Commander
US Army Test & Evaluation Command
ATTN: AMSTE-BB and AMSTE-TA
Aberdeen Proving Ground, MD 21005

2 Commander
Rock Island Arsenal
ATTN: SARRI-LR, Mr. Rankin
Rock Island, IL 61201

2 Commander
US Army Yuma Proving Ground
ATTN: STEYP-RPT, STEYP-TE
Yuma, Arizona 85364

1 Mr. Frank S. Mendez, P.E.
Technical Director
US Army Tropic Test Center
ATTN: STETC-TA
Box 942
Fort Clayton, Canal Zone 09827

1 Commander
US Army Natick Laboratories
ATTN: Technical Library
Natick, Massachusetts 01760

1 Director
US Army Human Engineering Laboratory
ATTN: Mr. Eckels
Aberdeen Proving Ground, MD 21005

2 Director
US Army Ballistic Research Laboratory
Aberdeen Proving Ground, MD 21005

3 Director
US Army Materiel Systems Analysis Agency
ATTN: AMXSY-CM, Messrs. D. Woomert, W. Niemeyer,
W. Criswell
Aberdeen Proving Ground, MD 21005

12 Director
Defense Documentation Center
Cameron Station
Alexandria, VA 22314

- 1 US Marine Corps
Mobility & Logistics Division
Development and Ed Command
ATTN: Mr. Hickson
Quantico, VA 22134
- 1 Mr. A. M. Wooley
West Coast Test Branch
Mobility and Support Division
Marine Corps Base
Camp Pendleton, CA 92055
- 1 Naval Sea Systems Command
Code PMS300A1
Department of the Navy
Washington, DC 20362
- 1 Naval Ship Research & Dev Center
Aviation & Surface Effects Dept.
Code 161
ATTN: E. O'Neal & W. Zeiffuss
Washington, DC 20034
- 1 Director
National Tillage Machinery Laboratory
Box 792
Auburn, Alabama 36830
- 1 Director
USDA Forest Service Equipment Dev Center
444 East Bonita Avenue
San Dimes, CA 91773
- 1 ~~Dr. R. A. Liston~~
Director, Keweenaw Research Center
Michigan Technological University
Houghton, MI 49931
- 1 Engineering Societies Library
345 East 47th Street
New York, NY 10017
- 1 Dr. M. G. Bekker
224 East Islay Drive
Santa Barbara, CA 93101

- 1 Dr. I. R. Ehrlich, Dean for Research
Stevens Institute of Technology
Castle Point Station
Hoboken, NJ 07030
- 2 Grumman Aerospace Corporation
ATTN: Dr. L. Karafiath, Mr. E. Markow
Plant 35
Bethpage, Long Island, NY 11714
- 1 Dr. Bruce Liljedahl
Agricultural Engineering Department
Purdue University
Lafayette, IN 46207
- 1 Dr. W. G. Baker
Dean, College of Engineering
University of Detroit
4001 W. McNichols
Detroit, MI 48221
- 1 Mr. H. C. Hodges
Nevada Automotive Test Center
Box 234
Carson City, NV 89701
- 1 Mr. W. S. Hodges
Lockheed Missile & Space Corporation
Ground Vehicle Systems
Department 50-24, Bldg 528
Sunnyvale, CA 94088
- 1 Mr. R. D. Wismer
Deere & Company
Engineering Research
3300 River Drive
Moline, IL 61265
- 1 Oregon State University
Library
Corvallis, Oregon 97331
- 1 Southwest Research Institute
ATTN: Mr. R. C. Hemion
8500 Culebra Road
San Antonio, TX 78228

- 1 FMC Corporation
Technical Library
P.O. Box 1201
San Jose, CA 95108
- 1 Mr. J. Appelblatt
Director of Engineering
Cadillac Gauge Co.
P.O. Box 1027
Warren, MI 48090
- 2 Chrysler Corporation
Mobility Research Laboratory,
Defense Engineering
ATTN: Dr. B. VanDeusen, Mr. G. Cohron
Department 6100
P.O. Box 751
Detroit, MI 48231
- 1 Library
CALSPAN Corporation
Box 235
4455 Genessee Street
Buffalo, NY 14221
- 1 Mr. Sven E. Lind
SFM, Forsvaretsforskningsanstalt
Avd 2
Stockholm 80, Sweden
- 2 Mr. Rolf Schreiber
c/o Bundesamt Fuer Wehrtechnik
Und Beschaffung - KGII 7 -
5400 Koblenz
Am Rhein 2-6 Germany
- 1 Foreign Science & Technology Ctr
220 7th Street North East
ATTN: AMXST-GEL
Mr. Tim Nix
Charlottesville, VA 22901

1 General Research Corporation
 ATTN: Mr. A Viilu
 7655 Old Springhouse Road
 Westgate Research Park
 Mc Lean, VA 22101

1 Commander
 US Army Materiel Command
 ATTN: AMCRD-T (Dr. Norman Klein)
 5001 Eisenhower Avenue
 Alexandria, VA 22333

reverte

1 Commander US Army Materiel Command
 ATTN: AMCRD-GV, Mr. Robert Green
 5001 Eisenhower Avenue
 Alexandria, VA 22333

reverte

UNCLASSIFIED

SECURITY CLASSIFICATION OF THIS PAGE (When Data Entered)

REPORT DOCUMENTATION PAGE		READ INSTRUCTIONS BEFORE COMPLETING FORM
1. REPORT NUMBER Technical Report 12109(LL152)	2. GOVT ACCESSION NO.	3. RECIPIENT'S CATALOG NUMBER
4. TITLE (and Subtitle) Development of Mathematical Model for Pneumatic Tire-Soil Interaction in Layered Soils		5. TYPE OF REPORT & PERIOD COVERED Final
7. AUTHOR(s) Leslie L. Karafiath		6. PERFORMING ORG. REPORT NUMBER RE -
9. PERFORMING ORGANIZATION NAME AND ADDRESS Grumman Aerospace Corporation Research Dept Bethpage, NY 11714		8. CONTRACT OR GRANT NUMBER(s) DAAEO7-75-C-0066
11. CONTROLLING OFFICE NAME AND ADDRESS US Army Tank Automotive Development Com- mand (Prov), Rsch Div, Warren, MI 48090		10. PROGRAM ELEMENT, PROJECT, TASK AREA & WORK UNIT NUMBERS 6.11.02A 1T161102B52A 347EH
14. MONITORING AGENCY NAME & ADDRESS (if different from Controlling Office)		12. REPORT DATE November 1975
		13. NUMBER OF PAGES 120
		15. SECURITY CLASS. (of this report) UNCLASSIFIED
		15a. DECLASSIFICATION/DOWNGRADING SCHEDULE
16. DISTRIBUTION STATEMENT (of this Report)		
17. DISTRIBUTION STATEMENT (of the abstract entered in Block 20, if different from Report) Approved for public release, distribution unlimited.		
18. SUPPLEMENTARY NOTES		
19. KEY WORDS (Continue on reverse side if necessary and identify by block number) Mathematical Models Tire-Soil Interaction		
20. ABSTRACT (Continue on reverse side if necessary and identify by block number) Mathematical models of tire-soil interaction have been de- veloped for nonhomogeneous soil conditions where the soil strength varies either continuously or discretely with depth. New methods of solving the differential equations of plasticity for soils have been developed for the bearing capacity problem in two-layer soils		

UNCLASSIFIED

SECURITY CLASSIFICATION OF THIS PAGE(When Data Entered)

Composite slip line fields obtained by these methods and the associated bearing stresses are shown for two cases: upper layer stronger than the lower layer and upper layer weaker than the lower layer. An approximate procedure, based on these composite slip line fields, is given for the estimation of bearing stresses in two-layer soils. This approximate procedure is applied in a tire-soil model expanded for the consideration of two-layer soils. The simulation of tire performance by this expanded model is compared with results of small-scale mobility tests performed at the U.S. Army Engineer's Waterways Experiment Station (WES) in layered soils.

Field methods of determining soil properties in layered soils are examined, and a modification of ring shear tests is recommended for the determination of the strength of individual layers in layered soils.

UNCLASSIFIED

SECURITY CLASSIFICATION OF THIS PAGE(When Data Entered)